# 1. INTRODUCTION, BACKGROUND, AND PRINCIPAL RESULTS OF LEG 135, LAU BASIN[1]

Shipboard Scientific Party[2]

## INTRODUCTION

The western Pacific Ocean basin is rimmed by island arcs, trenches, and marginal seas. These are closely associated with convergent oceanic plate margins where inclined seismic zones (Wadati-Benioff zones) mark the location of subducted oceanic lithosphere plates. Intraoceanic island-arc volcanic chains, situated above the Wadati-Benioff zones, represent regions where new crust is generated by the transfer of magmas derived from partial melting of the mantle with various contributions of constituents from recycled oceanic crust. The intraoceanic volcanic arcs are important sites for the generation of new crust in areas far removed from the mid-oceanic ridges, but other equally important sites are the small ocean basins (i.e., backarc basins) that lie "behind" the island arcs. Here, in the backarc basins, new oceanic crust is formed that has petrologic properties broadly similar to the basalts formed at mid-oceanic ridges.

Wegener (1929), perhaps, was among the first to suggest that "the island arcs, and particularly the eastern Asiatic ones, are marginal chains which were detached from the continental mass, when the latter drifted westwards, and remained fast in the old sea floor which was solidified to great depths. Between the arcs and the continental margin later still-liquid areas of sea floor were exposed as windows." Wegener's insight to the evolution of the western Pacific basin was not supported at that time by any geological or geophysical data; nonetheless, it parallels his ideas about continental drift. The models for backarc genesis have become more elegant than this simple description, but Wegener should be given credit for suggesting the importance of crustal extension in the origin of these basins. The relation of backarc basins to the broader arc-trench systems at convergent oceanic plate margins has been explored by many researchers in recent years, beginning with the works of Karig (1970, 1971), Packham and Falvey (1971), and Moberly (1972).

The western Pacific drilling projects of the Ocean Drilling Program (ODP) included several studies of backarc basins and their adjacent forearcs with the goal of gaining a better understanding of their geology, their relation to plate convergence processes, and their evolution. The broad scientific objectives for Leg 135 were (1) to assess the nature of the oceanic crust in the Lau Basin and the adjacent Tonga Platform in the forearc and (2) to understand the geologic history of the Lau Basin and its relationship to the geologic processes that formed the island-arc systems on its west and east boundaries. Leg 135 drill sites and their geologic setting are shown in Figures 1 and 2. The science plan for Leg 135 comprised a research program that would complement previous work in the Lau Basin and Tonga arc-trench region and studies on the Mariana, Izu-Bonin, and Vanuatu arc systems performed on previous DSDP and ODP drilling legs.

## BACKGROUND

### Introduction

The significance of crustal extension in the origin of backarc basins was recognized by Karig (1970), who postulated that the Lau and Tonga ridges were arcs—the former extinct, the latter active (Fig. 1)—separated by oceanic crust. He later extended this interpretation to the Mariana Trough (Karig, 1971). Support for the hypothesis came from data for Mariana Trough samples that were generally similar to mid-oceanic-ridge basalts (MORB), although these samples showed distinctive characteristics such as enrichment in volatiles, alkali elements, and alkaline earth elements (Hart et al., 1972). These characteristics suggested that there was an affinity to island-arc tholeiites and that Mariana Trough "basin basalts" were transitional to arc system magmas (e.g., Gill, 1976; Fryer et al., 1981). Data from the Lau Basin (Sclater et al., 1972; Hawkins, 1974, 1976, 1977) and from the North Fiji Basin (Hawkins and Batiza, 1975) showed differences from the Mariana Trough basalts and helped establish that some western Pacific backarc basins were floored by tholeiitic basalt that was similar to MORB in most mineralogic, major and trace element, and isotopic characteristics. Further studies of the margins of the Lau Basin suggested that it was zoned, passing from older crust having a "transitional" chemistry to more MORB-like lavas on the active axial ridges (Hawkins and Melchior, 1985). Detailed sampling with *ALVIN* on the axial ridge of the Mariana Trough shows that it too is zoned and has fresh MORB-like lavas interspersed with "transitional" basalts (Hawkins et al., 1990).

The distinctive characteristics of Mariana Trough samples were well documented by Fryer et al. (1981), who used their analyses of glasses to argue that backarc basin basalts (BABB) constituted a distinct type of basalt and were intermediate between MORB and the island-arc tholeiite series. Their enrichment in water relative to MORB and their high $H_2O/CO_2$ was demonstrated by Delaney et al. (1978) and Garcia et al. (1979). However, as more data were acquired, it became apparent that the basalts of backarc basins exhibit a range in composition from MORB-like to arc tholeiitic and that no single designation was appropriate for all backarc basins.

### Petrologic Problems

Backarc basins form in close proximity to island arcs, and it is generally agreed that their origin is closely related to the subduction process. The nature of this relationship is subject to much debate. For example, is there a mechanical coupling between subduction and the backarc extension process or not; and is there a chemical exchange or a contribution of melt from the subducted lithosphere or not? Understanding the origin of the magmas that form backarc basin crust requires that we test the same types of models as are proposed for the generation of arc magmas. The petrogenetic processes in the early stages of arc evolution, in which island-arc tholeiites are abundant, may be similar to magma genesis in backarc settings. It is argued by some that partial melting of the supra-subduction zone mantle wedge is the primary source of the arc tholeiitic island-arc magmas and that very little is contributed by the subducted lithosphere itself. Arc tholeiitic

[1] Parson, L., Hawkins, J., Allan, J., et al., 1992. *Proceedings of the Ocean Drilling Program, Initial Reports,* 135: Ocean Drilling Program (College Station, TX).

[2] Shipboard Scientific Party is as given in the list of participants preceding the contents.

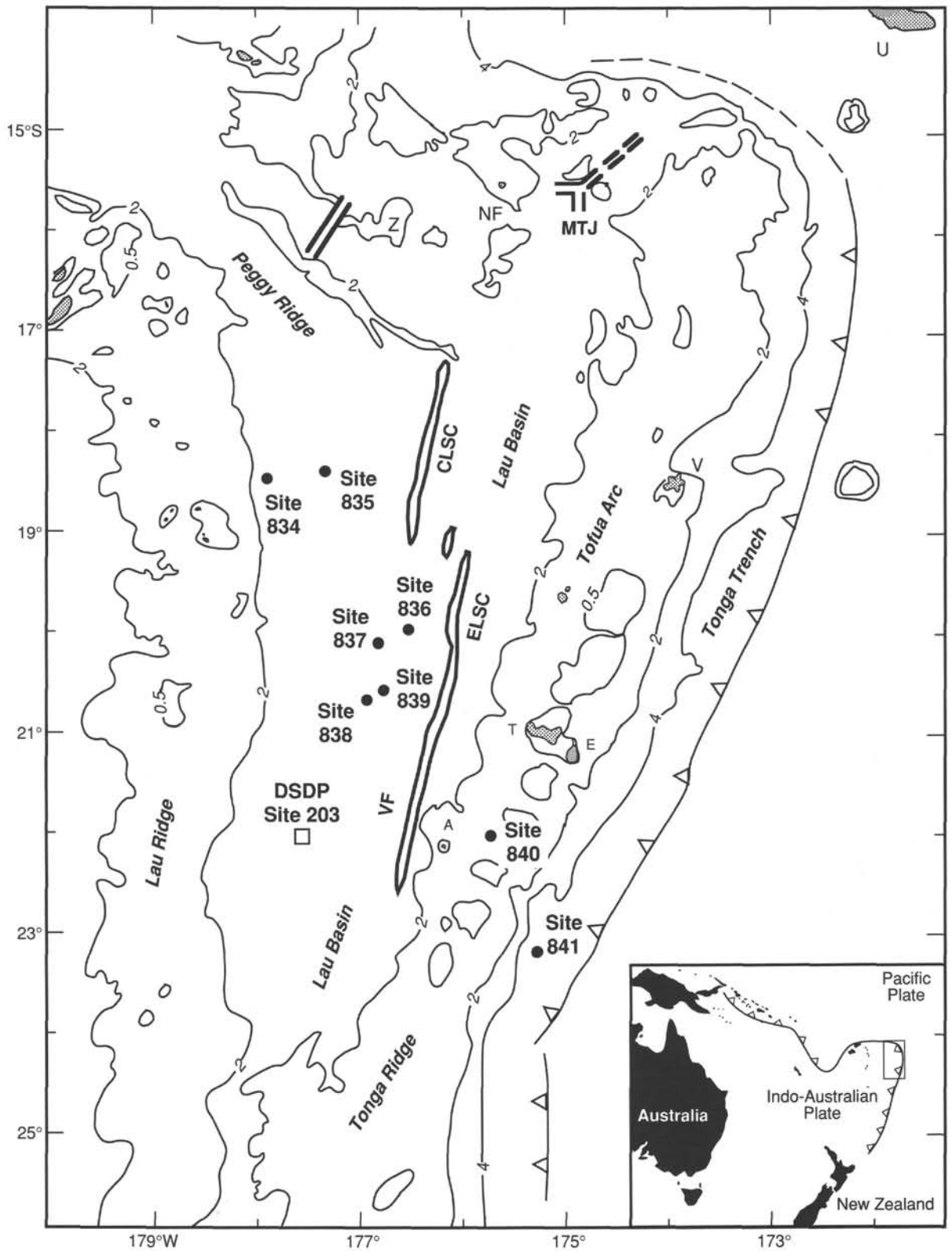


Figure 1. Regional setting for Sites 836 through 839 with locations of other drill sites in the Lau Basin and the major geologic features of the Tonga Trench and Lau Basin system. Z = Zephyr Shoal; islands include T = Tongatapu, E = 'Eua, V = Vavau, A = Ata, and NF = Niua Fo'ou Island. The locations of the Central Lau (CLSC) and Eastern Lau Spreading Centers (ELSC), Valu Fa Ridge (VF), and Mangatolu Triple Junction (MTJ) are from von Stackelberg (1990), Parson et al. (1990), Hawkins et al. (1989), and Nilsson et al. (1989). The location of DSDP Site 203 is shown as an open box. Contour interval in kilometers.

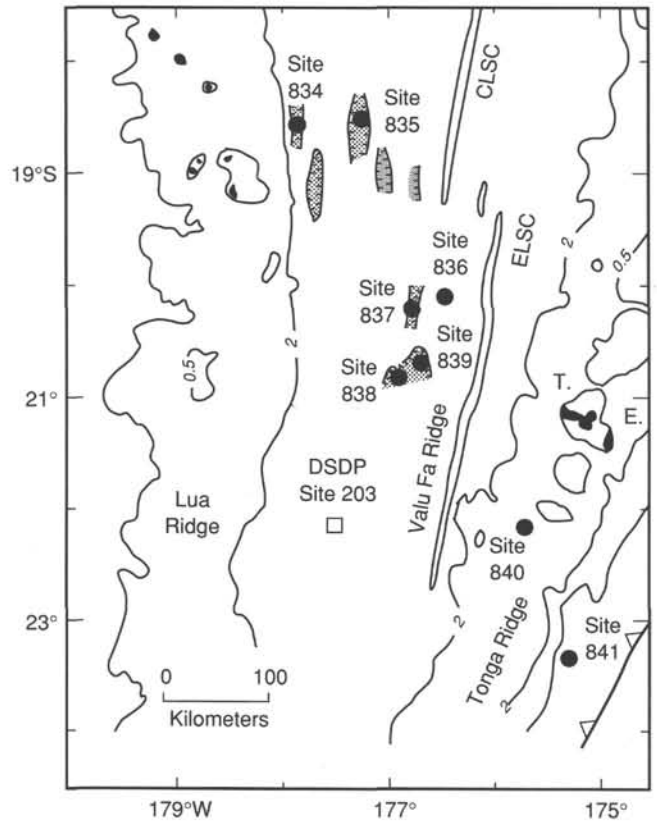


Figure 2. Map of backarc sites drilled in the Lau Basin during Leg 135 with outline bathymetry (500 and 2000 m isobaths). Known sub-basins are stippled. ELSC = East Lau Spreading Center and CLSC = Central Lau Spreading Center. Contour interval in kilometers. T = Tongatapu and E = 'Eua.

magmas are enriched relative to MORB in K, Rb, Ba, light-rare-earth elements (LREE), $^{87}Sr/^{86}Sr$, and water, and they display relative depletion in many high-field-strength elements (HFSE). Volatiles, enriched in large-ion-lithophile elements (LILE), are considered to be important modifying agents of the mantle wedge and give rise to some of the characteristics of island-arc tholeiites. The source of these volatiles is the hydrous minerals of altered subducted oceanic crust and sediment (Tatsumi et al., 1986). Much of the data for backarc basins suggests that the chemical signatures, typical of the supra-subduction zone magmas of island arcs, are characteristic of some of the magmas formed in the backarc setting as well.

The nature, variability, sources, and petrogenetic history of backarc basin magmas has remained a major problem. One of the major objectives of Leg 135 was to sample the crust of the Lau Basin along a transect between the Lau Ridge remnant arc and the active spreading axis. Petrologic studies of these samples were expected to give further information on the history of magma genesis and variations in the composition of magma sources with time.

## Regional Geophysical Setting

The Tonga Trench, and its associated Wadati-Benioff zone, are the major bathymetric and geophysical features of the region (Fig. 3). A well-defined, curved seismic zone dipping westward from the trench at 174°W extends to depths of nearly 700 km at 178°E (Isacks and Barazangi, 1977; Giardini and Woodhouse, 1984). The top of the seismic zone is at a depth of about 140 km beneath the active volcanoes of the Tofua Arc and about 250 km below

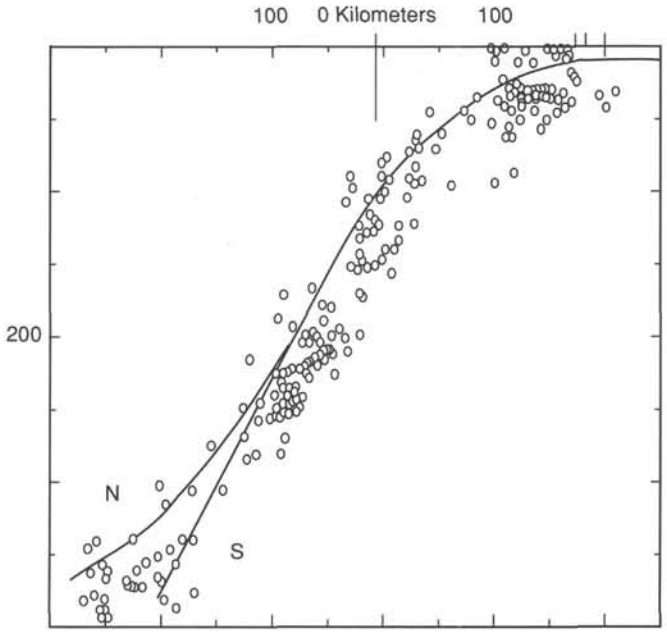


Figure 3. Composite cross-section of earthquake hypocenters for the Tonga Trench. The "0" km on the horizontal scale corresponds to the volcanic arc, and the projection of volcanoes and trench axes is shown by the vertical lines. Scale is in kilometers (Isacks and Barazangi, 1977).

the axes of the spreading ridges of the Lau Basin (Isacks and Barazangi, 1977). The estimated convergence rate between the (subducted) Pacific Plate and the Tonga Ridge ranges from 16 to 23 cm/yr (Pelletier and Louat, 1989). These unusually high rates are the consequence of the added east-directed component from the opening of the Lau Basin at an estimated 8 cm/yr. The geometry of the upper surface of the seismic zone has been modeled as a strongly curved and irregular surface (Figs. 4A–B) that terminates at its northern end where the Tonga Trench curves sharply to the west and the plate boundary becomes a trench–trench transform fault (Billington, 1980). Billington describes the deeper parts of the seismic zone (deeper than 300 km) as having considerable variability in form: "the strike of the deep seismicity does not exactly parallel that of the shallower seismicity in the southern Tonga region and strongly deviates from it in the northern Tonga region." The southernmost section of the Tonga Trench seismic zone dips smoothly at about 42° between depths from 300 to 600 km and then steepens to nearly vertical. Between 25° and 20°S, there is a strong discontinuity or inflection in the dip of the seismic zone that gives rise to a flattening or seatlike shape at depths ranging from 525 to 575 km. A subsequent study by Louat and Dupont (1982) interpreted the inflection as caused by imbrication of the subducted plate. The inferred age of the subducted lithosphere at the depth of this inflection is about 7–8 Ma. This is close to our estimate as to when the basin opening began, as determined from the drill core data, and suggests the possibility that the inflection is related to the beginning of lithosphere extension in the Lau Basin at about 5.5 Ma. A zone of strong seismic wave attenuation (Figs. 5A–B) has been recognized on the west side of the Tonga Ridge and beneath the crust of the Lau Basin (Barazangi and Isacks, 1971; Aggarwal et al., 1972). Barazangi and Isacks discussed various possible causes for this strong attenuation and attributed it to high temperature or partially melted upper mantle.

Few published heat flow data are available for the Lau Basin. Heat flow values in the northwestern Lau Basin (Fig. 6) range from 0.36 to 1.70 $\mu cal/cm^2$; these are low relative to theoretical

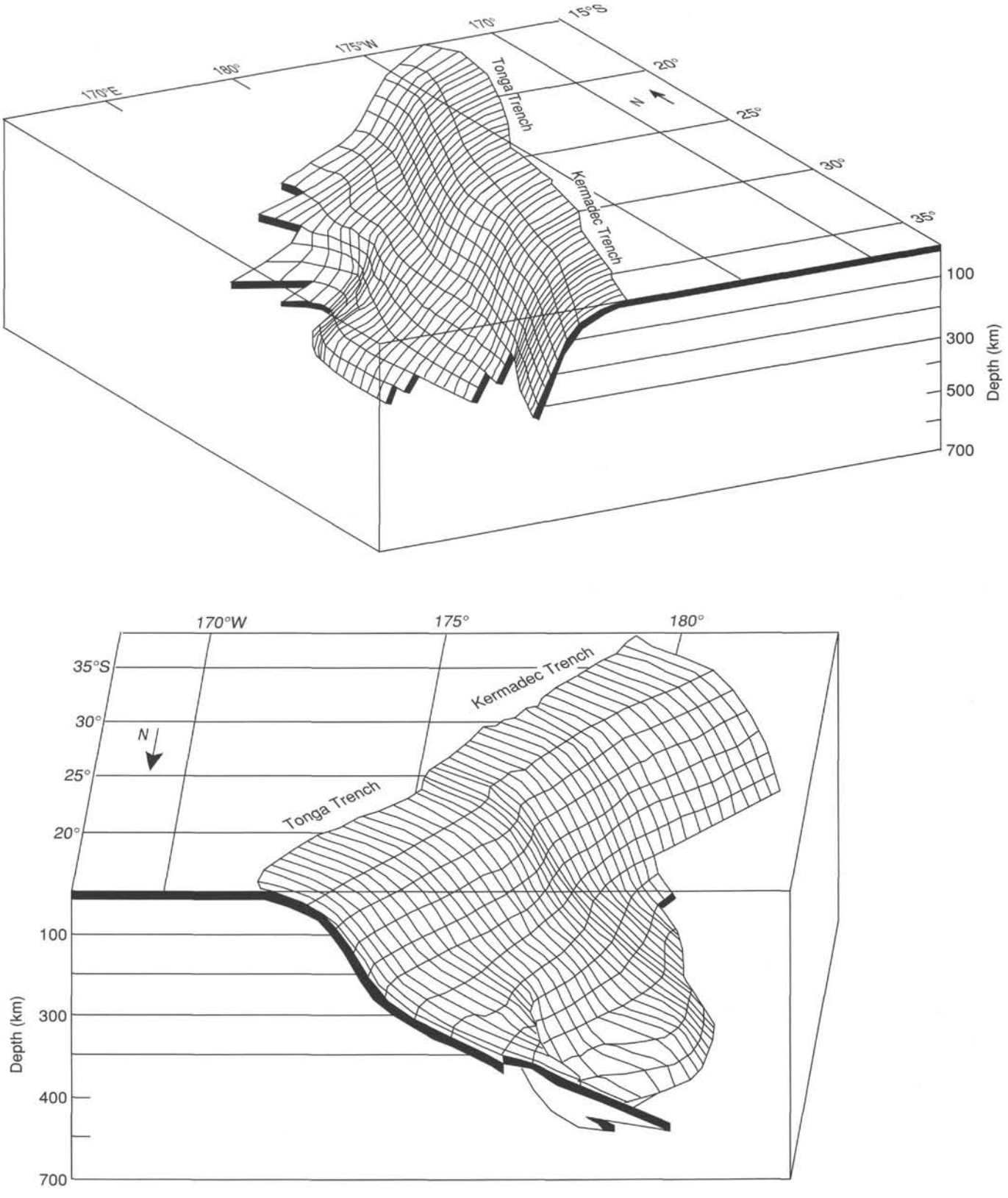


Figure 4. Views of a grid representing the upper surface of the Wadati-Benioff Zone of the Tonga-Kermadec subduction zone. The projections are slightly distorted in that they do not take into account the Earth's sphericity (after Billington, 1980).

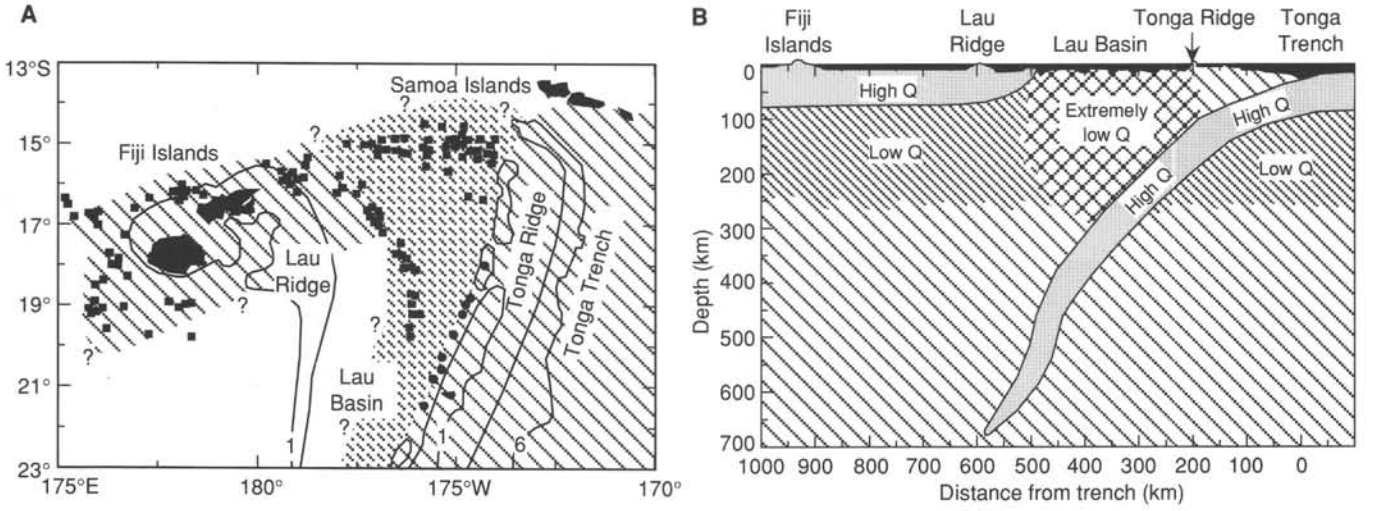


Figure 5. Map (**A**) and cross-section (**B**) of the North Fiji Basin–Lau Basin–Tonga Trench region showing inferred and extrapolated extent of the region of high and low attenuations in the uppermost mantle. Historically active volcanoes of the Tofua Arc are shown as solid circles. Depth contours are at 1 and 6 km. Loci of shallow earthquakes are shown as solid squares. Note that the Lau Basin is underlain by mantle with extremely low Q (high attenuation). After Barazangi and Isacks (1971).

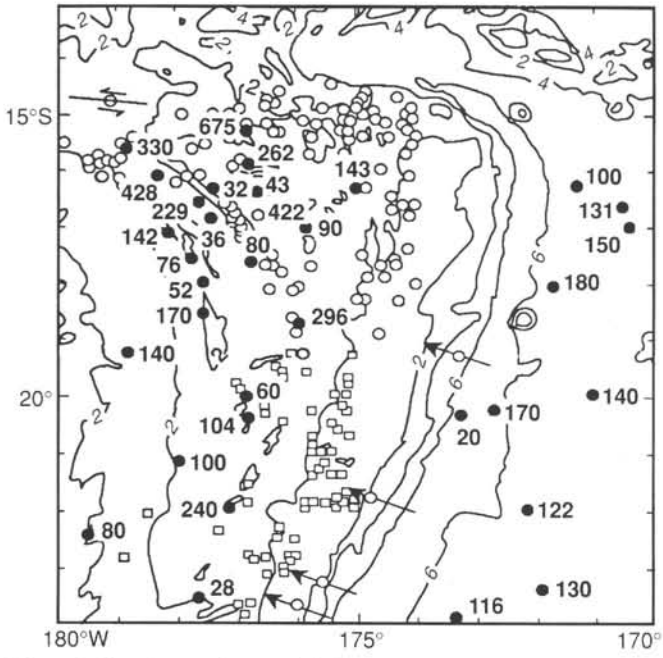


Figure 6. Heat flow stations and shallow focus seismic events in the Lau Basin. Solid circles are heat flow stations, open symbols are shallow focus earthquakes as of 1969. Depths shown are 2, 4, and 6 km isobaths. Arrows show directions of earthquake mechanisms. Northern end of Lau Basin and Tonga Plate is well defined by an east-west band of shallow earthquakes (after Sclater et al., 1972).

values for 5-m.y.-old oceanic crust (Sclater et al., 1971) and are lower than expected from the general observation that southwestern Pacific backarc basins have high heat flow relative to their topographic elevation (Sclater, 1972). Most measurements in the Lau Basin are significantly lower than values between 2.82 and 2.39 μcal/cm$^2$ for crust generated at mid-oceanic ridges of various spreading rates over the past 10 Ma (Sclater et al., 1971); however, several of the measurements for the Lau Basin are as high as 6.75 μcal/cm$^2$ (Sclater et al., 1972).

In addition to the petrologic problems concerning the similarities or differences between MORB, arc, and backarc basin magmas, it was recognized early on that there was a problem in explaining the tectonic evolution of backarc basins. Karig (1970) first proposed that the basins evolved by the splitting of a volcanic island-arc chain. The still-active volcanoes were displaced toward the trench, leaving behind an inactive remnant arc, and new backarc crust formed by mantle upwelling and partial melting. Hawkins et al. (1984) proposed a different view that the zone of "backarc" rifting was initiated in the forearc and that the outer (near-trench) arc volcanoes were new volcanic edifices established on the outer edges of the new backarc (or old forearc crust) after the Wadati-Benioff zone had changed its location and inclination and a new locus of mantle diapirism and melting was established. A consequence of this would be a time gap in arc volcanism that coincided closely with the beginning of the "backarc" basin opening. Both of these models could be tested by drilling in the Lau Basin–Tonga Arc region.

Understanding the tectonic and petrologic processes operative in the Tonga arc-trench system has application to other arc-trench systems and would help in framing a better model to explain the origin of backarc basins. Other problems of more specific application to the Tonga system include studies on the Tonga Ridge and on the upper slope of the Tonga Trench. The Tonga Ridge is capped by upper Pliocene to Pleistocene reefal limestones, some of which have been uplifted to form such islands as Tongatapu and Vavau. Drill sites on the forearc ridge were planned to investigate the uplift and subsidence history of the Tonga Platform and the age and nature of the crust under the carbonate rocks.

## Geological Setting: Backarc

The Lau Basin is bounded on the west by the islands and atoll reefs of the Lau Ridge (the remnant arc) and on the east by the volcanic islands, atoll reefs, and uplifted platform carbonates that comprise the Tonga Ridge. The western side of the Lau Basin is characterized by a number of small, partly sedimented basins separated by uplifted elongated blocks of basement with only a thin sediment cover. Sites 834 and 835 lie in sub-basins between 100 and 200 km east of the axis of the Lau Ridge, whereas Sites 836, 837, 838, and 839 lie in subbasins much closer to the modern backarc spreading system (Figs. 1 and 2). Even though we presumably reached igneous basement at five sites during Leg 135,

the nature of the crust that underlies the western Lau Basin remains poorly known. Several interpretations are possible. For example, the crust comprises (1) remnants of the forearc that originally lay to the east of the Lau Ridge; (2) either allochthonous or autochthonous blocks of Lau Ridge volcanic/plutonic material; (3) remnants of both arc and forearc crust; or (4) newly formed crust of backarc basin basalt. Whatever the origin of the western Lau Basin basement, the clastic sedimentary fill of the lesser basins must have a significant proportion of material derived from the Lau Ridge. As we are able to demonstrate from the results obtained during Leg 135, a significant contribution to the sediments probably came from intrabasin volcanic centers that developed throughout the western Lau Basin from mid-Miocene to mid-Pliocene times, before the initiation of true seafloor spreading at the site of the Eastern Lau Spreading Center (ELSC). The timing, geometry, and tectonic style of crustal extension on the Lau Ridge may be genetically related to geological processes that resulted in crustal extension in the western Lau Basin. Our initial results support this inference as the beginning of the Lau Basin opening and the earliest volcanic activity in the basin, overlapped in time with extension and volcanism on the Lau Ridge. Thus, an understanding of the geology of the Lau Ridge may be helpful in understanding the evolution of the western Lau Basin.

The Lau Ridge comprises emergent and coral-capped parts of a remnant volcanic arc, active until the late Miocene or early Pliocene (5–3.5 Ma), according to Gill (1976), Cole et al. (1985), and Woodhall (1985). The Lau Ridge is presumed to have been part of the former "Melanesian island arc," which included what are now the Fiji Platform, New Hebrides–Vanuatu Ridge, and the Tonga Ridge (Woodhall, 1985; Cole et al., 1985). The Lau and Tonga ridges were separated during the extensional development of the Lau Basin (e.g., Karig, 1970; Woodhall, 1985; Cunningham and Anscombe, 1985). The oldest known rocks exposed on the Lau Ridge are pre-middle Miocene lava flows and pyroclastic and volcaniclastic rocks of the Lau Group. These display a broad range in composition from basalt to rhyolite; basaltic andesite and andesite are the major rock types of the Lau Group. Both tholeiitic and calc-alkaline low- to high-K magma series are represented. Intrusive rocks, found on several islands, represent the same magma types as the volcanic rocks (Woodhall, 1985).

The chemistry and petrology of the Lau Group volcanic rocks indicate that the Lau Ridge displays the early and mature stages of volcanic arc evolution (Cole et al., 1985). There is no direct evidence for pre-middle Miocene volcanism on the Lau Ridge, but Oligocene and early Miocene volcanism and sedimentation has been postulated based on the occurrence of rocks with these ages elsewhere in the region. Cole (1960) and Colley et al. (1986) report late Eocene and early Oligocene volcanic rocks on Viti Levu, Fiji, while early and middle Miocene volcanic rocks have been reported from the Tonga Ridge (Cunningham and Anscombe, 1985). Middle and late Miocene volcanism on the Lau Ridge has been confirmed by radiometric age dates that range from 14 to 6 Ma (Cole et al., 1985). Volcanic activity continued into Pliocene time, as indicated by 4.5–2.5-Ma rocks of the Korobasaga Volcanic Group and <2.5-Ma rocks of the Mago Volcanic Group (Cole et al., 1985).

The spectrum of radiometric ages indicates that the volcanic activity was more or less continuous from Miocene through Pliocene time. Crustal extension on the Lau Ridge was contemporaneous with this volcanism (e.g., 4.5–2.5 Ma basalts of the Korobasaga Group) during the time that Whelan et al. (1985) relate to the "early rifting stage" in the evolution of the Lau Ridge. The timing of this rifting and the associated volcanism on the Lau Ridge, which was dominated by tholeiitic basalt, broadly overlaps in time with the beginning of the crustal extension of the western Lau Basin. Our drilling results indicate coeval extension and volcanism for at least 3–4 m.y., in the Lau Basin and on the Lau Ridge.

The Central Lau Basin is dominated by two major backarc spreading segments: the Central Lau Spreading Center (CLSC) and the Eastern Lau Spreading Center (ELSC) (Parson et al., 1990). The CLSC is a major morphologic/tectonic feature of the Lau Basin and is presently the site of magma leakage and backarc spreading at the latitude of Sites 834 and 835. The CLSC is propagating southward into the basin at the expense of the ELSC, approximately along the 176°30′W longitudinal line. The regional fabric is defined by the predominantly inward-facing fault pattern, which in this area varies from 350° to 10° in azimuth. This fault pattern can be seen to be locally controlling rifting as well as being cut by the propagator. The age of the CLSC is equivocal because the magnetic anomaly pattern is unclear, but it appears to have initiated from the southeastern termination of the Peggy Ridge and to have advanced southward for at least 1 Ma and possibly as much as 2 Ma. The propagator tip is located at around 19°16′S, 176°32′W, some 120 km from Site 835. Rocks from the CLSC include depleted N-MORB type tholeiitic basalts and fractionated basalts, "oceanic andesites and dacites," and Fe-Ti basalts (Hawkins, 1974, 1976, 1988, 1989; Hawkins and Melchior, 1985; Hawkins et al., 1990; Ernewein et al., in press).

The ELSC is the closest major morphotectonic feature lying to the east of the central basin drill sites (Parson et al., 1990). The ELSC can be traced for over 180 km from near 19°20′S at longitude 175°55′W to about 21°S where it merges with the Valu Fa Ridge. The ELSC has a well-defined central rift zone 5–10 km wide, characterized on high-resolution seismic profiles and echosounder profiles by a strong acoustic return interpreted as bare rock, or thinly sedimented extrusive seafloor. GLORIA sidescan sonar data images the axial zone as a wider, strongly backscattering region up to 20 km wide, cut by axial-parallel fault scarps (Parson et al., this volume). SeaBeam data show that the axial zone separates major rift walls, which rise as much as 500 m (to depths of about 2200 m) above the axial valley floor. Inward-facing fault scarps form a series of small terraces that step down to the axial floor; in some places the innermost part of the axial zone is a 1.5–3-km-wide notch about 50–100 m deep. The axial floor of the ELSC is about 2600 m near 19°40′S and deepens to over 2700 m near 20°20′S. It is thinly sedimented and fresh basalt glasses have been dredged along the axis between 19°20′S and 21°00′S (Hawkins et al., 1989; Ernewein et al., in press). Magnetic anomaly data together with the fresh glass and aphyric rock dredged from the axial zone support the interpretation that it is a young active zone of rifting and magmatism.

To the northwest, the northwest-striking Peggy Ridge truncates the western sector of the central Lau Basin (Fig. 1). The ridge rises to depths <1000 m below sea level and then extends over 300 km northwest from the northern limit of the CLSC axis. It presently marks a line of right-lateral motion associated with the spreading on the CLSC coupled with a component of east-west backarc extension. It was originally proposed that the Peggy Ridge was a spreading center (Chase, 1971), but Sclater et al. (1972) demonstrated that this speculation could not be supported by the magnetic data and proposed instead that it marked the location of a major subplate boundary that was possibly acting as a transform fault. This interpretation is supported by the first-motion earthquake data of Eguchi (1984) and more recently by Hamburger and Isaacs (1988). Rocks from the Peggy Ridge are tholeiitic basalt and are generally similar to the depleted N-MORB type basalts that characterize the CLSC (Hawkins, 1974, 1976; Hawkins and Melchior, 1985).

On a regional scale, the submarine topography of the western part of the Lau Basin is characterized by a series of upstanding crustal blocks that have a variety of dimensions (Parson et al., this

volume). These blocks are as long as 80 km and range from 35 to 4 km wide; they are aligned on north to northeast trends, between the strike of the ELSC and that of the Lau Ridge. The high-standing blocks separate troughs and linear basins that have dimensions comparable to the shoal areas. To the east of approximately 176°45′W, the seafloor morphology is dominated by a finer topographic grain, defined by linear scarps and ridges closely spaced at intervals from 1 to 5 km, and is locally continuous over lengths of up to 25 km. This fabric continues eastward and merges with the neotectonic faulting associated with the ELSC. This contrast in seafloor fabric can be traced along a line running approximately north-south that approaches the southern end of the Central Lau Spreading Center to the north and extends southward into the unsurveyed south-central portion of the Lau Basin. We confirm the suggestions of Parson et al. (this volume) that a major break in style of crustal formation occurs across this zone of contrasting seafloor fabric.

## Tectonic Setting

Structural interpretations of the Lau Basin have been based on the integration of seismic reflection data with data from SeaBeam swath bathymetric mapping and long-range sidescan sonar (GLORIA) records. The basement ridges dominating the western Lau Basin bathymetry separate linear, sediment-filled basins. Many of the basement blocks are morphologically asymmetric in profile, suggesting a small amount of rotation on the fault zones. The sense of asymmetry is not consistent, and thus interpretations of the style of rifting in the western basin are speculative.

Single-channel seismic reflection data acquired during the *JOIDES Resolution* survey are shown throughout the site chapters in the background and objectives sections, together with interpretive stratigraphic columns summarizing the lithologic units. Vertical exaggeration is about 15:1. The uppermost part of the section is generally overprinted by the decaying water-gun bubble pulse; however, below about 0.06 s two-way traveltime (TWT), the seismic stratigraphy is essentially unmodified.

Seismic units A, B, and C recognized in these records correspond to similar acoustic units identified elsewhere in the Lau Basin. Seismic unit A, the youngest unit, is a planar, weakly laminated unit, uniformly distributed throughout the basin and found on both elevated topography and in the deepest basins. Seismic unit B is defined by a series of regular and well-stratified laminations occupying the lower sections of the deepest sedimentary basins. Finally, seismic unit C is composed of a complex pattern of low-frequency, discontinuous reflectors that defines the lower surface of seismic units A and B throughout the basin. We refer to seismic unit C as the acoustic basement.

## Magnetic Data

Magnetic anomaly data for the Lau Basin have proved to be difficult to interpret, and attempts to model the crustal structural fabric and ages of magnetic lineations in terms of plate tectonic theory have met with only limited success. Several workers have developed models that presented widely varying interpretations for the age of the earliest backarc crust in the Lau Basin. These uncertainties range from an original estimate of 5–10 Ma (Sclater et al., 1972) to 2.5–3 Ma (Malahoff et al., 1982). One of the primary reasons for comparing drilling at the western and central backarc sites was to attempt to resolve uncertainties about the age of the igneous basement and, thus, by inference, to determine the age of the beginning of the basin opening.

Lawver et al. (1976) presented the first interpretation of the crustal accretion pattern in the Lau Basin based on magnetic anomaly data, and they demonstrated the discontinuous and nonparallel nature of the anomalies. Expanding on these data, Weissel (1977) proposed that there were north-south striking anomalies as old as 2′ (3 Ma; 2A of Harland et al., 1982) in the western Lau Basin between 17°00′S and 18°45′S. Furthermore, he suggested that the seafloor occupying the intervening basin between these anomalies and the eastern flank of the Lau Ridge was an earlier zone of magmatic accretion generated at some time between 3 and 6 Ma. These inferred ages are equivalent to the age of some of the Lau Ridge volcanic rocks (Gill, 1976). An extensive set of aeromagnetic data were used by Malahoff et al. (1982) to make a comprehensive interpretation of the Lau Basin and surrounding areas. They proposed that the oldest anomaly at the extreme western part of the basin (along longitude 177°00′W) was Anomaly 2′ (3 Ma). A more recent revision of the aeromagnetic data (Malahoff et al., in press) has extended the range of spreading anomalies to Anomaly 3′ in the far western part of the basin along the eastern foot of the Lau Ridge slope. The oldest magnetic anomaly in the western margin of the Lau Basin is identified as Anomaly 3′ (5.8 Ma; 3A of Harland et al., 1982). Site 834 lies on the older (i.e., western side) of this anomaly on crust postulated to be between 3 and 6 Ma old, according to the various interpretations of crustal age given here. If all of the crust of the Lau Basin formed by spreading from the present axial ridge systems, then a half spreading rate of 32 mm/yr can be estimated for the generation of the western part of the Lau Basin near Site 834. However, the results of Leg 135 drilling do not support this simple interpretation of the crustal fabric and its evolution.

## Geologic Setting: Arc/Forearc

The Tonga Ridge has existed in some form since at least Eocene time, when it was a component of an ancestral Melanesian proto-arc, comprising parts of the present Fiji, Lau, Tonga, and New Hebrides arcs. This ancestral arc probably came into existence after the initiation of a subduction zone at sometime during early Eocene time. The Melanesian arc was building during the time of the early history of the South Fiji Basin, when a proto-Tonga Trench represented the site of a west-dipping subduction zone. Magnetic anomalies 12–7 (dated as 32.5–26 Ma, earliest to late Oligocene) have been identified in the South Fiji Basin (Weissel, 1977; Davey, 1982; Malahoff et al., 1982), and are interpreted as having been derived from a ridge-ridge-ridge triple junction that migrated southwestward during the late Oligocene. Following the interpretations of the magnetic anomalies of Malahoff et al. (in press), it appears that there was no active spreading west of the Lau Basin since 29 Ma. During the late Miocene, approximately 10–12 Ma, the New Hebrides arc appears to have separated from the Lau-Tonga-Fiji segment following the initiation of subduction beneath the westerly facing New Hebrides Trench. The opening of the Lau backarc basin from the late Miocene onward and the initiation of the presently active Tofua arc to the west of the Tonga Ridge have further contributed to the uplift/subsidence history and regional tectonic development of the Tonga Ridge. Parts of the Tonga Ridge have been extant in some form throughout this history, and the rationale for drilling Sites 840 and 841 was that the history of subsidence and uplift thought to be associated with each of the regional tectonic events should be recorded in the stratigraphy.

The Tonga Ridge may be described in terms of three structural provinces: the southern, central and northern platforms. The southern platform extends from Tongatapu to the intersection with the Louisville Seamount Chain. The southern platform shoals to 200 m and has a surface incised with northwest-southeast distributary channels, probably structurally controlled, that subdivide the platform into several morphological blocks. The Tofua volcanic arc is submarine south of Tongatapu, except for the volcanic island of Ata. The central platform extends from Tongatapu northward to Vavau. Water depths are shallower than on the southern platform, and there are many islands and reefs.

The structural segmentation of the block is more pronounced here, with deep incisions of the seafloor by the northwest-transverse canyons. The northern platform extends from Vavau to the northernmost (and least well-charted) part of the Tonga Ridge, at around 15°S. Here the ridge topography is more subdued, with few subaerial expressions, except for the volcanic islands of the Tofua Arc, and little clear evidence exists for subdivision into component blocks.

The northern and central blocks have received the most attention in terms of surveying because of their greater potential for the accumulation of hydrocarbons, and consequently the southern block is less well understood. Surveys completed by the United States Geological Survey (USGS) during 1982 and 1984 (Scholl and Vallier, 1985) provided considerable background data for Leg 135 drilling. Furthermore, commercial wells drilled on the island of Tongatapu have provided some reconnaissance control. The data from these sites, unfortunately restricted to well logs and chippings, have been useful to tie in seismic stratigraphy in the Tongatapu block; but the correlation of these units across boundaries between adjacent blocks becomes increasingly difficult as the units pass to the south.

Extensive reviews of the seismic stratigraphy of the southern platform of the Tonga Ridge have been reported by Scholl et al. (1985), Herzer and Exon (1985), and Tappin et al. (1991). Comparable syntheses of the Tonga Ridge to the north of Tongatapu have been completed by Austin et al. (1989).

Multichannel seismic reflection data collected during the USGS Tripartite programs in 1982 and 1984 (Scholl and Vallier, 1985) and proprietary commercial seismic data have been used to establish a seismic stratigraphy for the central and southern Tonga Ridge. This stratigraphy has been presented by a number of authors, including Herzer and Exon (1985), Austin et al. (1989), and Tappin et al. (1991). The lack of published data on the northern platform precludes extrapolation of the seismostratigraphic control farther north than 18°30′N. The seismic stratigraphy for the rest of the platform has been subdivided into five principal units. In order of decreasing age, the boundary horizons delineating these units are denoted as V, C, B, and A (Herzer and Exon, 1985). The units have been described in terms of their lithologies by earlier workers primarily using dredge data from the exposed western flanks of the Tonga Ridge. Limited support for the correlations discussed below is provided by subaerial exposures (and commercial well data) on Tongatapu and 'Eua, respectively. Despite these data, precise stratigraphic controls on the unconformities that mark the unit boundaries have not been possible until Leg 135 drilling.

Data from five industry exploration wells drilled on Tongatapu (Maung et al., 1981; Scholl et al., 1985; Katz, 1986) have been used to constrain partially the interpretation of the geophysical data. Interpretations have been derived from analyses of rock chips from holes to a depth of 2000(?) m, from outcrop information at 'Eua, and from dredge samples from the western scarps of the Tonga platform. On the basis of these data, tentative dates were ascribed to the seismic events recognized as angular unconformities in the Tonga platform multichannel data over the platform (Herzer and Exon, 1985).

The above regional seismostratigraphic events can be correlated throughout much of the Tonga Ridge. More localized smaller scale tectonism of the platform is evidenced in the faulting affecting the uppermost seismic units, seen on both single-channel and multichannel seismic reflection profiles. A wide range of structures are identified, including normal and reversed, synthetic and antithetic, and growth faults. GLORIA sidescan records also image a number of outcropping faults (L. Parson, unpubl. data), the configuration of which suggests a rectilinear conjugate pattern. The synthesis of detailed fault patterns will constrain recent deformation of the platform.

Horizon V marks the upper surface of acoustic basement, generally considered to be of middle to late Eocene age. These basal lithologies are suggested to comprise mainly volcanic arc components, equivalents of which crop out on 'Eua. Horizon C, a conformable horizon traced throughout the central and southern platform, overlies a predominantly volcaniclastic/pelagic mixed arc sequence suggested to contain a limited amount of shallow-shelf carbonate facies. The unconformity is thought to span at least the late Oligocene, but this date is largely derived from regional correlations supported by dredged material. In the early Oligocene, around the time of Anomaly 12/13 (35 Ma), the Lau–Tonga–Fiji–New Hebrides protoarc was rifted and the south Fiji Basin was spreading as a complex backarc basin, suggested to be dominated by a ridge-ridge-ridge triple junction for most of its history. If the provisional dating of Horizon C is correct, then it correlates directly with the timing of the tectonic decrease in the southern Tonga Ridge as backarc extension in the South Fiji Basin began to wane around 26 Ma (Davey, 1982; Malahoff et al., 1982). While this decline in deformation of the south and central Tonga Ridge took place, the effects of the extensional system continued in the northern platform (Tappin et al., 1991). A major biostratigraphic hiatus involving nondeposition also occurred at the end of the Oligocene, where several complete foraminifer zones are missing throughout the Pacific (G. Chaproniere, pers. comm., 1991). It is tentatively postulated that this corresponds to a proposed major drop in sea level during the upper Oligocene. Additional regional events may have influence on the tectonic history of the Tonga Ridge. At about the same time (10 Ma), there was a reversal of subduction direction along the New Hebrides arc-trench system, reconfiguring the plate geometry to approximate that of the present day. A shallow-water paleoenvironment for the Lau-Tonga ridges is supported by the absence of middle to late Miocene faunal zones (e.g., Zone N15 foraminifers; G. Chaproniere, pers. comm., 1991), presumably at a low sea-level stand.

Horizon B marks the early Miocene and overlies volcaniclastic materials characterized by discontinuous, lenticular seismic units that may be reefal bodies. The age of Horizon A has been suggested to be latest Miocene/earliest Pliocene (Scholl and Vallier, 1985), and the findings from Leg 135 appear to support this date. The identification of the horizon on lithologic grounds is less clear. Physical property and downhole log data are conclusive in the identification of velocity and density variations across the boundary. Each of Horizons A–C can be correlated to regional tectonic events affecting the Lau-Tonga region, with Horizon B dated as lower Miocene and Horizon C as lower or middle Oligocene (Austin et al., 1989). A period of uplift, corresponding to the time of Horizon A, is proposed as a consequence of the initiation of Lau Basin rifting, now well established from our drilling as dated between 5 and 6 Ma. After rupture and basin subsidence, the Tonga platform subsided in the west to form the paleosurface onto which the early Pliocene sediments could progressively onlap. Horizon A has been recognized widely throughout the Tonga Arc, but its occurrence has not been reported on the Lau Ridge.

The Tonga Ridge is a high-standing block of crust that trends north-northeast and comprises two concentric belts of fundamentally different rocks. The principal eastern belt (Tonga platform) is formed of uplifted carbonate rocks with interbedded volcaniclastic material. The island of 'Eua has exposures of uplifted pre-middle Eocene igneous basement that has been intruded by early Oligocene and early Miocene age dikes (Ewart and Bryan, 1972; Hawkins and Falvey, 1985). Deformation of the Tonga platform has resulted in a complex arrangement of normal faults

that give rise to a reticulated pattern with intersecting west-northwest and north-northeast trends (Herzer and Exon, 1985). Northerly trending structures flank downdropped blocks to the west. The subparallel, western linear component of the Tonga Ridge is formed of the active and inactive volcanoes, seamounts, and (volcanic) shoals of the Tofua Arc. These are largely basaltic or basaltic andesitic, but some shoals have erupted rhyolitic pumice in historic times (Melson et al., 1970).

Detailed summaries of the Tonga platform geology have been given by Herzer and Exon (1985), Exon et al. (1985), Cawood (1985), Cunningham and Anscombe (1985), and Packham (1985) and may be summarized as follows. A pre-late Eocene igneous basement is exposed on 'Eua. These igneous rocks, formed largely of arc tholeiitic series igneous rocks (Hoffmeister, 1932; Ewart and Bryan, 1972; Hawkins and Falvey, 1985) have been radiometrically dated as 46 Ma (Ewart et al., 1977) and 40–43 Ma (Duncan et al., 1985). The age dates have been determined on clasts rather than *in situ* rocks, but the large size of the clasts is used to infer that they are representative of the igneous basement. The igneous rocks are overlain by Eocene (to Oligocene?) platform limestone, a foraminiferal/algal wackestone-packstone with remains of echinoids, bryozoans, molluscs, and rare corals (Cunningham and Anscombe, 1985). The Oligocene age has been questioned and only late-middle Eocene and late Eocene limestones are considered to be present (G. Chaproniere, pers. comm., 1991). These limestones are, in turn, overlain by late middle Miocene to early Pliocene volcaniclastic turbidites. The contact is interpreted as a paraconformity or, locally, a fault (Tappin and Ballance, 1991). The volcaniclastic rocks are reworked deposits, and the nature of the original protolith is obscured because of the severe alteration (Cunningham and Anscombe, 1985). The mineral constituents given in descriptions suggest that the protolith was of broadly andesitic to dacitic composition, and the Lau Ridge as a source is likely but has not been proven. Pliocene to Quaternary coral and foraminiferal limestones overlie the volcaniclastic series without an apparent break on 'Eua, but they onlap Eocene and Oligocene limestones to the north and south. Reworked volcanic detritus is present at the base of the limestones (early Pliocene) but notably absent in the younger part of the limestone sequence.

An interpretation of the geologic history of the area, according to Herzer and Exon (1985), follows. The Tonga Ridge and Trench are considered to be parts of a convergent plate margin system that has been active at least since Eocene time. The Tonga Ridge has migrated eastward relative to the Lau Ridge, as a consequence of lithospheric extension and formation of the Lau (backarc) Basin. In the Miocene the southern Tonga platform accumulated a thick sequence of clastic rocks in a forearc basin lying to the east of a volcanic arc. The sedimentary filling thickened westward and accumulated to thicknesses on the order of 2000 m. Sedimentation was accompanied, or followed shortly, by the emplacement of hypabyssal intrusives that form dikes or sills in the volcaniclastic series of Tongatapu. These intrusive bodies were radiometrically dated at 21.3 ± 0.4 Ma (early Miocene) and 13.9 ± 1 Ma (middle Miocene) and have intruded late Eocene and older volcanic rocks. It is assumed that the intrusive rocks were feeders to the overlying Miocene volcanic rocks, but the authors (Cunningham and Anscombe, 1985) caution that the radiometric dates are minimum ages and may reflect alteration. The sedimentary and volcanic fill thinned to the east onto an outer ridge. In late Miocene, or early Pliocene time, regional uplift resulted in the development of a regional unconformity, accompanied by the reactivation of large normal faults that strike nearly at right angles to the trend of the arc. In late Pliocene or Quaternary time, continued normal faulting caused (1) further downthrow on preexisting conjugate faults cutting the platform and continued downdrop of blocks to the west as the Lau Basin opened and (2) accentuation of block boundaries of the Tonga Ridge along faults at right angles to the trend of the arc.

Herzer and Exon (1985) proposed that the Miocene volcanic arc was split off from the active arc and carried *westward* as the Lau Basin opened beginning in Pliocene time. This contrasts with the models proposed by Karig (1970) and Hawkins et al. (1984) that visualized the Lau Ridge (remnant arc) as remaining fixed while the Tonga arc-trench system retreated eastward. The end result remains the same despite the absolute direction of the trench and remnant arc displacement. Hawkins et al. (1984) and Herzer and Exon (1985) have proposed that the Tofua Arc was a young feature that has developed since the crustal extension and rifting that led to the development of the Lau Basin. Identification of the rhyolitic arc lithologies at the base of Hole 841B (as discussed below) supports this suggestion, in that the Tonga Ridge may represent the site of an ancestral arc that has been repeatedly rifted eastward from a series of partially successful or failed zones of attempted backarc rifting, namely, the Tasman Sea, the New Caledonia Basin, the Norfolk Basin, the South Fiji Basin, and, most recently, the Lau Basin.

## Tonga Trench

The Tonga Trench is a major tectonic feature in the southwestern Pacific basin. As such, it marks the zone of plate convergence that has been the most important control on the evolution of the Earth's crust in this area for at least the last 40 m.y. Oceanic crust presently being subducted into the trench is at least as old as the Late Cretaceous (Vallier et al., 1985). There is only meager evidence for the accretion of seafloor rocks on the inner wall of the Tonga Trench (Vallier et al., 1985), but there is good evidence for crustal erosion (Bloomer and Fisher, 1985; Lonsdale, 1986). Upper Cretaceous age pelagic sediment has been recovered from the bottom of the inner-trench slope near the intersection of the Louisville seamount chain (Vallier et al., 1985). Fisher and Engel (1969) described a collection of mafic and ultramafic rocks from five dredge collections made at depths of 700–9400 m. The mafic rocks appear to be from the incoming Pacific Plate, but they are actually parts of a horst on the oceanic plate and are not material accreted to the trench wall. The landward slope of the trench includes harzburgite on its lower levels and andesitic clasts on its upper levels. The composition of much of the forearc basement has been postulated to be part of an Eocene arc complex (Vallier et al., 1985; Bloomer and Fisher, 1985).

The exposure of these arc rocks within 40 km of the trench axis and the morphologic characteristics of the trench have been used to argue for subduction erosion along the Tonga Trench, perhaps accelerated by the subduction of the Louisville Seamount Chain (Lonsdale, 1986; Bloomer and Fisher, 1985). If this is the case, we expected the sedimentary section at Site 841 on the trench-slope break to show evidence of substantial subsidence since the Eocene.

## Lord Howe Rise and Norfolk Ridge

The Lord Howe Rise, located at approximately 163°E, and the Norfolk Ridge, at 168°E, are far removed from the Tonga arc-trench system. However, a brief review of their geologic history is useful as background material for Site 841 at Tonga Ridge. It has long been recognized that the area lying east of Australia and extending to the Tonga Trench has been the site of successive rifting and the development of volcanic arcs and backarc basins (e.g., Karig, 1970; Burns and Andrews, 1973; summary in Kroenke, 1984). Beginning in Late Cretaceous time, the eastern margin of Australia was rifted away and the rifted blocks were further segmented into the Lord Howe Rise and Norfolk Ridge (Burns and Andrews, 1973; Bentz, 1974). Shor et al. (1971) presented data showing that the Lord Howe Rise and Norfolk

Ridge were underlain by quasicontinental crust, but both ridges are capped in places with Miocene basaltic rocks (e.g., Lord Howe and Norfolk islands). The New Caledonia Basin, separating the Lord Howe Rise and Norfolk Ridge, was formed by seafloor spreading before late Paleocene time. The opening of the Tasman Basin and Coral Sea continued until early Eocene time, displacing the Lord Howe Rise to the east from Australia. Although locally overlain by basalt, the Lord Howe Rise is likely to be a continental fragment. DSDP Site 207, drilled on Lord Howe Rise, recovered rhyolitic lapilli tuffs, produced by explosive eruptions and vitrophyric rhyolite flows that are partly autobrecciated. Both rock types formed in a subaerial or shallow-water subaqueous setting. The rhyolitic units were dated by the K/Ar method and yielded an age of 93.7 ± 1.2 Ma. The rhyolite is overlain by Maestrichtian sandstone and silty claystone (van der Lingen, 1973).

A number of workers, as summarized in Kroenke (1984), have proposed that the Tonga and Lau ridges were derived by the break up of a common parental ridge first by the formation of the South Fiji Basin and then by the Lau Basin. We postulate that this parental ridge, in turn, may have been derived from the Norfolk Ridge arc. The details of the geometry and trajectories of the successively formed splinters of the ancient Lord Howe Rise-Norfolk Ridge land mass split off from the Australian continent are unclear.

## PRINCIPAL RESULTS

### Lithostratigraphy

#### *Introduction*

During Leg 135, six sites were drilled in the western Lau Basin (Sites 834–839), one site on the Tonga Ridge (Site 840), and one site on the Tonga forearc (Site 841). The sites drilled in the western Lau Basin were drilled in a series of small, elongate, north-trending, sedimentary sub-basins. Sites 834 and 835 were drilled in two separate sub-basins, 48 km apart, proximal to the Lau Ridge. Sites 836–839 were drilled about 220 km to the southeast of Sites 834 and 835, in three fault-bounded sub-basins on the western flank of the ELSC (Fig. 2). These four sites are <90 km apart. Sites 838 and 839 were drilled in the same sub-basin. The sites drilled during Leg 135, therefore, fall into three separate geotectonic and sedimentary provinces: the backarc (Sites 834–839), platform/arc (Site 840), and forearc (Site 841). The backarc sites can be further divided into those proximal to the Lau Ridge and distal to the ELSC (Sites 834 and 835) and those fairly distal to the Lau Ridge and proximal to the ELSC (Sites 836–839).

#### *Sites 834 and 835*

##### *Lithostratigraphy*

The sedimentary sequences recovered at Sites 834 and 835 consist predominantly of clayey nannofossil oozes, clayey nannofossil mixed sediments, and volcanic silts and sands. At Site 834, 115 m of pelagic and turbiditic sediments were cored that range from lower Pliocene to middle Pleistocene in age (Fig. 7). At Site 835, 156 m of pelagic, turbiditic, and debris flow deposits were recovered, ranging from late Pliocene to middle Pleistocene in age (Fig. 7). The two sites possess a similar lithostratigraphy, with pelagic clayey nannofossil ooze containing turbiditic foraminifer sands and ooze interbeds and pyroclastic fallout ash layers overlying a sequence of clayey nannofossil mixed sediments interbedded with turbiditic volcanic sands and silts that increase in thickness downsequence.

The upper part of the sediment column at both sites consists of a sequence of brown, iron oxy-hydroxide stained, pelagic clayey nannofossil ooze. Apart from a few thin pyroclastic fallout ash layers and isolated pumice clasts, the clayey nannofossil ooze contains very little volcaniclastic material. However, the clayey nannofossil ooze does contain occasional thin- to thick-bedded foraminifer sand and ooze interbeds, interpreted as turbidites, possibly derived from carbonate reefs built upon the eroded Lau Ridge. These are thinner and finer grained at Site 835 than at Site 834, suggesting a more distal deposition.

The sequence of clayey nannofossil ooze (termed Unit I at both sites) is much thicker at Site 835 (130 m thick) than at Site 834 (42 m thick). However, the base of the sequences are of approximately the same age at both sites (2.6–2.8 Ma). Unit I at Site 835 contains several medium to very thick beds of matrix-supported mud-clast conglomerate. These are interpreted as muddy debris-flow deposits. The total thickness of the mud-clast conglomerates is at least 20 m. Micropaleontological data have also identified an additional 12.4-m-thick resedimented deposit in the lower Pleistocene. This redeposited sediment contains a few thin beds of mud-clast conglomerate, but it mainly consists of structureless mud that closely resembles the background pelagic deposits. Assuming a constant rate of background pelagic deposition at the two sites, Unit I at Site 835 contains 88 m of additional redeposited sediments as compared with Site 834, which contains 12 m. The mud-clast conglomerates and the resedimented block in the lower Pleistocene account for 30–35 m of this in Site 835. The remaining extra thickness may be a result of the presence of thick structureless, redeposited clayey nannofossil muds that resemble the background pelagic ooze deposits. Indeed, the resedimented block in the lower Pleistocene appears to consist largely of such structureless mud.

Redeposited sediments comprise about 70% of the total sediment thickness deposited in Unit I at Site 835 compared with 10% for the same time-equivalent unit at Site 834. This probably reflects that Site 835 is more proximal to the Central Lau Spreading Center. Seismic activity associated with the spreading center may have caused more sediment instability on the slopes adjacent to the sub-basin containing Site 835.

There is much more volcanic glass in the sediments at Site 834 older than 2.6 Ma. The proportion of volcaniclastic material increases with age, becoming the dominant lithology before 3.5 Ma. Most of this material is present as vitric turbidites consisting predominantly of optically fresh, colorless vitric shards (up to 90 vol%). The interbedded oozes also show an increasing clay content downcore. A similar pattern of sedimentation before 2.6–2.8 Ma is seen at Site 835, although here the sedimentary sequence only dates back to the late Pliocene (about 3.4 Ma). As at Site 834, there is an abrupt increase in the amount of volcanic glass in the sediments deposited before 2.6–2.8 Ma, and much of the upper Pliocene section consists of clayey nannofossil mixed sediments interbedded with vitric turbidites, consisting predominantly of optically fresh, colorless vitric shards. As at Site 834, there is a gradual increase in the clay content of the interbedded oozes downcore. Toward the base of the sequence at Site 835 (153–154 mbsf), sparse, sand- to pebble-size, angular to subrounded fragments of black manganese oxide (identified as todorokite) are scattered within the clayey nannofossil ooze.

The lithostratigraphic units distinguished in the sedimentary sequence at Sites 834 and 835 are clearly correlatable and time-equivalent; however, in contrast to Unit I at Site 834, Unit I at Site 835 contains a very high proportion of redeposited material, accounting for its much greater thickness.

##### *Volcaniclastic Sedimentation*

The volcaniclastic sediments at Sites 834 and 835 are mainly epiclastic and predominantly mass-flow deposits that are interpreted as turbidites. Their deposition began at the end of the formation of backarc basin crust at each site, at about 4 Ma (Site

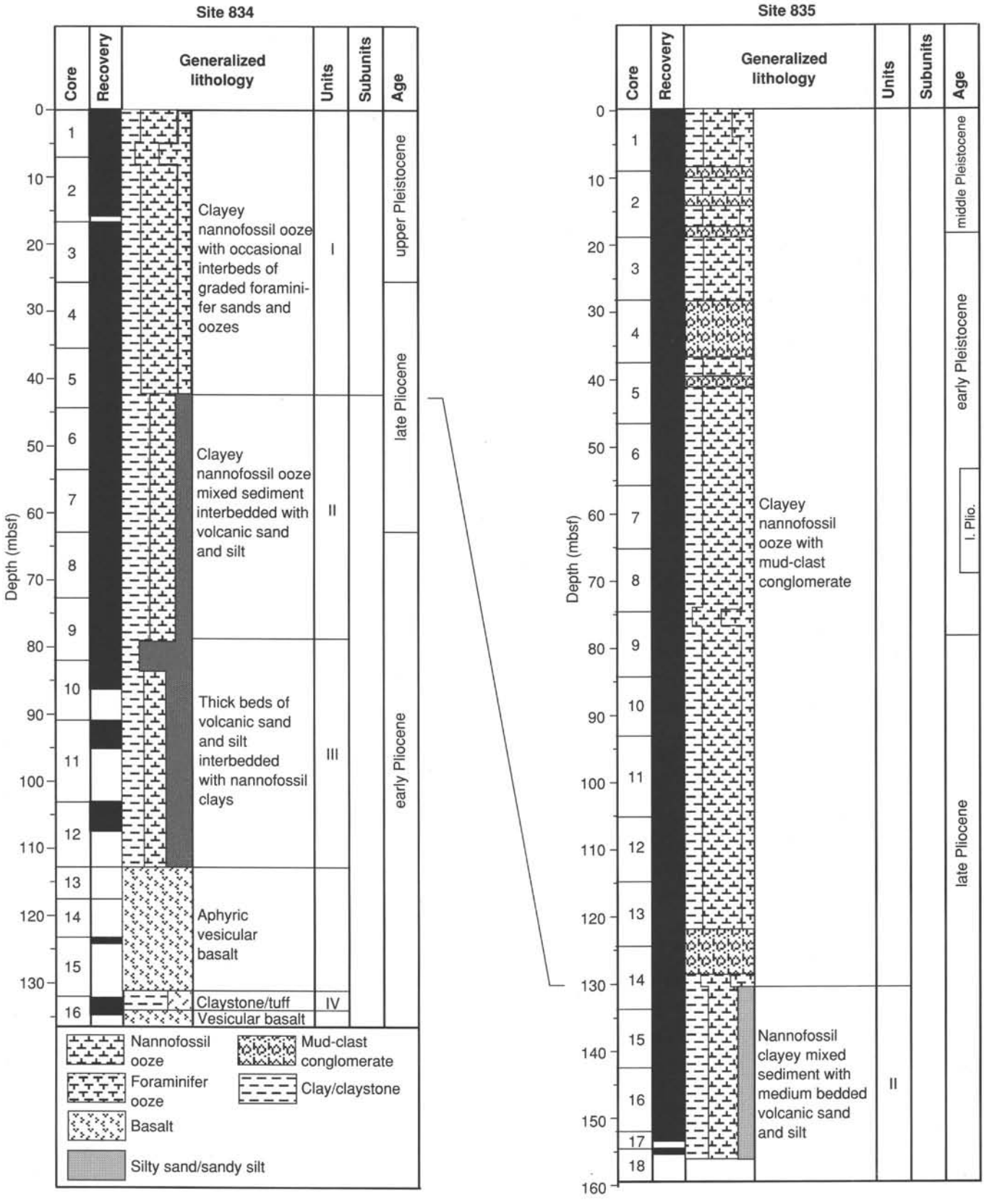


Figure 7. Lithologic summaries for Holes 834A and 835A, illustrating the main lithologic units and ages as well as a generalized graphic lithology.

834) and 3 Ma (Site 835). Vitric shards are silt- to sand-size and occur enriched at the bases of turbidite units, where they make up 80–90 vol% of the deposits. They are mainly colorless, clear, and optically fresh angular, bubble-wall and bubble-junction shards. The larger grain-size fraction present in individual samples is normally dominated by fibrous pumice shards and pumice shards with very elongate, tubular vesicles. Characteristic to all these turbidites with bases enriched in vitric shards is the scarcity of igneous minerals. Plagioclase, pyroxene, and opaques occur only in trace amounts.

Volcanic glasses at both sites are predominantly evolved andesitic to rhyodacitic compositions. Less silicic, basaltic andesitic to andesitic shards contribute minor amounts to most of the turbidites (Fig. 8). Overall, samples studied from Site 834 are distinctly more silicic with abundant rhyodacitic glass, whereas those from Site 835 have a larger proportion of andesitic and dacitic shards.

About 28 individual depositional events were distinguished at Site 834 and 20 at Site 835. This is consistent with the greater distance of Site 835 from the most likely source area, the Lau Ridge, when compared with Site 834, and also with the different crustal ages at the two locations. The thickness of vitric-enriched turbidites or parts of turbidites at Site 834 extends to 1.85 m, but usually they are 20–100 cm thick. However, Site 835 may receive material from more proximal sources because the vitric-rich turbidites at Site 835 do not exceed 37 cm in thickness, which is distinctly thinner than those at Site 834. Nevertheless, maximum grain sizes at the base of the turbidites are markedly larger at Site 835 than at Site 834, which may indicate that these sites were parts of different sediment distribution systems with different source areas and that individual units may not be directly correlatable. This is consistent with the differences in chemical composition of the shards; this needs to be confirmed by more detailed study.

A distinct epiclastic unit at 69.56 mbsf at Site 834 is about 1.35 m thick and is made up of alternating medium gray to black layers. Its age is about 3.3 Ma. Overall, the unit fines upward with a maximum grain size of about 1 mm at the base, greater than that of other volcaniclastics at this site. The deposit is characterized by basaltic andesitic, scoriaceous shards with up to about 60 vol% vesicles, and by the presence of neritic foraminifers. The volcanic component in these epiclastic deposits is interpreted as originating primarily from the eruptions of a shallow seamount.

Well-preserved, distal primary fallout tephras (3.2–2.4 m.y. old) are mainly restricted to the interval from 42.85 to 64.66 mbsf at Site 834, where they form weakly graded beds 3–11 cm thick. They are characterized by predominantly colorless vitric shards (10–600 μm in diameter) and a complex phenocryst assemblage that includes plagioclase, clinopyroxene, orthopyroxene, biotite, amphibole, and opaques, occurring in varying proportions and not always all present.

At Site 835, a proximal to medial primary fallout tephra consisting of colorless shards of rhyodacitic composition with a very minor population of brownish andesitic shards as recovered from 141.39 mbsf, which corresponds to an age of about 2.8 Ma. This tephra layer is ungraded and 23 cm thick; it is characterized by being extremely well sorted and by the presence of very delicate glass shards of extreme length-to-width aspect ratios (up to 1:25).

### *Sites 836–839*

#### *Lithostratigraphy*

These four sites, about 220 km to the southeast of Sites 834 and 835, are clustered in an area of about 100 × 50 km directly to the west of the ELSC. Basement ages range from approximately 0.6 Ma (Site 836) to about 2.1 Ma (Site 837).

Sites 836–839 were drilled in three fault-bounded sub-basins on the western flank of the ELSC. The four sites are <90 km apart; in addition Sites 838 and 839 were drilled in the same sub-basin, although separated by a low-relief flexure. All of the sites display a very similar sequence of brown, iron oxy-hydroxide stained, pelagic clayey nannofossil oozes containing rare volcaniclastic horizons overlying thick sequences of volcaniclastic silts, sands, and pumiceous gravels, with clayey nannofossil ooze and mixed sediment interbeds (Fig. 9). This general sequence of a thick sequence of pelagic clayey nannofossil ooze containing sparse allochthonous interbeds overlying another very thick sequence dominated by redeposited volcaniclastics is very similar to the ones seen at Sites 834 and 835, except that the volcaniclastic units at Sites 836–839 are very much thicker and coarser grained than at Sites 834 and 835.

Site 836 was drilled on middle Pliocene crust in a small basin, 48 km east of the propagating rift (CLSC) in the central Lau Basin. Only 20 m of pelagic and volcaniclastic sediments were cored until basaltic basement was reached. These sediments range from the middle to late Pleistocene in age (Fig. 9). The general sedimentation pattern follows that for all the other backarc sites, with 12 m of clayey nannofossil ooze containing thin- to medium-bedded volcaniclastic interbeds, overlying a sequence of clayey nannofossil mixed sediments, volcanic sand, and hyaloclastites.

Site 837 was drilled in a narrow, north-trending basin, 30 km southwest of Site 836. The sedimentary sequence recovered at Site 837 consists of 82 m of clayey nannofossil ooze and vitric volcaniclastics ranging from middle Pleistocene to late Pliocene in age (Fig. 9). Like all the other backarc sites, the uppermost part of the sequence consists of brown, iron oxy-hydroxide stained, pelagic clayey nannofossil oozes containing rare, thin, calcareous and volcaniclastic allochthonous interbeds (Unit I). This overlies a 68-m-thick sequence of thick volcaniclastic sands and silts interbedded with clayey nannofossil ooze (Unit II). This sequence consists of beds (up to 17 m thick) of upward-fining vitric sands and silts. These beds are interpreted as turbidites on the basis of their sedimentary structures and normal grading. Many of the units appear to have been deposited in rapid succession as there is often very little pelagic sediment between the turbidite beds. Within the turbidite sequence, five major upward-fining cycles are identified that form the basis for the subunit division (Subunits IIA–IIE; Fig. 9). This volcaniclastic-dominated sequence directly overlies basaltic basement, and deposition of this lithofacies ceased around 0.7 Ma.

Sites 838 and 839 were deposited within a sub-basin on the western flank of the ELSC, 60 km south of Site 837. However, they are separated by a flexure that forms a low ridge (400–600 m relief), which seismic data suggests may be associated with an angular unconformity that occurs near to the boundary of lithologic Units II and III. Both sites display a very similar sequence with brown, iron oxy-hydroxide stained, pelagic clayey nannofossil ooze overlying a very thick volcaniclastic-dominated sequence that directly overlies basalt.

The sedimentary sequence recovered at Site 838 consists of 103 m of clayey nannofossil oozes and volcaniclastic sediments ranging in age from the middle Pleistocene to the upper Pliocene. However, the sedimentary sequence is known to extend to at least 260 mbsf, although recovery below 98 mbsf was very poor. Sediments that were recovered from below 98 mbsf suggest that volcaniclastic sediments may dominate the sequence at least to the base of the cored section (260 mbsf). Like the other backarc sites, the uppermost part of the sequence consists of pelagic clayey nannofossil ooze containing rare thin- to thick-bedded volcaniclastic interbeds (0–23 mbsf). This overlies a thick sequence (>80 m) dominated by very thick (up to 20 m thick) massive vitric sands and silts and pumiceous gravels. Redeposited

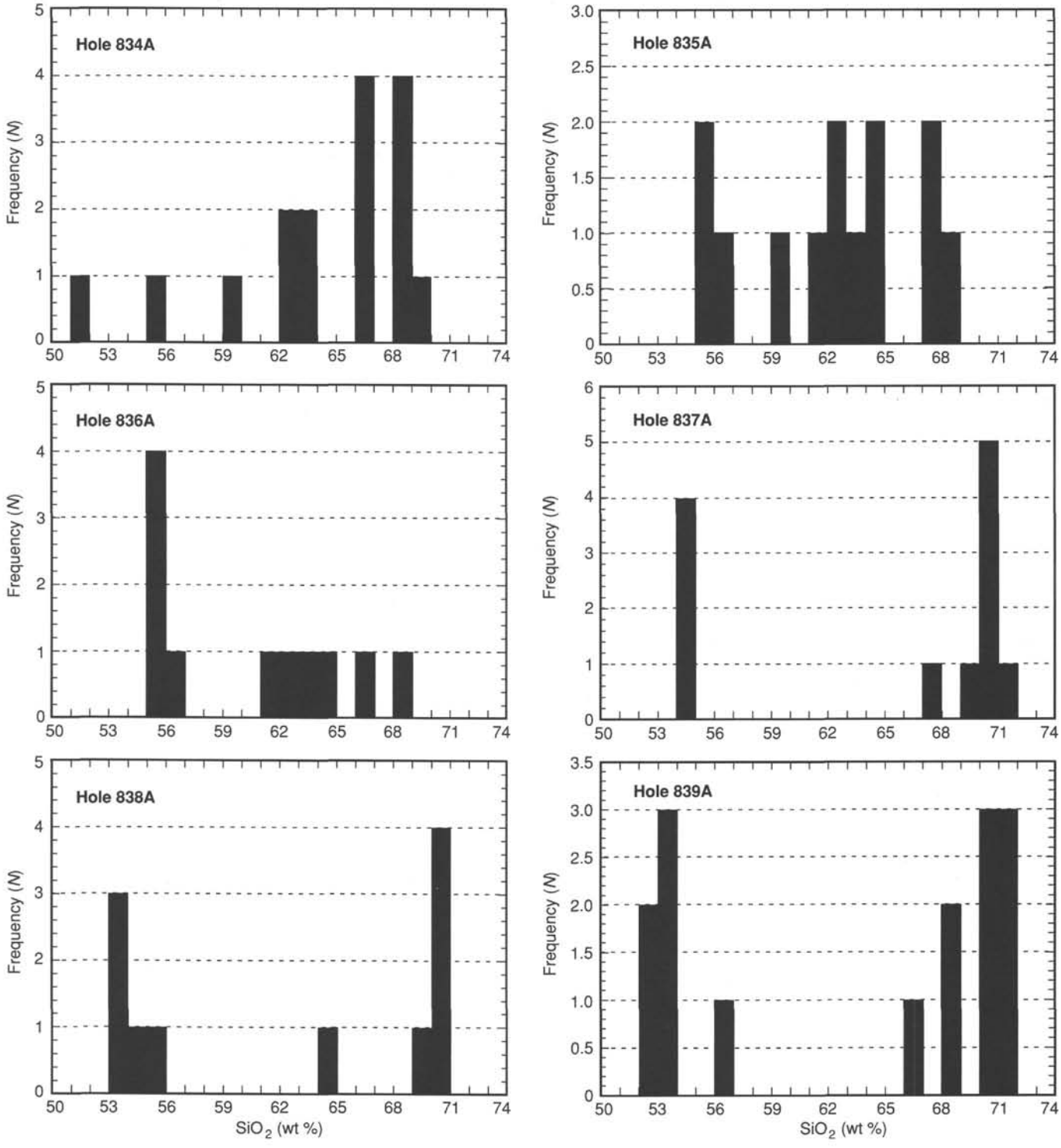


Figure 8. Histogram illustrating silica variation in volcanic glasses recovered from Lau Basin backarc sites (Sites 834–839). Note that the histogram is not weighted for the modal composition of the samples studied.

volcaniclastic silts, sands, and gravels comprise 63% of the upper 100 m of the sediment column. These beds typically show normal grading but are otherwise fairly structureless, except for occasional short planar-laminated intervals. Three very thick pumiceous gravels (up to 20 m thick) were recovered between 45 and 98 mbsf. In this interval, poorly sorted, matrix-supported, disorganized gravels or sandy gravels make up 65% of the sediment sequence. These are composed of angular to rounded granule- to pebble-size clasts of altered and fresh pumice, mafic volcanic rock, and reddish brown indurated mud clasts, set in a matrix of sand-size volcanic glass. Some gravel intervals show a crude overall normal grading, although most of the beds are generally structureless. Deposition of the volcaniclastic-dominated lithofacies (Unit II) ceased around 1.0–1.1 Ma.

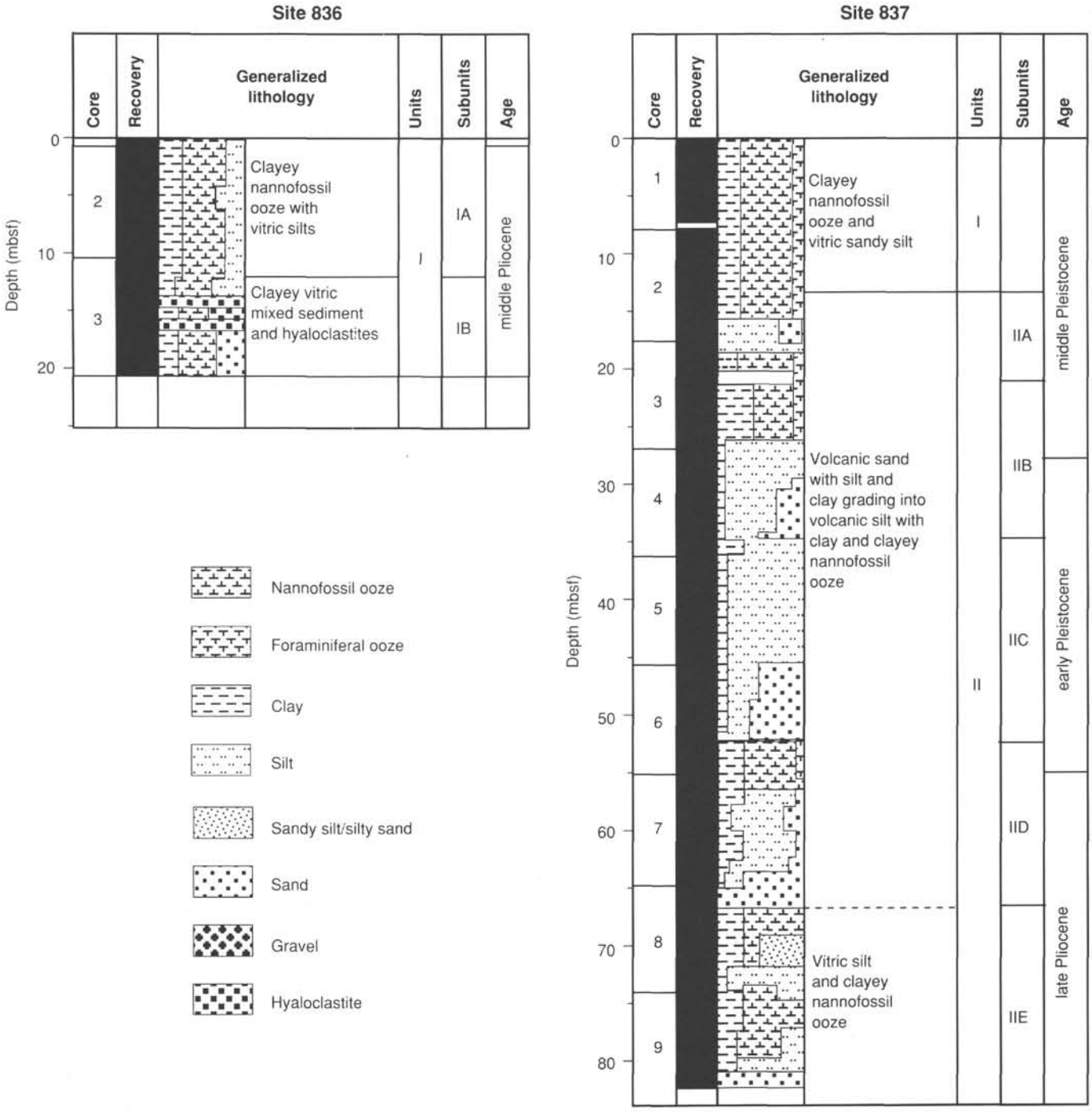


Figure 9. Lithologic summaries for Holes 836A through 839A, illustrating the main lithologic units and ages as well as a generalized graphic lithology.

Site 839 was drilled 20 km to the northeast of Site 838. It consists of a very similar sediment sequence to Site 838, except that the pumiceous gravels are much rarer (Fig. 9). The sedimentary sequence at Site 839 consists of 215 m of clayey nannofossil ooze, turbiditic sands and silts, and rare pyroclastic fallout ashes, ranging in age from the middle Pleistocene to the upper Pliocene. At Site 839, a lesser thickness of brown, iron oxy-hydroxide stained, pelagic clayey nannofossil ooze (18 m) (Unit I) overlies the main volcaniclastic sequence (Units II/III) than at Site 838. However, preliminary data suggest that deposition of the volcaniclastic dominated sequence (Unit II) ceased around 0.7–1.1 Ma. The volcaniclastic lithofacies (Unit II) at Site 839 is generally finer grained than at Site 838. The very thick pumiceous gravels, characteristic of the volcaniclastic sequence at Site 838, are generally absent from the equivalent sequence at Site 839. Both sites are proximal to scarps bounding the basin, although the gradient of the slope adjacent to Site 838 is steeper than that adjacent to Site 839. Greater instability on this steeper slope may account for the coarser epiclastic lithofacies seen at Site 838. Alternatively, if the volcaniclastic sands, silts, and gravels are laterally extensive

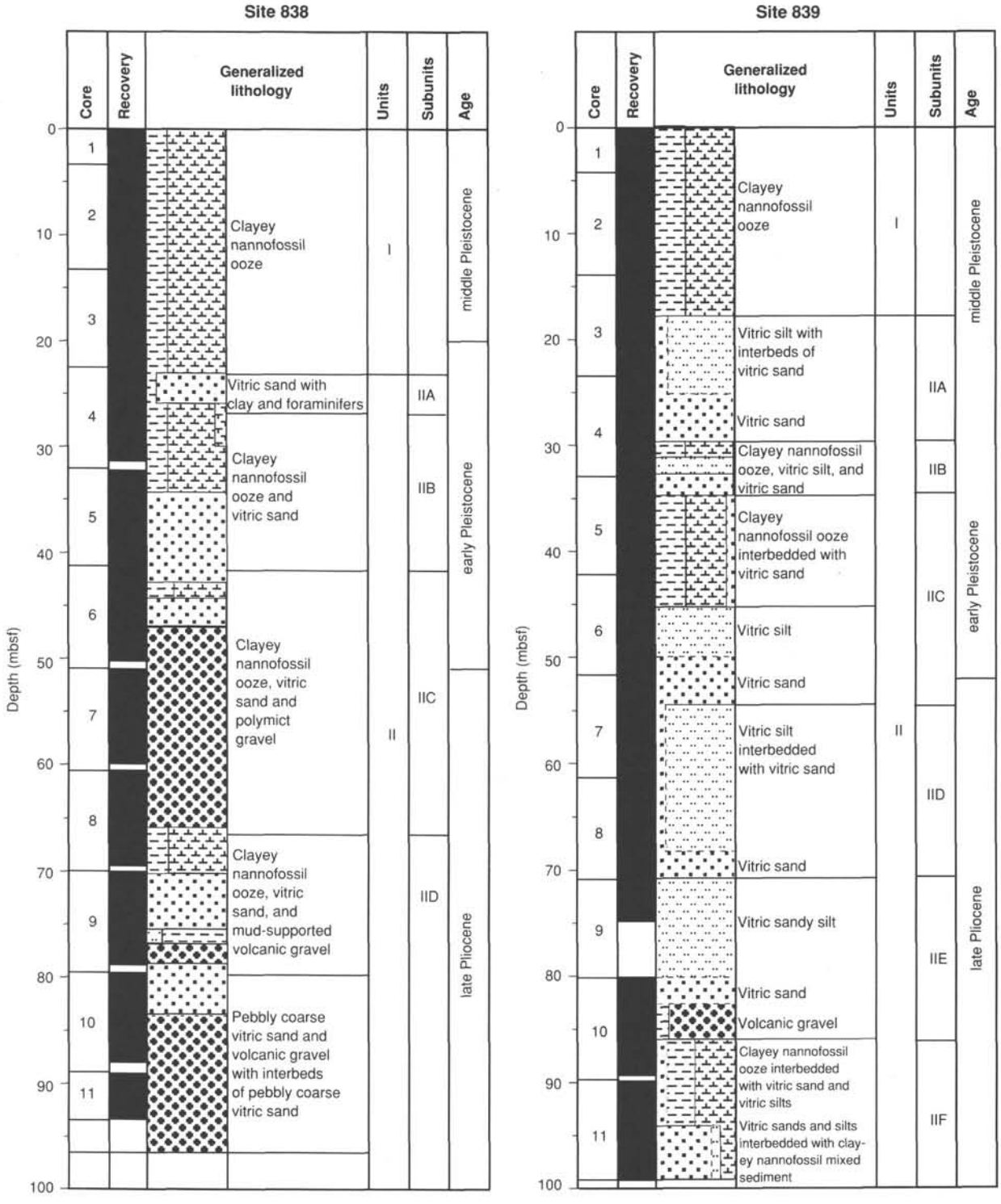


Figure 9 (continued).

deposits, those at Site 838 may represent a more proximal facies. Only one 3-m-thick pumiceous gravel was recovered at Site 839 (Subunit IIE; Fig. 9). This poorly sorted, disorganized deposit consists of angular to rounded granules and pebble-size clasts of pumice mixed with very coarse black hyaloclastite (which comprises 10 vol% of the deposit). Redeposited volcaniclastic silts, sands, and gravels comprise 65% of the upper 100 m of the sediment column at Site 839, the same proportion as at Site 838.

The volcaniclastic sediments present at Sites 838 and 839 consist of three different types of deposits: (1) very thick, massive, silts, sands, and gravels; (2) thin turbidites with glass-rich bases (typically up to 30 cm in thickness); and (3) rare thin primary fallout tephra layers. The massive volcanic silts, sands, and gravels occur as typically graded but otherwise structureless beds that are often several m thick. They are absent from Unit I but very common in Unit II and probably in Unit III (poor recovery) at both sites. Volumetrically, they are the most important type of volcaniclastic unit. The gravels are predominantly pumiceous and matrix supported, and they often grade upward into vitric sands that may themselves grade into vitric silts. The

gravels are typically poorly sorted and show no organized internal structure. These may be cohesive debris-flow deposits. The thick vitric sands and silts are typically structureless and therefore fall into the massive sandstone facies rather than into classical turbidites in the scheme introduced by Walker (1978). These beds usually consist of Bouma Ta divisions up to several meters thick. These may have been deposited from sandy turbidity currents developing into fluidized sand flows before being deposited.

All the pelagic clayey nannofossil oozes recovered at the backarc sites (Sites 834–839) are stained a distinctive reddish brown by hydrothermally derived, iron oxy-hydroxides, suggesting that hydrothermal activity has been ongoing throughout the history of the Lau Basin.

*Volcaniclastic Sedimentation*

*Fallout Tephras.* Primary fallout tephras are only rarely preserved at the four sites (3–9 occurrences at each site), and they range in thickness from about 1 to 9 cm. They mainly occur in the uppermost parts of the sequences. Their estimated ages range from 70 ka to 1.2 Ma.

*Epiclastic Deposits.* These deposits, rich in volcaniclastic material, consist predominantly of two types at Sites 837, 838, and 839: (1) vitric turbidites and (2) vitric mass-flows of pumiceous gravel. These sediments account for up to 65% of the total sediment cored.

Vitric turbidites are normally graded overall with few internal structures, apart from some planar lamination and rare water-escape structures. They are composed of up to 90 vol% silt- and sand-size vitric shards with a composition clearly dominated by highly evolved rhyodacites containing 70–71 wt% $SiO_2$. A second population of medium brown to brownish green shards is much less common and lies in the compositional range of basaltic andesites to andesite (52–57 wt% $SiO_2$). Vitric turbidites are up to 17 m thick at Site 837 and up to 5.2 m thick at Site 838. At Site 839 vitric turbidites exceed 10 m in thickness.

One 4.5-m-thick vitric turbidite in Hole 838A (at 75.45 mbsf) is dominated by shards of basaltic andesitic composition. Geochemically, the glasses resemble basaltic andesites from the basement of Site 836. Their distinctly lower $TiO_2$, Zr, and Y concentrations indicate a mantle source, different and more depleted than for N-MORB and many of the Lau Basin spreading-center magmas.

Volcaniclastic beds/sediments rich in lapilli-size pumiceous detritus dominate the epiclastic deposits at Site 838. Three of these major mass-flow units, 7.6–18 m in thickness and with maximum grain sizes of pumice clasts of about 7 cm at the bases, constitute up to about 30% of the total thickness of the cores recovered at Hole 838B. At Site 839 only one mass-flow unit, 21.3 m thick, was found at 86.2 mbsf. The basal 3 m contains large pumice clasts up to 3 cm in diameter. At Site 837, lapilli-size, well-rounded pumice clasts up to 1.2 cm in diameter are restricted to a single well-sorted unit, 2 m thick, recovered from 74.52 mbsf.

Three X-ray fluorescence (XRF) analyses were made of pumice clasts from Sites 837, 838, and 839. Each analysis represents a bulk analysis of several pumice clasts, and they demonstrate that the pumice clasts are derived from highly evolved, rhyodacitic to rhyolitic magmas with 71–77 wt% $SiO_2$, agreeing with $SiO_2$ estimates made by refractive index measurements of glasses from the same intervals. Pumice samples from Holes 837A and 838A are very similar in major and trace elements with 2.2 and 3.0 wt% CaO, 2.2 and 3.1 wt% $FeO_T$, 4.1 and 4.3 wt% $Na_2O$, 1.7 and 1.5 wt% $K_2O$, 164 and 145 ppm Zr, 62 and 49 ppm Y, 36 and 33 ppm Ce, and 19 and 29 ppm V, respectively. The rhyodacitic pumice from Hole 839A possesses a higher $FeO_T$ (4.32 wt%) and V (71 ppm), which may reflect a smaller proportion of Fe-Ti oxides in the fractionating assemblage. The HFSE and REE concentrations of 85 ppm Zr, 30 ppm Y, and 19 ppm Ce are very low for a highly evolved magma and could suggest a different, strongly depleted mantle source for the magmas parental to this sample.

The grain-size variations and the thicknesses of the pumiceous mass flows and vitric gravels at Sites 837, 838, and 839 display no systematic spatial variation and preclude any correlation of individual units as well as determination of a common origin. This is most likely directly related to the structural division of the western Lau Basin into elongate, north-extending sub-basins that range from about 1 to 15 km in width and about 10 to 85 km in length. Furthermore, the chemical data indicate distinct variations that are not compatible with a single magma source. The bulk of the highly evolved volcaniclastic detritus at Sites 837, 838, and 839 was probably derived from siliceous volcanic centers in as-yet undetermined locations.

*Hyaloclastites.* Hyaloclastites, the dominant type of volcaniclastic sediment at Site 836, make up about 50% of the lower half of the sedimentary section. Individual hyaloclastite layers are up to 1 m in thickness. They are predominantly made up of medium brown glass shards with blocky, angular morphologies and medium to low vesicularity. Grain sizes of up to 3 cm in diameter (averaging around 700 μm) indicate relative proximity to the source. These hyaloclastites are composed mainly of basaltic andesites to andesite with 55–57 wt% $SiO_2$; there is good agreement between the refractive index and XRF data.

Hyaloclastites are interpreted to originate from the spalling of glassy rinds of active pillow tube and/or sheet lava flows in the vicinity (1–10 km?) of the site. They may be related to spreading, as they are only slightly younger than the underlying basement or they could be from isolated volcanic centers. Evolved basement lavas are probably rare in the Lau Basin (e.g., Hawkins, 1976), but lavas with major and trace element characteristics very similar to the hyaloclastites of Site 836 have been recovered from the top of the basement at neighboring Site 837.

In the other Lau Basin sites, hyaloclastites are much rarer and are only found in the lowermost cores and as intralava sediments, consistent with a direct genetic relationship to the basement volcanism. In the thick pumiceous mass-flow deposits of Hole 838A, angular black hyaloclastites occur in varying amounts, with increasing abundance and grain size in the basal parts, especially of the lowermost two mass flows.

*Alteration.* Vitric shards and igneous minerals in all the Lau Basin sites are typically very fresh. However, slight birefringence of shards, indicative of hydration and early stages of hydration, may occur throughout the cores. Enhanced alteration was encountered at Hole 838 below 98.7 mbsf, where all the volcanic glasses are replaced by brownish yellow smectite, and pore spaces are completely filled by fibrous zeolites (probably natrolite-thompsonite) and minor carbonate.

### *Site 840*

*Lithostratigraphy*

Site 840 was drilled on the shallow carbonate platform of the Tonga Ridge (Fig. 2). The sedimentary sequence consists of at least 600 m of clayey nannofossil ooze, vitric siltstones and sandstones, pumiceous gravels, volcaniclastic breccias and conglomerates, and clayey nannofossil chalks. The sequence ranges in age from the late Pliocene to the Miocene, and is divided into three lithologic units based on texture, composition, sedimentary structures, and degree of lithification. The uppermost part of the sequence consists of white or grey, mottled, clayey nannofossil oozes interbedded with normally graded, vitric silts and sands, which become increasingly common downhole (Unit I). The vitric sands and silts usually have sharp, scoured bases and are interpreted from their grading and sedimentary structures as turbidites.

Small amounts of pumiceous gravel were recovered between 47 and 69 mbsf. The clayey nannofossil oozes and interbedded sands, silts, and gravels of Unit I overlie a sequence of heavily bioturbated, nannofossil chalks and calcareous mudstones, which in turn overlie a thick sequence of redeposited, normally graded, vitric siltstones, vitric sandstones, and fairly monomict pumiceous gravels (Unit II). Such volcaniclastic sediments are the most common lithologies recovered between 124 and 260 mbsf. This sequence was deposited between 5.2 and 5.4 Ma; therefore, sedimentation rates at this time were very high. These beds overlie a 337-m-thick sequence of thin- to thick-bedded volcaniclastic turbidites interbedded with heavily bioturbated, nannofossil chalks and calcareous claystones, interpreted as hemipelagites (Unit III). The interbedded turbidites increase in thickness downcore as does overall grain size. This is interpreted as reflecting a change from distal to more proximal deposition, with the turbidites in the upper part of Unit III being deposited farther from the source area than those in the lower part of the unit. The turbidite sequence comprises thin- to thick-bedded vitric siltstones and sandstones and volcaniclastic clast- and matrix-supported breccias and conglomerates. These deposits generally consist of granule- to pebble-size, angular to subrounded, gray pumice clasts in a matrix of medium- to very coarse-grained sandstone. The breccia and conglomerate beds are either structureless or planar-stratified. The volcaniclastic breccias and conglomerates range from 0.02 to 2 m in thickness and increase in thickness and number downhole. These coarse-grained beds are interpreted as the deposits of cohesive debris flows.

The sequence at Site 840 shows that between 5.1 and 6.6 Ma, sedimentation on this part of the Tonga Ridge was dominated by volcaniclastic turbidites and debris flows. Low in the sequence, these are fairly proximal deposits, but they become more distal and hence finer grained upsection. These beds were deposited in water depths comparable with those of today (around 800 m). Between 5.1 and 5.3 Ma, deposition of proximal, coarse-grained volcaniclastics again occurred. This was followed by a rather long period (corresponding to 3.0–5.1 Ma) of very slow deposition and possibly local erosion. Since 3.0 Ma, sedimentation has been of mainly pelagic, clayey nannofossil oozes with only minor volcaniclastic input.

### *Site 841*

Site 841 was drilled on the Tonga forearc, about 140 km south-southeast of Site 840 (Fig. 1). The sedimentary sequence at Site 841 consists of 605 m of clays, vitric siltstones, vitric sandstones, volcanic conglomerates and breccias, and calcareous volcanic sandstones. These sediments range in age from the middle Pleistocene to the late Eocene. Below 605 mbsf, the hole penetrated a rhyolite volcanic complex. Recovery below 72 mbsf was poor (approximately 30%).

The sedimentary sequence at Site 841 consists of a sequence of greenish gray and yellowish brown, structureless clays containing very thin- to medium-bedded vitric sand and silt turbidites and thin fallout tephra interbeds (Unit I, 0–56 mbsf). This sequence ranges from middle Pleistocene to Pliocene? in age. The sediments here overlie a 277-m-thick sequence of thin- to thick-bedded vitric siltstones and sandstones that increase in thickness downsequence (Unit II, 0–333 mbsf). The proportion of sandstone also increases downcore, and the sediments correspondingly become coarser grained. Individual beds show sharp, often scoured, basal contacts and normally graded bases. Convolute-, planar-, and cross-laminated intervals are common. We have interpreted the sediments here as being a sequence of turbidites. The upsequence thinning and fining of the beds may be the result of a change from proximal to more distal deposition. This sequence overlies a 125-m-thick sequence of poorly sorted, matrix-supported, volcanic conglomerates and breccias interbedded with vitric siltstones and sandstones (Unit III, 333–458 mbsf). This unit is dated as late Miocene in age. The volcanic conglomerates and breccias consist of mainly subrounded to rounded, pebble-size clasts of altered lava, held in a sandy matrix. The conglomerates, breccias, vitric sandstones, and siltstones are interpreted as debris-flow and proximal turbidite deposits. This sequence of beds overlies a 91-m-thick layer of deformed, greenish volcanic sandstones and siltstones, which show an overall coarsening downsequence to volcanic conglomerates (Unit IV, 458–549 mbsf). These beds are separated from the overlying unit by a brecciated, mineral-veined zone, interpreted as a fault breccia. This sequence is dated as early middle Miocene and is moderately deformed.

There is a general increase in the inclination of the bedding downsequence, and meso- and microscopic faults and fractures are common. The most common faults are high-angle, normal faults with listric or planar fault planes. Bed displacements are on millimeter or centimeter scales. The vitric siltstones are frequently banded and show reticulate patterns caused by hydrothermal alteration along bedding planes and along convolute, wavy-, cross- and planar laminae within the beds. These paler colored, altered zones are typically 2–3 mm thick and are probably a result of migrating hydrothermal fluids. These beds are interpreted as a series of turbidites, possibly deposited on a submarine fan. Conglomerates within the lower part of the sequence are interpreted as proximal gravity-flow deposits. This sequence overlies a 56-m-thick series of calcareous volcanic sandstones with thin interbeds of sandy claystone, clayey sandstone, and claystone (Unit V, 549–605 mbsf). Faunal evidence indicates that these rocks were deposited in shallow water under low energy conditions, probably on an open platform shelf. These beds directly overlie a rhyolitic volcanic complex. The boundary between Units IV and V is a major unconformity, spanning approximately 13 m.y. from the early Oligocene to the early middle Miocene.

## Structural Studies

### *Introduction*

Leg 135 sites were drilled in three distinct tectonic provinces within the supra-subduction zone of the Tonga arc-trench convergent margin. Sites 834–839 were situated within the western part of the actively spreading Lau backarc basin; Site 840 lies on the Tonga platform, to the east of the presently active Tofua volcanic island arc; and Site 841 was drilled farther to the east again, on the trench slope in the forearc.

### *Sites 834–839*

Sites 834–839 were drilled in the western part of the Lau Basin between the remnant volcanic island arc of the Lau Ridge and the active Lau backarc spreading centers. The regular, subdued topography (typically 100–200 m relief) thought to have been created by normal seafloor-spreading processes at the CLSC and ELSC was not observed across the entire Lau Basin; instead, a transition to a much more rugged bathymetry, with relief of up to 1500 m, occurs in the western part. The regional topography in this western area is made up of elongated, predominantly north-trending horsts, separated by linear grabens. The graben floors are on the order of 1–15 km wide and 10–85 km long. Sites 834–839 were drilled within several of these basins at differing distances from the Lau Ridge and Lau spreading centers so as to examine the opening history of the Lau Basin.

Sites 834 and 835 are situated in the oldest part of the basin, closest to the Lau Ridge, in small, roughly north-trending basins that are superimposed upon a more regional deepening of the Lau Basin as a whole toward the north. The oldest sediments in Basin 834 are late Miocene–early Pliocene in age, and those in Basin

835 are middle Pliocene. Neither site preserves evidence for tectonic activity on the structures that bound the basins during the period of sediment deposition. At Basin 834, the infill of pelagic sediments and volcaniclastic turbidites dip regularly at ≤1° throughout. At Site 835, there is evidence for tectonic disturbance in the form of mud-clast conglomerates and slump rafts within the sequence; however, the general northward dip of turbiditic sediments there is thought to be essentially depositional, reflecting sediment transport direction rather than tectonic tilting. Basin 835, therefore, appears to have acted as a passive channelway to externally derived turbidite deposits being transported northward into the deeper parts of the Lau Basin. The igneous rocks from both sites are traversed by fractures, interpreted as extension joints, that are parallel to the north-south elongation direction of the basins.

Sites 836–839 are situated to the south and east of Sites 834–835, close to the transition from the horst-and-graben topography of the western part of the Lau Basin to regular, topographically subdued seafloor associated with the ELSC (Fig. 2; Parson et al., this volume). Site 836, drilled into a small basin bounded by north-south lineaments, penetrated only a thin carapace of sediment before encountering igneous rocks. The sediments are 20 m thick and of middle Pleistocene age. Site 837, drilled into another basin nearby, preserves an 80-m-thick succession dominated by turbidites of late Pliocene to middle Pleistocene age. Sediments from both sites have a general dip toward the east, which may indicate activity on the basin-bounding structures with minor concomitant block rotation in the Pleistocene. Sites 838 and 839 lie approximately 50 km south of Basins 836 and 837. In contrast to the previous sites, they are associated with northeast-trending lineaments. Sidescan sonar records suggest that they are separated from each other by a north-south structure that truncates the northeast-southwest lineaments. Seismic reflection profiles show clearly that Basin 839 is bounded to the northwest by a steeply southwest-dipping normal fault; moreover, they reveal an angular unconformity within the sedimentary sequence between a lower sequence dipping 4° northwestward and an upper sequence dipping 0.5°–1° northwestward. Basin 838, however, is less well constrained. Northwest-dipping sediments measured from core at the top of the section in Hole 838A contrast with southeast-dipping sediments measured from logging data lower in the sequence in Hole 838, and appear to suggest that tectonic rotation of part of the sequence, possibly coupled with large-scale slumping, may have occurred. The location of the angular unconformity at Site 839, and of the horizon at which the dip direction in Site 838 appears to change, suggest that normal faulting along the northeast-southwest structures took place in this region in the late Pliocene–early Pleistocene. Creation of the north-south lineament that separates Basin 838 from Basin 839 must have postdated this episode.

Set in the context of SeaBeam, GLORIA, and seismic reflection data from the western Lau Basin, the basins within which Sites 834–839 were drilled appear to have been formed by an episode or episodes of tectonic extension that were broadly coeval with magmatism on a regional scale. The horst-and-graben topography of this part of the Lau Basin, with its considerable relief, contrasts with the uniform low-relief fabric typical of regular seafloor spreading. It is, however, more similar to the tectonic fabric documented within the presently subaerial or shallow submarine portions of the Lau Ridge to the west. Woodhall (1985) and Cole et al. (1985) have described episodes of rifting and subsidence accompanying the submarine extrusion of basaltic arc-tholeiite type volcanics of the Korobasaga Volcanic Group on the Lau Ridge from 4.5 to 2.5 Ma (i.e., at a similar time). Seismic reflection profiles from the Lau Ridge (collated in Woodhall, 1985) show similar topographic highs and small basins at shallow depths, and a rapid, probably fault-controlled basin margin stepping down from water depths <500 m to depths in excess of 2 km.

Initial interpretations suggest, therefore, that the western portion of the Lau Basin shows more structural similarity to the Lau Ridge than to the present-day Lau spreading centers. Lithologic evidence suggests that the sedimentary sequences of Sites 834–839 were deposited at comparable water depths to those of the present day. The volcanic basement of these sites, therefore, must either have been rifted and subsided to abyssal depths very rapidly after lava extrusion, for which there is little evidence; or volcanism, with associated rifting, must have been distributed over a broad zone and over a range of water depths from shallow submarine to abyssal. The age ranges shown by the sites suggests that the principal eruptive center migrated eastward with time.

The regional horst-and-graben topography across both the Lau Ridge itself and the western Lau Basin suggests that the whole area has been stretched. No evidence for this is preserved within the sedimentary sections of Sites 834 and 835, and even in Sites 836–839 the amount of extension apparently accommodated by syndepositional faulting is small. The creation of the grabens by normal faulting appears largely to have occurred before the deposition of the sediments, and possibly before the eruption of some of the lava succession. Estimates of the degree of extension undergone by the western Lau Basin over the period spanning the initiation of rifting in the late Miocene until the onset of regular seafloor spreading along the ELSC and CLSC in the early Pleistocene is difficult, therefore, and must be based principally upon the detailed interpretation of seismic profiles from the area.

### *Site 840*

Site 840 was drilled on the Tonga platform, which is situated to the east of the Lau Basin and immediately east of the presently active Tofua island-arc chain. Seismic reflection profiles show that the platform is dissected by a large number of normal faults (e.g., Herzer and Exon, 1985; Austin et al., 1988), the majority of which are north-northwest to north-northeast trending. The platform is also segmented laterally into discrete blocks by east-west to northwest-southeast structures. The profiles show that many faults extend up to the seafloor, suggesting that they have been active in geologically recent times.

No direct evidence for this faulting is preserved in core recovered from Site 840. Bedding dips computed from formation microscanner (FMS) data (extending from 100 to 500 mbsf only) reveal two, or possibly three, structural "units," or domains of similar orientation. Between 100 and 260 mbsf, dips range from 0° to 5°, with random strike. In marked contrast, sediment orientations from approximately 260 to 500 mbsf are far more regular, with the dip directions displaying a very consistent northward trend. The 260-mbsf boundary corresponds to the subdivision between lithologic Units II and III, separating sediments dominated by coarse pumiceous gravels above from more regular turbiditic volcaniclastic sediments below. Below the boundary, the dips themselves increase progressively from an average of 2° at 260 mbsf to 4°–5° at around 500 mbsf. Scatter of 2°–3° on either side of the mean was observed throughout this interval and is cyclical on a scale of tens of centimeters to a few meters. This cyclical variation is on the same scale as the thickness of individual turbidite influxes in this stratigraphic interval. It is possible, therefore, that the scatter may reflect a component of depositional dip at the erosional bases of the turbidites that is superimposed upon a background dip recorded by the pelagic interbeds.

A slight increase in sediment dip is evident in the lowermost FMS dipmeter data, at approximately 500 mbsf. Core-derived dip measurements, which continue to 590 mbsf, also show an increase at around this depth, some to as much as 25°–30°. No lithologic or biostratigraphic discontinuities have been noted at this depth,

which falls within upper Miocene volcaniclastic turbidites; however, it does correspond to a change in the physical properties of the sediments, which show a marked increase in sonic velocity, and a concomitant increase in bulk density, at 494 mbsf. The significance of this boundary remains uncertain, although it is perhaps the most realistic candidate at Site 840 for the "Horizon A" seismic reflector that has been widely recognized across the Tonga platform, and it is situated at a two-way traveltime that corresponds approximately to this depth.

The regular increase in dip present between 260 and 500 mbsf is most easily interpreted in terms of growth faulting. It implies a progressive northward tilting of the block during deposition in the late Miocene. Bathymetric and seismic evidence (Herzer and Exon, 1985) shows that Site 840 is situated close to several small north-trending faults that are truncated by an east-trending lineament. It is possible that these or other comparable structures were responsible for the growth faulting, in which case the east-west fault may have acted as a normal fault, and the north-south faults in a hinge mode, with significantly greater throws at their northern terminations than to the south.

### *Site 841*

Site 841 was drilled slightly inboard of the trench-slope break to the forearc of the Tonga Trench. It is the only site drilled on Leg 135 for which evidence of significant deformation can be documented from the core. Sedimentary bedding is inclined in excess of 15°, even within 1 m of the mud line. Microfaults, with consistent normal displacements on the order of a few millimeters, were observed throughout the core. Paleomagnetic evidence suggests that sediments at this depth are probably of a lower-middle Pleistocene age. Therefore, the site was undergoing extension at least as recently as that time, and extension may well be continuing to the present day.

Two major fault zones intersect Hole 841B. The higher fault zone separates upper Miocene from earliest middle Miocene volcaniclastic sediments at 458 mbsf. Three nannofossil and at least seven foraminifer zones are omitted across the structure, suggesting that it had a normal sense of displacement. This is confirmed by the normal throws to microfaults associated with the fault zone. Some fault gouge is preserved, together with several epidote-bearing fragments. Significant hydrothermal alteration has affected the footwall for a distance of at least 80 m below the fault zone: microfractures and veins are surrounded by halos of intense leaching, and the originally coarser grained portions of the volcaniclastic sequence have also been completely leached.

The second major fault zone was encountered at a depth of 605 mbsf; it separates shallow-water upper Eocene limestones above from sheared rhyolites and rhyolitic tuffs below. Although all core beneath the fault is barren of fossils, normal motion is again implied from the disposition of the overall lithologic relationships and from the sympathetic microfaults with normal senses of displacement. Within the fault zone itself, 0.64 m of extremely soft white clay was recovered. This clay contains euhedral quartz crystals, pumice, mineralized lithic fragments (including vein quartz, ?andesitic lava fragments, and jasper), and disseminated sulfides. Several minor discrete shear strands traverse the clay; these are probably derived from the latest stage of movement, as the weak clay would have been destroyed had significant displacement along the fault zone continued after its deposition.

Several further zones of cataclasis, fault gouge, and shattering are preserved within the core, at depths of 498, 573–585, 645, and 757 mbsf. These represent fault zones, but they do not juxtapose differing lithologies, nor are they associated with gaps or repetitions in the biostratigraphic record. Thus, they are thought to be of lesser magnitude than those described above. All show evidence for normal displacement.

The structural history of Site 841 is complicated by the presence of reverse microfaults at certain intervals in the core. The reverse faults are restricted to the approximate intervals 170–360 and 460–530 mbsf (entirely within the Miocene parts of the succession). None has a displacement of more than a few centimeters. In the higher stratigraphic levels, at 200–220 mbsf, slump folds and other structures clearly indicative of soft-sediment deformation are preserved. Microthrusts were observed in the axes of some of these slump folds, and these have displacements parallel to the sense of motion of the slumps. This may suggest that the sediments were being affected by compression before or during lithification (i.e., at a very early stage). The microfaults may be cut by hydrothermal veins that have extensional geometries, implying that the compression predated the episode of extension and normal faulting described above. If this is so, a change from a compressional to an extensional regime in the forearc is implied in late Miocene times.

### *Rotation of the Forearc*

The southward-convergent, trapezoidal-shaped form of the Lau Basin leads to the supposition that part of the shape of the basin may have have derived from the progressive rifting and rotation of the Tonga platform and forearc from the Lau Ridge. If this is the case, then the Tonga forearc today should be rotated clockwise on the order of 20°–30° from a relative position adjacent to the Lau Ridge. This hypothesis can be tested paleomagnetically by looking for northeasterly declined remanent magnetization vectors in discrete samples from the core. To accomplish this, accurate orientation of the core is necessary. Piston cores only can be oriented using the multishot orientation tool; therefore, only soft sediments can be oriented. A further means of core orientation is possible, however, by integrating paleomagnetic sampling with the core-based structural measurements and FMS downhole logging data. The FMS tool carries a magnetometer, allowing orientation of its microresistivity images. Dip measurements of inclined strata from distinctive intervals within the core can be restored, therefore, back to the orientation of their counterparts on the FMS images, and the paleomagnetic declinations of samples from the same strata can be rotated by the same amount to give an original declination direction. Preliminary analysis of logging, structural, and paleomagnetic data from Site 840 tend to confirm the initial paleomagnetic results reoriented using the multishot tool; this suggests that some rotation of the Tonga platform has indeed taken place.

## Biostratigraphy

Calcareous planktonic microfossils were been studied from sites in the Lau Basin (backarc) as well as the Tonga platform (forearc). At most sites, assemblages were well preserved and of moderate to high diversity. Some evidence of dissolution was apparent in some planktonic foraminiferal faunas from Sites 834 and 835 in the Lau Basin; dissolution was strong in the deepest water site, Site 841 on the Tonga platform, where much of the upper Miocene to Quaternary section was barren. For most sites, the top part of the sedimentary sequence was made up of nannofossil-foraminifer oozes, with a few thin volcaniclastic deposits. Passing downsection, these sediments become increasingly rich in volcaniclastic material and, at the same time, the microfossil assemblages deteriorate. Only one site was penetrated to sediments older than upper Miocene; in Site 841 the top of the lower middle Miocene unit of volcaniclastic sands and conglomerates was faulted against the upper Miocene, and the base was disconformably underlain by lowermost Oligocene to upper Eocene sediments.

Figures 10 and 11 summarize the biostratigraphic correlations for the Lau Basin and the Tonga platform, respectively, in terms

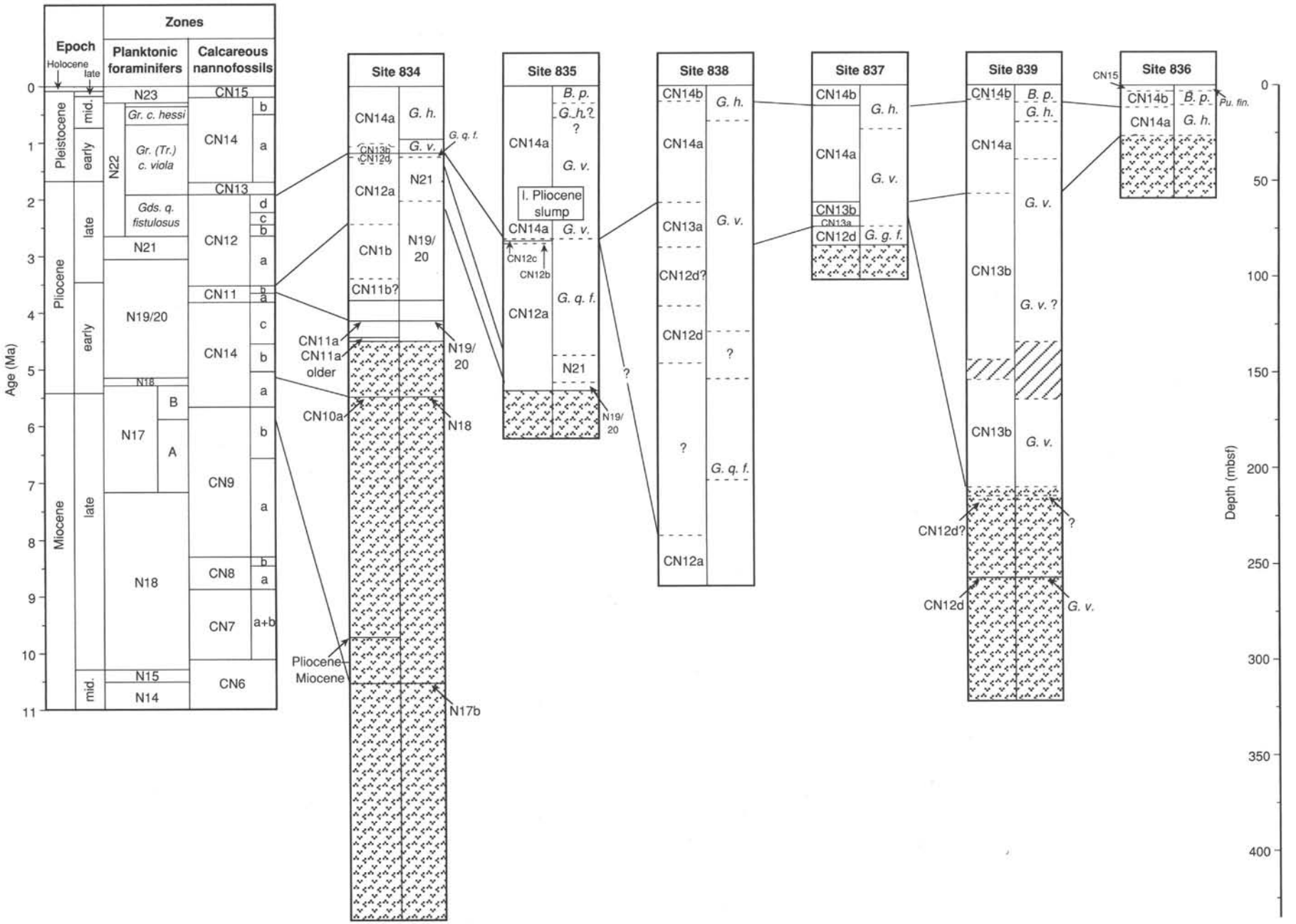


Figure 10. Biostratigraphic vs. depth correlations between Lau Basin (backarc) Sites 834–839 based on planktonic foraminifers and calcareous nannofossils.

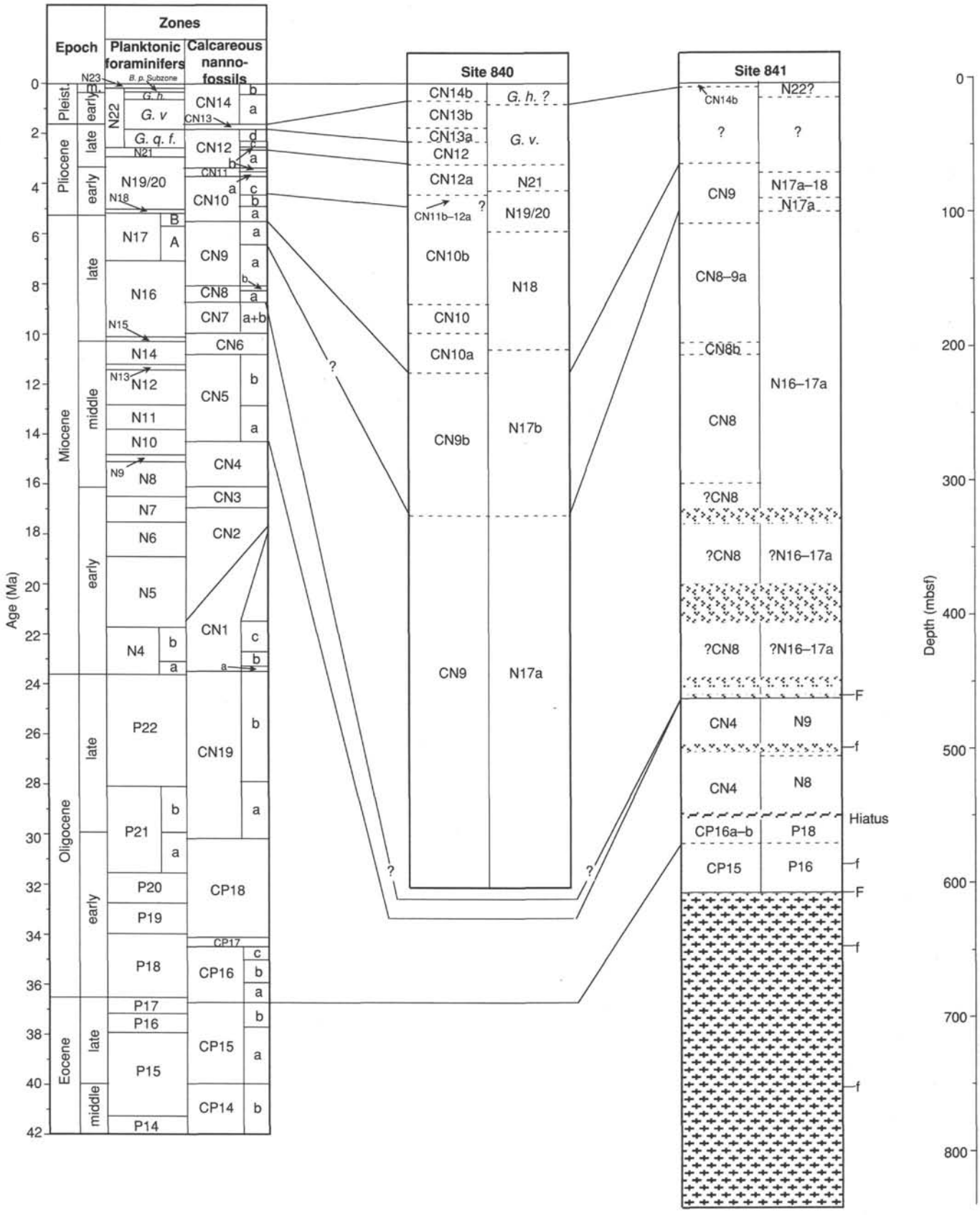


Figure 11. Biostratigraphic vs. depth correlations between Tonga platform (forearc) Sites 840 and 841 based on planktonic foraminifers and calcareous nannofossils.

of section thickness. The relationship between the planktonic foraminiferal and nannofossil biostratigraphic schemes is also illustrated. Figure 12 compares the sections at each site in terms of age. In general, the tropical and subtropical planktonic foraminifer zonal scheme of Blow (1969), with modifications of Kennett and Srinivasan (1983), Bolli and Premoli Silva (1973), and Chaproniere (in press), adequately described the Quaternary to upper Eocene sequences where planktonic foraminifers were present. The East Indian Letter Stage Classification (Adams, 1970) was used for the upper Eocene, larger foraminiferal sequence in Site 841. Similarly, the nannofossil zonal schemes of Martini (1971), Bukry (1973, 1975), and Okada and Bukry (1980) with minor modifications were successfully employed.

For the Lau Basin sites, the main objective of Leg 135 was to sample and date the igneous basement. Of the six sites, five were penetrated through the sediment cover into basalt. For Site 834, the oldest sediments directly overlying basalt were probably from within Zones N19/N20 and Subzone CN11a, and from sediments interbedded within the pillow basalt sequence, Zone N17B, and the boundary between Subzones CN10a and CN10b. At Site 835, the microfossil assemblages indicate that Zones N19/N20 and Subzone CN12a overlie the basalts. Assemblages become progressively younger from Site 837 (Zone N22, *Globigerinoides quadrilobatus fistulosus* Subzone; Subzone CN12d) to Site 839 (Zone N22, *Globorotalia [Truncorotalia] crassaformis viola* Subzone; Subzone CN13b), with the youngest assemblage at Site 836 (Zone N22, *Globorotalia [Truncorotalia] crassaformis hessi* Subzone; Subzone CN14a). At Site 839, assemblages from Zone N22, *Globorotalia (Truncorotalia) crassaformis viola* Subzone, and Subzone CN12d were recovered from interbeds within the basalt sequence. Igneous basement was not reached at Site 838, but the oldest sediments recovered were slightly older than those from Site 837, being typical of Subzone CN12a. A slump block of upper Pliocene sediments (CN12a–CN13b) was found within the lower Pleistocene (CN14a) of Site 835. This block was probably derived from the slopes above the basin in which Site 835 was located.

Site 840 was situated on the Tonga platform in 755 m of water and was drilled to date the seismic unconformity Horizon A, which is thought to occur within the upper Miocene part of the sequence. Paleontologic data, however, did not identify this horizon as a chronostratigraphic surface. The hole bottomed in upper Miocene Zone N17 or Zone CN9. Nannofossil studies indicate that a hiatus is present which spans the interval from the base of Subzone CN12a to the base of Subzone CN10a; this was not recognized in the planktonic foraminiferal zonal scheme. Foraminiferal faunas, which are diverse and well preserved in the Pleistocene and Pliocene parts of Site 840, deteriorate in the lower part of the sequence as volcaniclastic deposits make up a large part of the section.

Site 841 was drilled in water depths of 4821 m on the Tonga forearc to test the nature of the igneous basement. The absence or paucity of microfossil assemblages typify the upper Miocene to Quaternary interval, indicating that the site was at or below the carbonate-compensation depth (CCD) for most of this time, as it is today. The lower part of this sequence contains reworked upper Eocene, larger benthic foraminifers (*Asterocyclina, Discocyclina,* and *Pellatispira*) scattered throughout the conglomeratic phases. The presence of these fossils indicates that an upper Eocene sequence was being actively eroded during the upper Miocene. The upper Miocene to Quaternary section overlies, and is in faulted contact with, lower middle Miocene volcanic conglomerates, sandstones, and siltstones. In contrast to the overlying sequence, the faunal and floral assemblages are well preserved and were deposited at neritic or bathyal depths. Unconformably underlying the middle Miocene is a sequence of basal Oligocene to upper Eocene calcareous sands. The upper part of this sequence is dominated by planktonic and smaller benthic foraminifers and nannofossils. Below this, the assemblage gradually changes to one dominated by larger benthic foraminifers in which the planktonic component becomes very rare or absent. In these lower beds, *Halimeda* and coralline algae, bryozoa, and echinoids are also present, indicating water depths of <50 m. The age of this unit ranges from Zones P18 to P16 (CP16b to CP15) where planktonic microfossils are present. The lower part of the assemblage is made up of *Asterocyclina, Discocyclina, Spiroclypeus, Operculina,* and *Amphistegina; Pellatispira* was not recorded. This assemblage is typical of the East Indian Letter Stages Ta3 to Tb. However, the planktonic faunas and the lack of any evidence of a stratigraphic break suggest that this part of the section is part of the upper Eocene and probably therefore from Tb.

Although no study of smaller benthic foraminifers was made, there is no evidence to suggest major changes in depositional environment for any of the sequences studied except for that at Site 841. At this site it is obvious that water depths have changed from very shallow-water, inner-neritic depths in the upper Eocene, to neritic or bathyal depths during the early middle Miocene, to depths below the CCD down to depths close to 5000 m today.

## Sedimentation Rates

Sedimentation rates were estimated from age vs. depth data for each site, using nannofossil and planktonic foraminiferal datum levels and paleomagnetic reversal data. The results for the Lau Basin sites (backarc) are presented in Figure 13, and those for the Tonga platform and forearc in Figure 14. The backarc sites cover a time interval from the upper Miocene to the Quaternary. At Site 840 the time interval spanned the upper Miocene to the Quaternary, and at Site 841, the interval covered was from the upper Eocene to the Quaternary. Calcareous plankton assemblages for all of the Lau Basin sites were generally good to moderately abundant although dissolution effects were noted for some levels, as were those from Site 840 on the Tonga platform. For Site 841, however, dissolution resulting from deposition below the CCD through the upper Miocene to Quaternary prevented confident estimates of sedimentary accumulation rates. Furthermore, paleomagnetic data over the early middle Miocene interval were not used because of their lack of reliability. Sedimentation rates in the upper Eocene section also proved difficult to calculate because of their shallow-water nature and the lack of biostratigraphic resolution afforded by the larger foraminiferal faunas within the lower part of the unit. For all other sites, the biostratigraphic data were well constrained and provided good results.

For the Lau Basin sites, the sediment accumulation rates were high during periods of intense volcanic activity from the upper Miocene to the upper Pliocene. Rates of up to 383 mm/k.y. were obtained for a period in the upper Miocene (Site 834) when basalts and thick vitric ash beds were deposited. At Site 839, high sedimentation rates of 882 mm/k.y. were obtained from an upper Pliocene basalt and vitric ash sequence. For the other sites, sedimentation accumulation rates dropped to between 38 and 9 mm/k.y. for the upper Pliocene to Quaternary sections. At Site 835, the sedimentation rate curve is complicated by the presence of a slump block of upper Pliocene sediments within the lower Pleistocene.

A thick sequence of upper Miocene to Quaternary sediments was penetrated at Site 840 on the Tonga platform. Sedimentation accumulation rates range from 110 to 820 mm/k.y. during the upper Miocene when considerable thicknesses of arc-derived volcaniclastic sediments were deposited. With the decrease in volcanic activity during the Pliocene, sedimentation rates deceased to 39 mm/k.y., dropping to 14 mm/k.y. through the Pleistocene. A short hiatus was noted within the Pliocene. Site 841, on

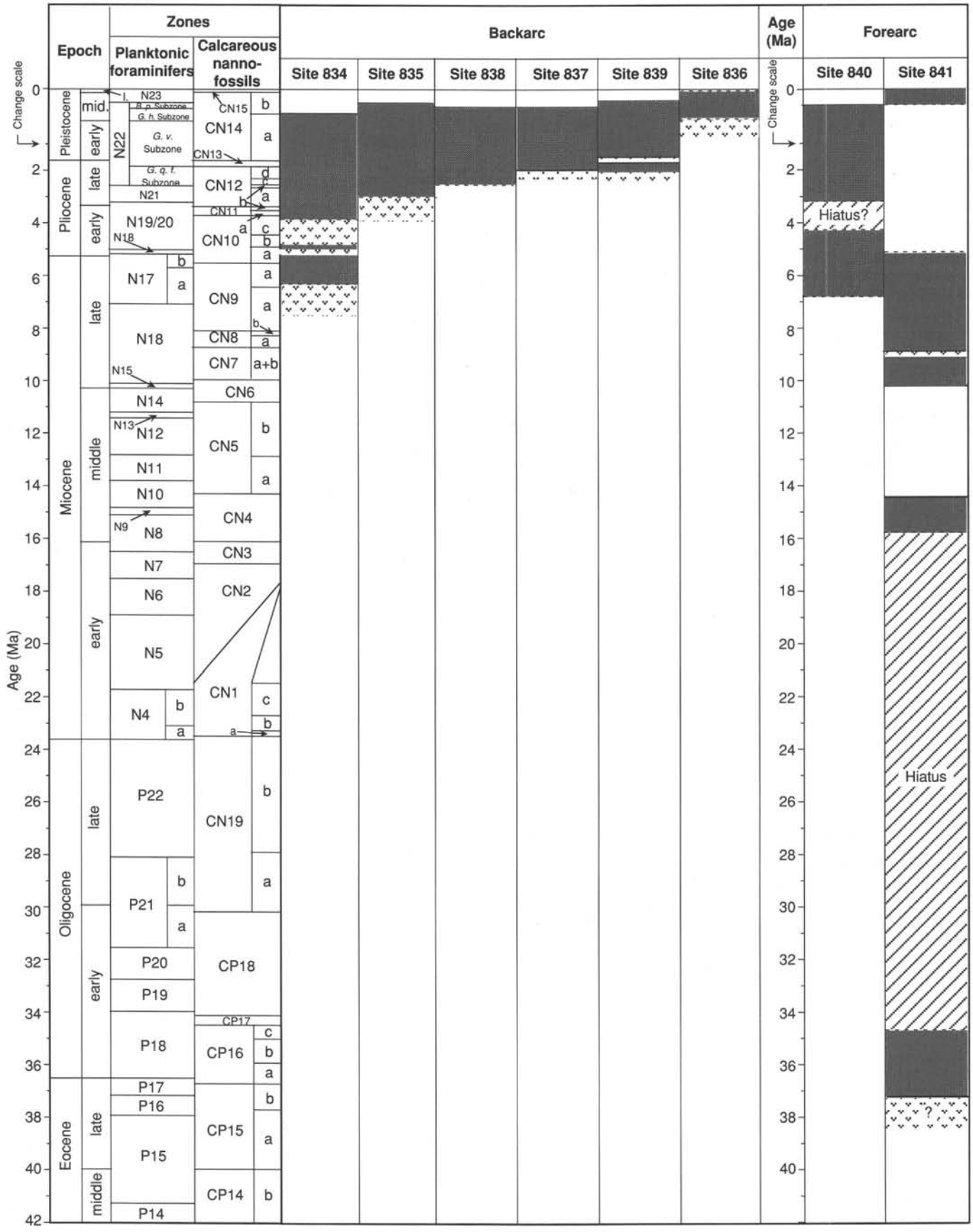


Figure 12. Biostratigraphic correlations, scaled by age, among Sites 834 to 841, based on planktonic foraminifers and calcareous nannofossils.

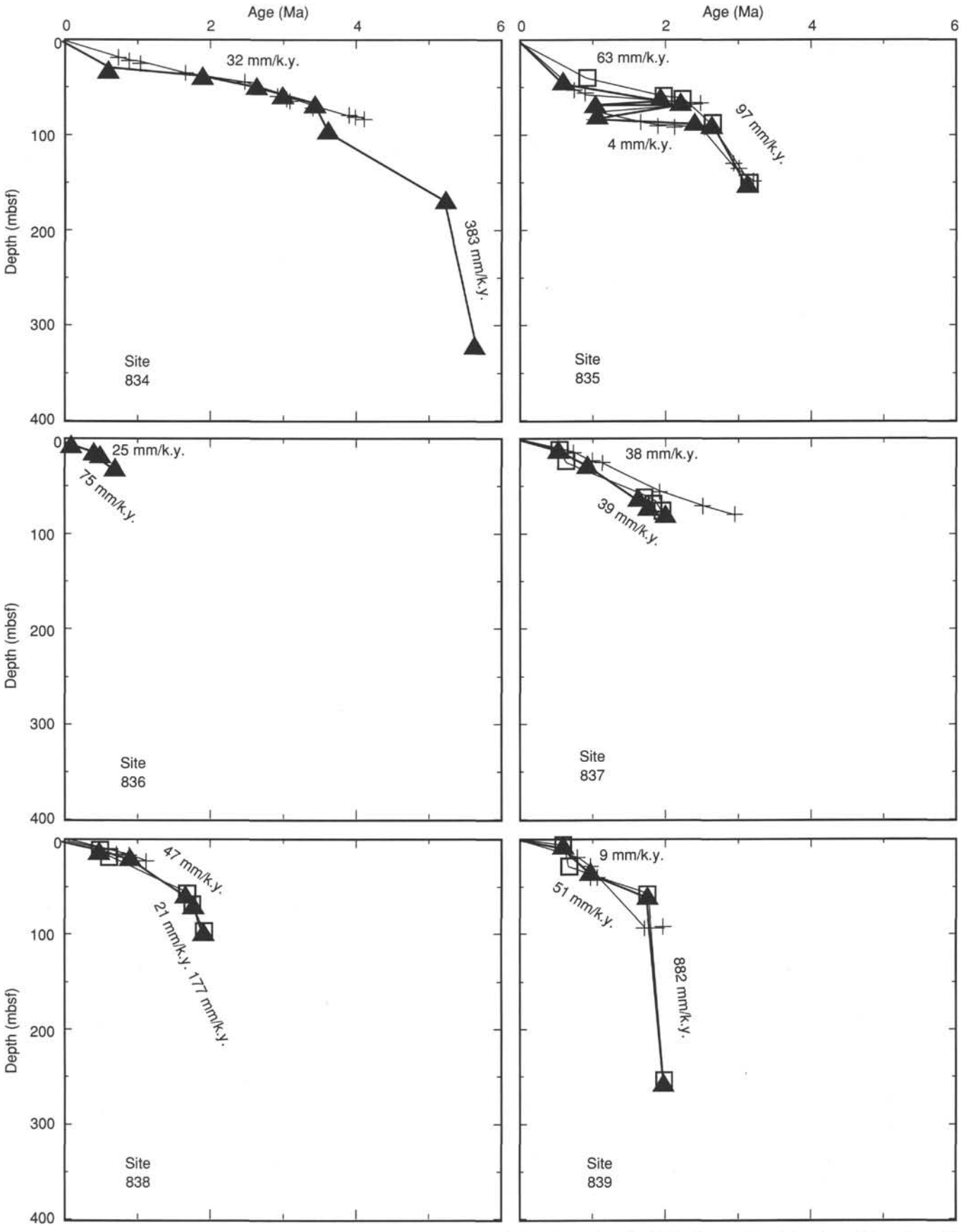


Figure 13. Summary of sediment accumulation rates (age vs. depth) for Leg 135 sites in the Lau Basin (backarc). Closed triangles = biostratigraphic data, open squares = biostratigraphic data with modified ages for *Globorotalia* (*Truncorotalia*) *tosaensis*, and crosses = paleomagnetic data.

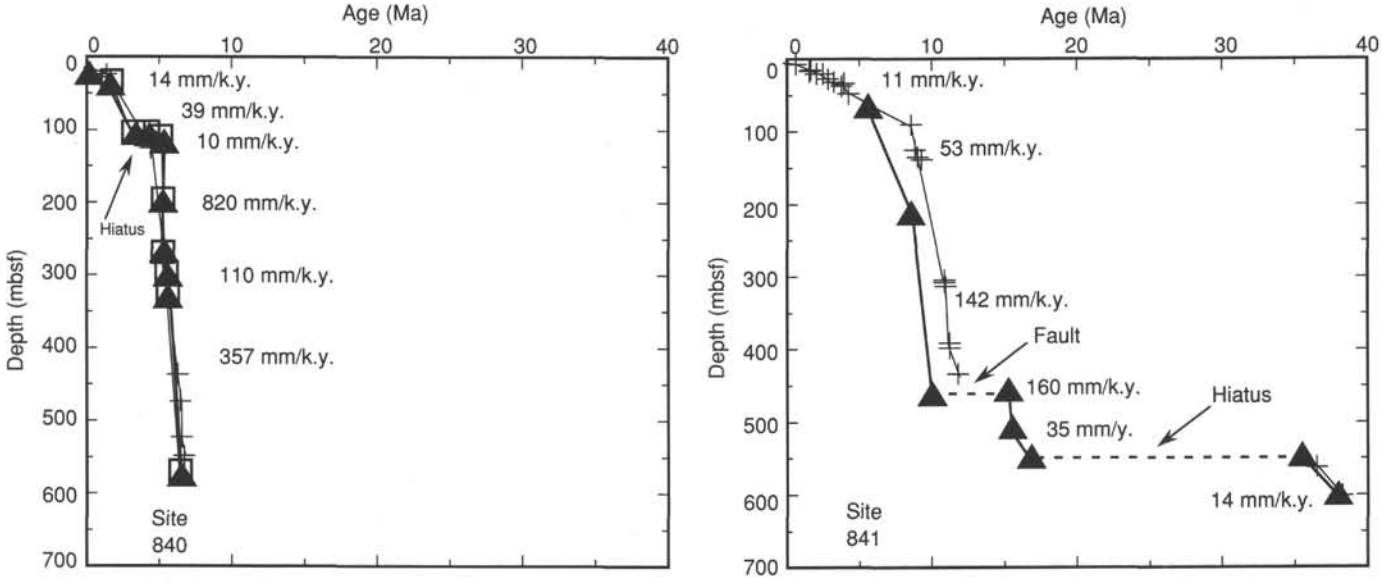


Figure 14. Summary of sediment accumulation rates (age vs. depth) for Leg 135 sites on the Tonga platform (forearc). Closed triangles = biostratigraphic data, open squares = biostratigraphic data with modified ages for *Globorotalia* (*Truncorotalia*) *tosaensis*, crosses = paleomagnetic data, and dashed line = hiatus or fault.

the forearc, proved to be complicated by faulting and poor fossil assemblages; despite this, there is good correspondence between paleomagnetic and biostratigraphic data. Sedimentation rates were low (14 mm/k.y.) during the upper Eocene to lower Oligocene when larger foraminiferal and planktonic sediments accumulated at neritic depths. Rates increased to 160 mm/k.y. over the lower middle Miocene sequence of volcanic siltstone, sandstone, and conglomerates. During the upper Miocene, sedimentation rates over an deposition interval of volcaniclastic conglomerates and sandstones reached 142 mm/k.y., decreasing to 53 mm/k.y. as volcaniclastic input decreased, and finally reaching 11 mm/k.y. during the Pliocene and Quaternary when the calcareous component was removed by dissolution.

## Paleomagnetism

### *Magnetic Properties*

Sediments from the Lau Basin and Tonga Ridge are strongly magnetic, with natural remanent magnetization (NRM) intensities as high as 7262 mA/m but more typically averaging 100–750 mA/m. To a large degree, the high NRM intensities result from the abundant volcanic material within most of the sediments. Also contributing to the high intensities were low-coercivity magnetic minerals, found in most Leg 135 sediments, that were susceptible to the acquisition of an isothermal remanent magnetization (IRM) from the drill string. Typical median destructive field (MDF) values for Lau Basin sediments were 2–5 mT. Tonga Ridge sediment MDF values were generally somewhat higher at 7–15 mT.

The highest recorded NRM in the igneous rocks (mostly basalts) was 9614 mA/m, but NRM values typically averaged around 1000–2500 mA/m. Although the drill string IRM was also observed to bias most igneous rock magnetizations, it was usually not as pervasive as in the sediment samples. The MDF values for the basalts were also usually higher, at about 10–20 mT.

The drill-string IRM was ubiquitous, contaminating the magnetizations of virtually all samples measured on Leg 135. This overprint was recognizable by its consistent vertically upward direction. Indeed, it was often possible to recognize mishandled samples, placed in the core liner upside-down, by the direction of this overprint. The drill-string overprint often masked the inherent magnetic polarities of reversely magnetized samples. However, because it resides mainly in low-coercivity grains, this IRM was easily removed by alternating-field (AF) demagnetization. Unfortunately, to remove the overprint, AF fields in excess of the 15-mT limit were often applied to archive core halves. Thus, archive half measurements sometimes yielded unreliable results.

### *Magnetic Polarity Stratigraphy*

Magnetic polarity determination and matching of the polarity sequence to geomagnetic reversal time scales was seldom straightforward at Leg 135 sites. Hampering such efforts were the ubiquitous and often strong drill-string overprint, slumps (Site 835), thick and unconsolidated ash turbidites (Sites 837–840), and spotty recovery (Sites 840 and 841). Nevertheless, plausible magnetic stratigraphy models were constructed for all sites (Fig. 15). Pliocene-Pleistocene reversals of the Gauss, Matuyama, and Brunhes chrons were recorded at Lau Basin sites. The deeper Tonga Ridge sites yielded cores that displayed parts of the Miocene and Eocene reversal sequences (Fig. 15). The high sedimentation rates in the basin enabled us to recognize even short subchrons at most sites. For example, the Cobb Mountain Event (Mankinen et al., 1978; Clement and Robinson, 1987) was visible just beneath the Jaramillo Subchron at Sites 834, 835, 837, 838, and 839. High sedimentation rates at the Tonga Ridge sites aided magnetostratigraphy by expanding polarity intervals to the point that most were recognizable even with low recovery.

The most reliable magnetostratigraphic model was obtained from the advanced hydraulic piston (APC) cores recovered at Hole 834A, in which recovery was good, sedimentation rates were fairly constant, biostratigraphic data were plentiful, and the drill-string overprint easily removed. The least reliable record is probably that obtained from the APC core section of Hole 841A, which yielded biologically barren and moderately disturbed sediments, with a drill string overprint that was not entirely removed by 15-mT AF demagnetization.

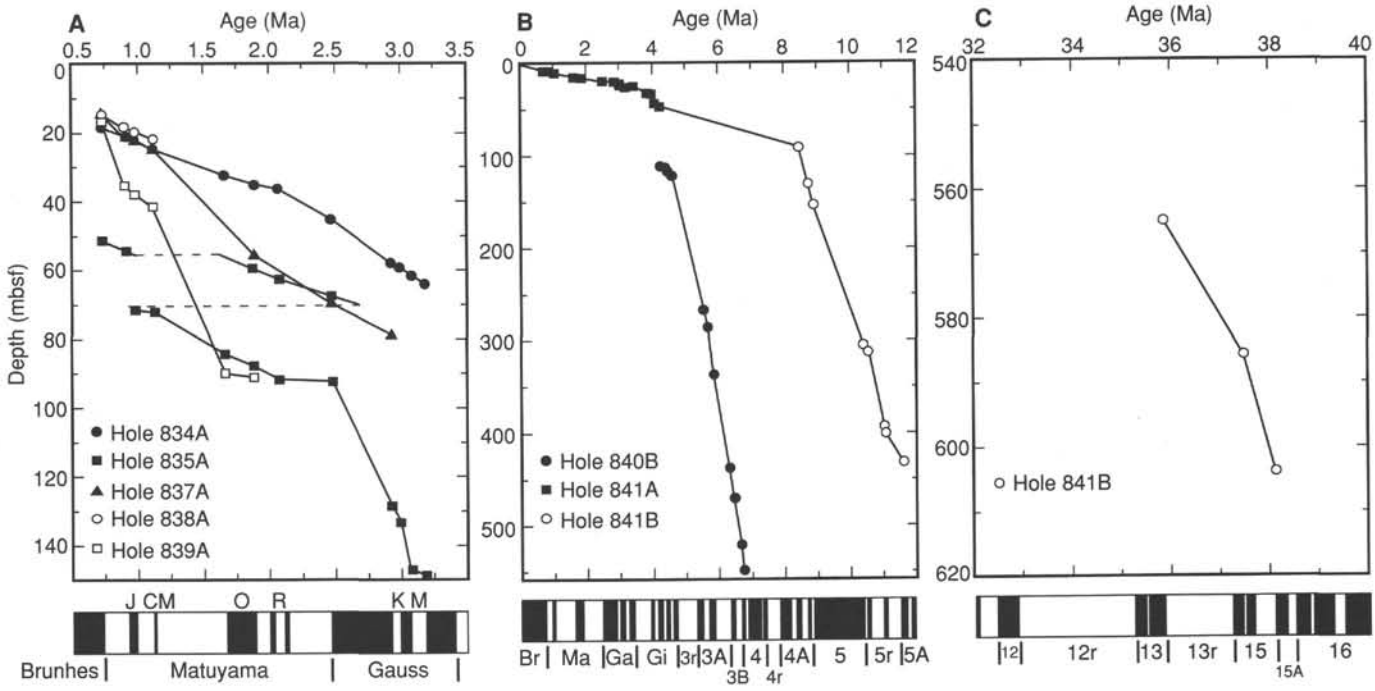


Figure 15. Summary of age vs. depth curves derived from magnetic polarity stratigraphy. **A.** Lau Basin sites. **B.** Tonga Ridge sites, Neogene. **C.** Tonga Ridge Site 841, Eocene section. Polarity models from geomagnetic reversal time scale provided at the bottom of the figure (Berggren et al., 1985, modified by inclusion of Cobb Mountain Event [Clement and Robinson, 1987] and Réunion Subchron [Harland et al., 1982]). J = Jaramillo, CM = Cobb Mountain, O = Olduvai, R = Réunion, K = Kaena, M = Mammoth, Br = Brunhes, Ma = Matuyama, Ga = Gauss, and Gi = Gilbert.

### *Oriented Cores and Paleomagnetic Declination*

Tectonic models suggest that the Tonga Arc has rotated 20°–30° clockwise, away from the Lau Ridge, since the early Pliocene (e.g., Weissel, 1977). To test this hypothesis, oriented APC cores were obtained at the Tonga Ridge sites, so that paleomagnetic declinations could be measured. Orientation data were obtained for 16 APC cores from Holes 840C and 841A; however, lithologic problems reduced the number of useful cores. In Hole 840C, loose volcaniclastic gravels and sand made up most of the recovered material. Moreover, lubricated by the water from the volcaniclastic core sections, some of the pelagic sediment sections broke free from the core liner and rotated, negating measurement of their orientations. In addition, one APC core from Hole 841A hit a resistant layer and returned empty.

Despite the scatter caused by these problems, a definite clockwise trend of paleomagnetic declinations was noted (Fig. 16). The average of all declination measurements is 16.5° ± 10.7° (95% confidence). Ignoring the results from cores with <3 measured samples, an average declination of 23.0° ± 13.1° was determined. These results are from sediments of middle Pliocene to early Pliocene age and imply that the Tonga Arc has indeed undergone a clockwise rotation of about the hypothesized amount and timing.

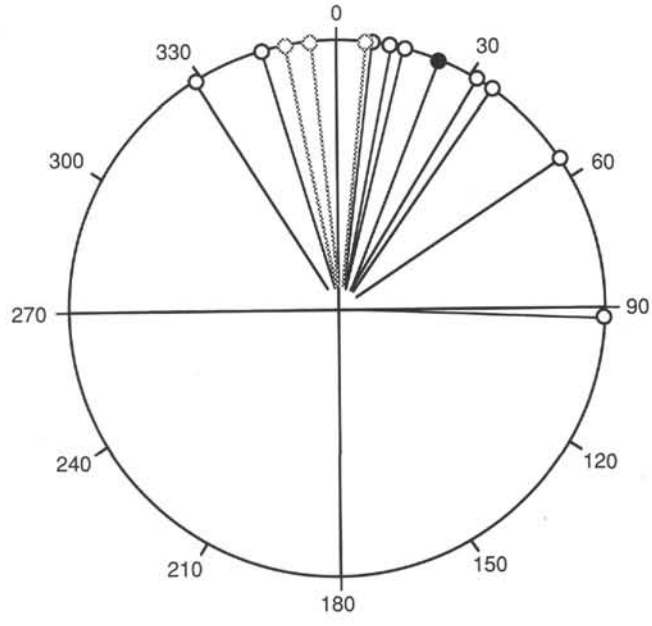


Figure 16. Summary of paleomagnetic declinations from oriented middle-early Pliocene APC cores, Holes 840C and 841A. Open circles show mean declinations for oriented APCs. Gray declinations are least reliable, being derived from only two samples. Mean declination, 23° ± 13°, is shown by filled circle.

### *Magnetic Susceptibility*

Susceptibility values from Leg 135 cores varied widely, from $1 \times 10^{-6}$ cgs to $5013 \times 10^{-6}$ cgs. Much of the variation observed within sediment cores reflects the amount of volcanic material. Ash layers and ash turbidites typically give high susceptibility values whereas nannofossil ooze yields low readings. Indeed, within the ooze sections, ash layers barely visible to the eye often stood out by their susceptibility peaks. Not surprisingly, the highest susceptibility values were recorded from basalt cores.

Several different types of susceptibility signatures were noted in Leg 135 cores. Aside from occasional ash-layer peaks, nannofossil oozes often showed low-amplitude oscillations (about $50 \pm 10^{-6}$ cgs) with wavelengths of several tens of centimeters. These oscillations appeared similar to susceptibility cycles noted in deep-sea cores elsewhere and attributed to fluctuations in magnetic grain input caused by Milankovitch climate cycles (e.g.,

Bloemendal and deMenocal, 1989). To reduce the effect of material variations, a modified Koenigsberger Ratio was calculated by dividing the magnetization intensity demagnetized at 15 mT by the susceptibility (Q15). Comparing Q15 cycles to the magnetic stratigraphy, approximate periodicities of 21 k.y. (Site 836) and 37–41 k.y. (Sites 834, 837, and 839) were calculated, similar to Milankovitch orbital perihelion and obliquity periods, respectively (Berger, 1978; Ruddiman and McIntyre, 1981).

In many Leg 135 cores, turbidites were evident from the presence of susceptibility signatures that showed exponentially increasing values toward the bottom of the graded layer. The susceptibility enhancement is apparently caused by the preferential settling of heavy magnetic minerals to the bottom of the turbidite while it is still a slurry (Sager and Hall, 1990). Particularly striking examples were observed from thick ash turbidites in Hole 837A. At Site 838, similar susceptibility signatures were observed in pumiceous gravel layers that showed no obvious grading, implying a subtle, gravity-induced compositional grading.

At several sites, broad-scale susceptibility variations were noted over tens of meters. Basalts from Holes 834B and 839B displayed susceptibility fluctuations with an amplitude of about 1 order of magnitude over 50–100 m of depth. Such variations indicate changes in the amount of magnetic minerals contained in the basalts, perhaps indicative of subtle shifts in melt chemistry. Sediments from the bottom part of Hole 840B showed similar variations, indicating a long-term drift in the concentration of magnetic minerals contained in turbidites, and, by extension, in the composition of their source rocks.

## Inorganic Chemistry

The main objective of the inorganic geochemistry studies for Leg 135 was to understand the causes of variations in the pore-water chemistry of the sediments of the Lau Basin–Tonga/Tofua arc. The pore-water chemical constituent of greatest interest is the calcium ion, concentrations of which are most directly related to alterations of the volcanogenic material in the sediments or the underlying basalts.

In sites located to the west of the present Lau Basin spreading centers (Sites 834 through 839), the concentration-depth profiles of calcium ion dissolved in the pore water are characterized by extremely low concentration gradients (Fig. 17). However, these Ca profiles exhibit a systematic trend with a slight increase in calcium in the upper part of the sedimentary column. Toward the bottom of the sediment, a pore-water Ca decrease was observed at Sites 834, 835, 837, and 839. At Site 838, below 30 mbsf, the Ca concentration gradient is lower than that observed at the other backarc sites. These features can be related to two major processes that probably varied in intensity in time and space: (1) diffusive exchange with the basement rock and (2) low advection of seawater at the boundary between hemipelagic sediment and basaltic basement. This circulation seems to be aided by the occurrence of permeable volcanic material overlying the basement, and it affected the chemical signature of the pore water. This hypothesis is also supported by the distribution in major (magnesium, chloride, sodium, potassium, and sulfate) and minor (manganese) chemical components determined in Sites 834 through 839.

Site 840 is located in the shallow platform sequence of the Tonga Ridge. The low recovery, the coarse-grained nature of the volcanic gravel lithologies, and the rather hard and well-lithified nature of the sediments, allowed us to collect only six samples at Site 840. Alteration of volcanic material in the sediments is the major factor causing the observed changes in the calcium, magnesium, and potassium gradients in the Site 840 pore waters. Concentrations of sulfate and ammonia do not vary much, indicating that the bacterial activity in these low organic carbon sediments is minimal. This is further substantiated by the low level of dissolved manganese. In the most enriched carbonate layer, the observed decrease in alkalinity is probably related to the relative amount of volcanogenic materials in lithologic Units I and II.

Site 841 is located on the Tonga forearc. The pore-water chemistry indicates that the collected interstitial water is some of the most intensively modified pore water of seawater origin yet sampled during the ODP/DSDP programs and can be defined as $CaCl_2$-rich brine. The pore-water chemistry of the sediments at Site 841 is similar to that obtained at only three other drilling sites

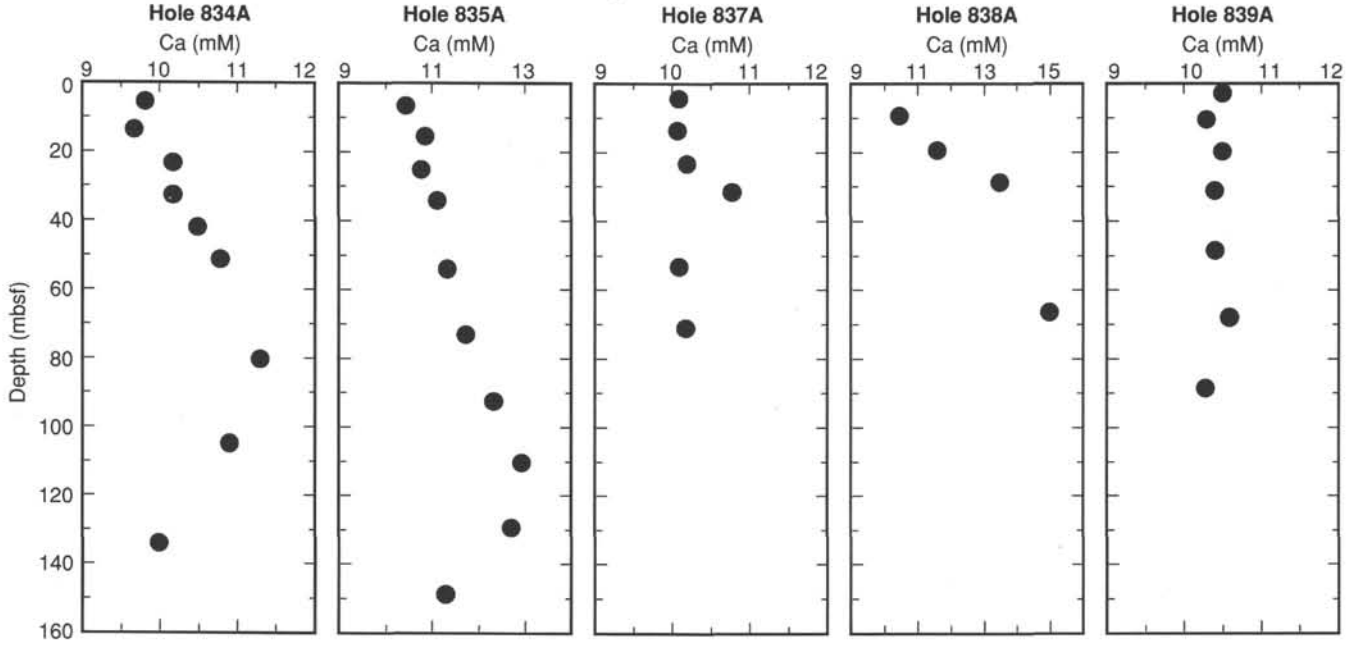


Figure 17. Geochemical profiles for calcium at Leg 135 sites.

in the world: Sites 792 and 793 occupied during Leg 126 in the Izu-Bonin arc sedimentary basin (Taylor, Fujioka, et al., 1990), and Site 802 occupied during Leg 129 in the central Mariana Basin (Lancelot, Larson, et al., 1990). Variations in the concentrations of Ca, Mg, K, Na, and Cl are abnormal for normal marine sediments and are probably caused by the combined effect of abundant volcanogenic material and the high rates of sedimentation leading to a very low diffusivity. Chloride concentrations are higher than those obtained in seawater and can be understood best in terms of water uptake by secondary minerals, as also recorded at ODP Leg 126 and 129 sites. The changes observed in dissolved sulfate, ammonia, and phosphate in the uppermost 200 mbsf are likely to be related to decomposition of the organic matter by sulfate-reducing bacteria. The changes observed in silica, strontium, and manganese concentrations are probably controlled by diagenetic reactions involving alteration of the volcanogenic material.

## Organic Geochemistry

Methane was not detected above laboratory background levels in any of the 123 head-space samples taken during Leg 135, except in three samples from Site 841. Even at Site 841, the maximum concentration of methane obtained was 15 ppm. These samples, from 670 to 756 mbsf, contained igneous rocks, which suggests that the methane was derived from a nonbiological process. The lack of methane in any of the other head-space samples indicates that methanogenesis is not occurring in the sediments encountered during Leg 135. Ethane and propane were not detected in any sample.

The average organic carbon content of the sediments recovered during Leg 135 is 0.14%. This is based on 148 measurements made with the Carlo-Erba NCS analyzer of total carbon and by subtracting the inorganic carbon value. This very low figure is an overestimate because of the tendency to avoid picking samples for NCS analyses that obviously were predominantly volcaniclastic. The highest organic carbon content (0.67%) was obtained from Eocene carbonate-rich sediments that contain the larger foraminifers at Site 841 (Core 135-841B-46R). When these and other samples with higher organic carbon contents were analyzed using the Rock-Eval instrument, the results indicated that their organic matter has no hydrocarbon potential and is probably reworked oxidized material (i.e., inertinite). The Leg 135 organic geochemical results are similar to those reported by other workers (Buchbinder and Halley, 1985; Sandstrom, 1985) who have made organic geochemical analyses of samples from the Tonga area and also found them to have low organic carbon contents, with the organic matter being mostly inertinite.

Open-ocean sediments with a large volcaniclastic contribution, such as those cored during Leg 135, were expected to have low total organic carbon (TOC) contents. Primary productivity in the upper waters of the open ocean is low, and efficient scavenging by organisms or oxidation deeper in the water column means that open-ocean sediments normally contain a low abundance of organic carbon (Hunt, 1979; Tissot and Welte, 1984). The addition of volcaniclastic sediments further dilutes this carbon, which is in any case mostly inertinite with no metabolic value for bacteria. The lack of enough carbon for the sulfate-reducing bacteria to metabolize is possibly the reason why sulfate levels at the Leg 135 sites show little change with depth. Hence, two of the diagenetic stages that are generally observed in marine sediments, sulfate reduction and methanogenesis, do not occur in these Leg 135 sediments, which should have important consequences for the diagenesis of inorganic species.

Nitrogen and sulfur were generally in very low abundance. In most samples, they were below the detection limits of the NCS analyzer. At Sites 834 and 835, nitrogen appeared to be associated with organic matter and sulfur with volcaniclastic material. At other sites, there was no obvious relationship between carbon or carbonate contents and the amount of nitrogen or sulfur.

## Igneous Petrology

### *Introductory Summary*

One of the major objectives for Leg 135 was to sample the igneous crust of the basin so as to understand the petrologic evolution of magmas that were erupted as the basin opened. The tectonic setting of the basin, between an active and a remnant volcanic arc, suggested that the mantle beneath the basin might be heterogeneous and could be expected to give rise to melts having variable expression of an "arc" signature as well as more MORB-like compositions. Data from other backarc basins such as the Mariana Trough (e.g., Fryer et al., 1981; Mattey et al., 1980; Hawkins and Melchior, 1985; Volpe et al., 1987; Hawkins et al., 1990) and previous studies of rocks dredged from the Lau Basin (e.g., Hawkins, 1976; Hawkins and Melchior, 1985; Volpe et al., 1988; Ernewein et al., in press) have provided evidence that this was the case and that there is spatially related compositional variation within these basins.

Six sites were drilled on Leg 135 in the Lau Basin so as to determine spatial variations in the composition of the crust and to make a detailed study of geochemical responses to the temporal and spatial evolution of mantle sources under the basin. Volcanic rocks, presumed to be igneous basement, were reached at five of the drill sites. The drill sites were situated in small north-trending sub-basins more or less subparallel to the present axial ridge system. Basal sediment ages indicate that there is a general west to east younging of minimum basement ages from 4 Ma (with the oldest recovered basement rock age being 5.6 Ma) in the northwest portion of the basin (Site 834) to 0.7 Ma at Site 836, about 50 km west of the ELSC. There does not seem to be any direct relationship between basement ages in these sub-basins and their position relative to the present spreading centers in the Lau Basin. The initial rifting of the basin may have proceeded with sequential crustal extension, subsidence, volcanism, and sedimentation operating in a number of small sub-basins that share a common trend and form. Volcanism and sedimentation no doubt were synchronous initially; either process may have been dominant at any one time, but eventually volcanic activity ended and the basins have continued to be filled with sediments. Rather than evolving by classic "seafloor spreading" processes, the early history of the Lau Basin may have been more similar to the formation of intracontinental rifts or basin range structure. This difference may have been important in the evolution of the erupted magmas as a "non-seafloor spreading" process may have provided opportunity for assimilation and mixing with older arc or forearc crust. Thermal gradients, depths of melt separation from mantle sources, and near-surface crystal fractionation processes all may have differed from those envisioned for true mid-oceanic-ridge settings during the early history of the backarc basin. Supra-subduction zone mantle-wedge chemistry, modified by prior depletion during previous extraction of melts and by subsequent addition of volatiles (and melts?) derived from subducted oceanic lithosphere, may have been the fundamental control on erupted magma compositions.

Results from the shipboard XRF analyses indicate that the Leg 135 igneous samples possess some trace and minor element abundances considered as typical of an "arc-source" signature. The most significant are a depletion in Nb relative to MORB and an enrichment in Rb, Ba, K, Sr, and Ce relative to Nb, Y, Ti, and Zr (Fig. 18). The model proposed by Hawkins and Melchior (1985) predicted that there should be a spatial, and by inference, a temporal variation from a greater to a lesser arc-like signature as

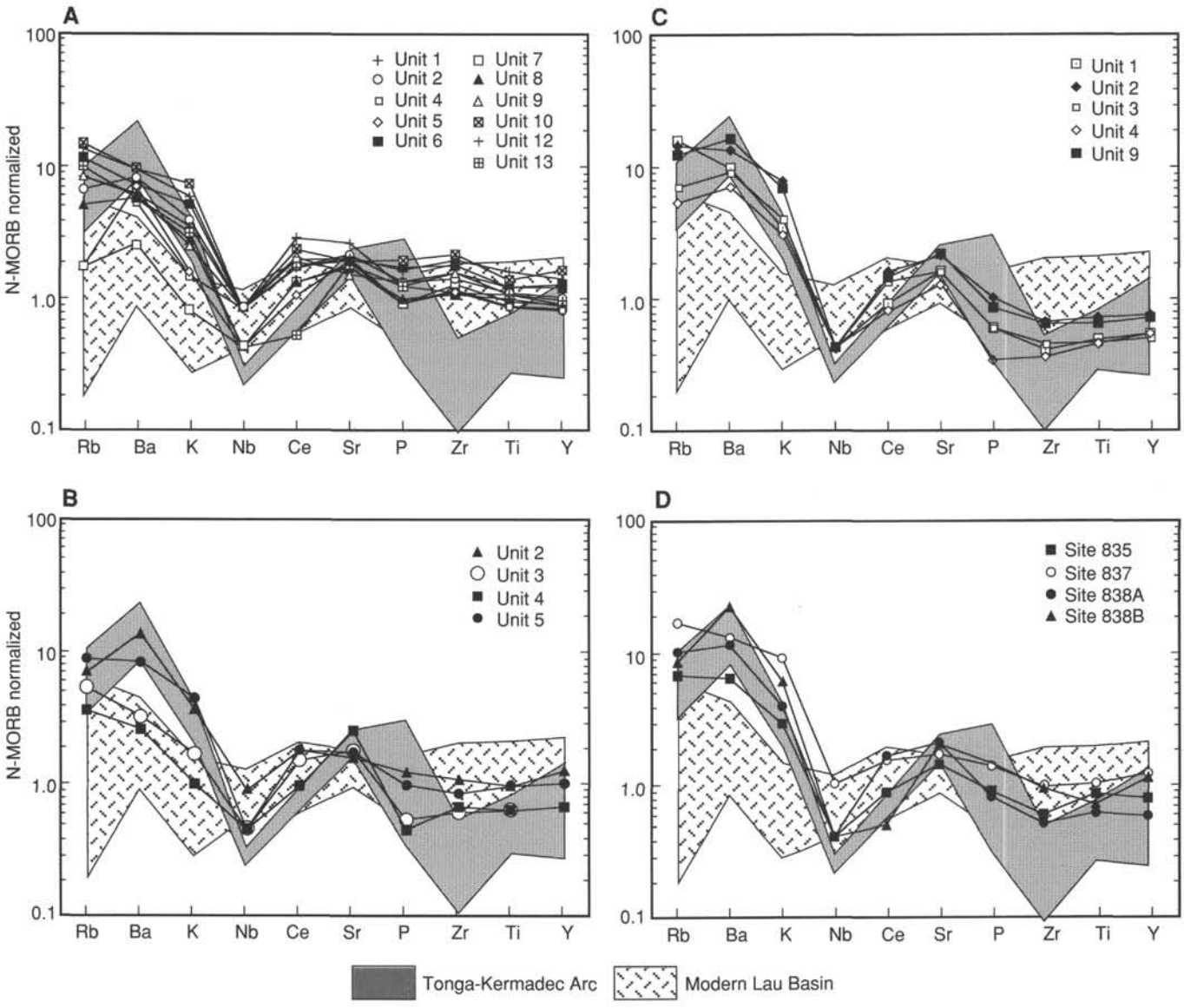


Figure 18. Average compositions of incompatible elements in igneous units from Leg 135 backarc sites normalized to values for N-MORB (from Sun and McDonough, 1989). **A.** Site 834. **B.** Sites 835, 837, and 838. **C.** Site 836. **D.** Site 839. Reference fields for modern Lau Basin and Tonga-Kermadec lavas from Ernewein et al. (in press) and Ewart and Hawkesworth (1987).

the basin opened. Drilling results show that there is no simple change in the chemical composition in space or with time. The erupted volcanic rocks vary from more "arc-like" to more "MORB-like," but the oldest basalts (recovered at Site 834 in the western basin), which presumably were erupted during the earliest stages of backarc rifting, are closer to normal MORB in composition, and to basalts that form at the present axial rift zones of the basin, than any of the samples from the other drill sites. The drill sites in basins with the youngest basement ages in the central Lau Basin have trace and minor element signatures that are more arc-like and are intermediate to those of normal MORB and the modern Tofua Arc. The most distinctive chemical signatures in the intermediate rocks are enrichments in Rb, Ba, and K, and pronounced depletion in Nb. Basaltic andesites and basalts recovered at Site 839 are the most arc-like recovered and show the most extreme relative enrichments in alkalis and alkaline earth elements. They resemble, respectively, the modern Tofua Arc basaltic andesites and the island-arc tholeiitic basaltic lavas thought to be parental to the more evolved rocks of the Tofua Arc (Ewart and Hawkesworth, 1987).

### *Tectonic Setting and Ages*

All six sites in the backarc were drilled in roughly north-trending sub-basins. Sites 834 and 835 are located along a latitudinal line at 18°30′S, west of the CLSC. Sites 836 and 837 were drilled in the central Lau Basin at about 20°10′S, and Sites 838 and 839 were drilled in the same sub-basin near 20°45′S. Sites 836, 837, 838, and 839 are all located west of the present ELSC.

Crust drilled at Sites 834 and 835 in the northwest portion of the basin has the oldest basement ages. Minimum basement ages are 4 Ma at Site 834 and 3.5 Ma at Site 835 (Fig. 10). Sediments interbedded with lavas at Site 834 confirm that volcanism was active at least 5.6 m.y. ago. The four sites drilled between 20° and 21°S are closely spaced in longitude and indicate a consistent younging eastward (Fig. 19). Basement was not recovered at westernmost Site 838, although the oldest sediments recovered

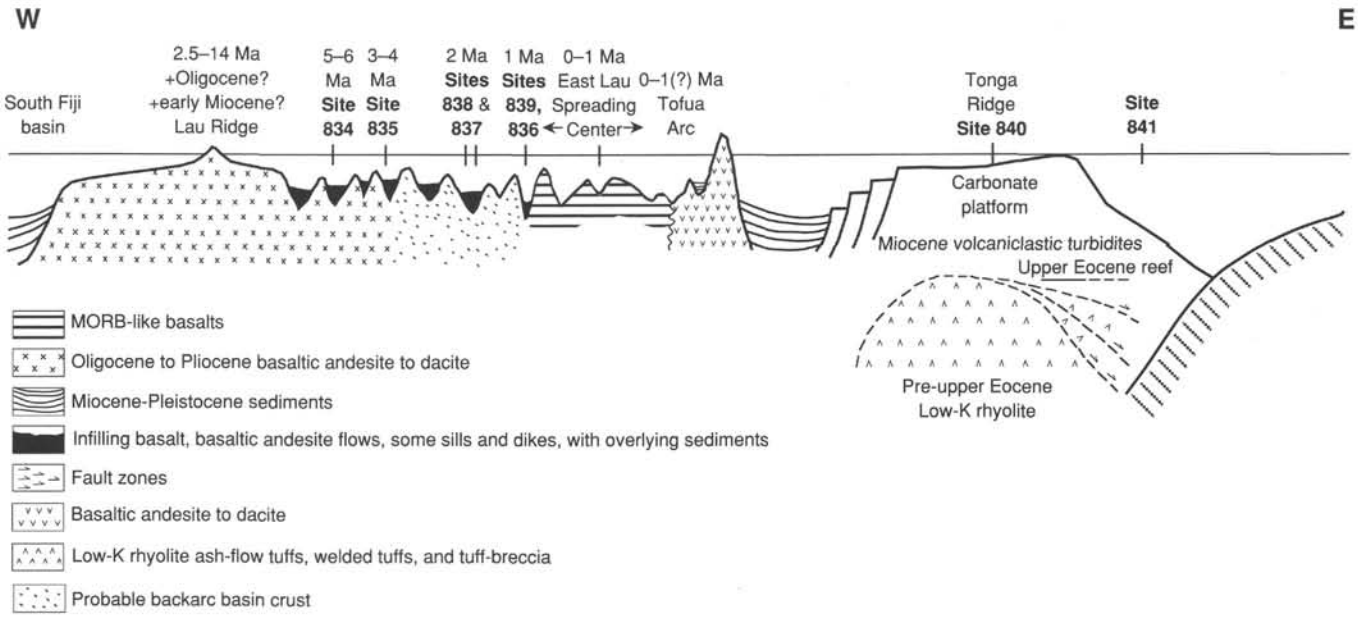


Figure 19. Schematic west-east cross-section across the Lau Basin, Tofua Arc, and Tonga Ridge. Depth and vertical dimensions are not to scale, but horizontal dimensions are to scale.

there require that volcanic basement be older than 3 Ma. The minimum basement ages at the other sites range from 0.7 Ma at Site 836 to 2.0 Ma at Site 837 (Fig. 10). Site 836 is nearly on the same north-south line, but it is more northerly and its basement is 1 m.y. younger than at Site 839. The very large-scale basin and ridge topography suggests that the rifting proceeded in a manner more akin to continental rifting than to normal seafloor spreading. The basement ages at the drill sites indicate sequential magmatic episodes younging eastward. However, neither these basement ages nor the regional magnetic anomaly patterns should be used to estimate rates of seafloor spreading during the early history of Lau Basin opening.

The cessation of volcanism at all of the sites was followed by a period of rapid sedimentation with a significant volcanic gravel, sand, or silt component (Fig. 20). This suggests that all of the basins continued to subside for some time after the end of volcanic activity. The volcaniclastic debris appears to be arc-derived (based on silica contents and trace element analyses). That such arc-derived debris occurs from 4 to 0.7 Ma at the different sites (Figs. 19 and 20) indicates that throughout the development of the Lau Basin there was synchronous arc volcanism within the basin or along its margins.

### *Petrologic and Geochemical Variability*

#### *Major Element Geochemistry*

The various units recovered in Holes 834–839 represent a remarkably diverse group of magma compositions, ranging from high-MgO olivine and quartz normative tholeiites through olivine and quartz normative tholeiites, to basaltic andesite, andesite, and low silica (low $K_2O$) rhyolitic pumices. The generalized compositions from each hole are presented in Figure 21 in terms of the normative Ol-Di-Hy-Q system ($Fe_2O_3/FeO = 0.2$). The data define a broad field extending from the basaltic andesites and andesites through to the olivine tholeiite field of Site 836, Unit 4, the most chemically undersaturated lava encountered. In Figure 21, there is a clear displacement of the strongly olivine phyric Units 3 and 6 from Site 839, relative to the other fields. The remarkable feature of these highly magnesian compositions, however, is that they are only mildly olivine-normative. In fact, the associated magnesian Unit 4 (Site 839), which is nearly aphyric in the hand specimen (olivine + clinopyroxene microphenocrysts) is quartz normative. These high MgO, relatively high $SiO_2$ units encountered at Site 839 are considered significant as they may be parental to the more siliceous quartz tholeiites and basaltic andesites recovered at this same site. Data fields for Site 839 again lie on a linear trend projecting away from the olivine composition (Fig. 21).

Major and minor element comparison of the chemistry of the sites is provided by Harker diagram plots (Fig. 22). An obvious feature in all of these plots is the chemical distinction between Sites 834 and 839. Sites 835 and 836 consistently plot close to the Site 834 data, whereas the unit from Site 837 is closest to the basaltic andesites of Site 839.

The behavior of individual elements on these diagrams provides insights into possible phase controls on the liquid compositions and also suggests likely primary magmatic differences (and presumably source differences). The most striking variations are shown by MgO and $Al_2O_3$. The MgO vs. $SiO_2$ (Fig. 22) clearly shows the high MgO and yet high $SiO_2$ characteristics of Units 1, 3, 4, and 6 in Site 839. This is unmatched by the lavas in any of the other sites. $Al_2O_3$ decreases with increasing $SiO_2$ at all sites (Fig. 22) except at Site 839, which shows a distinct positive correlation. The most obvious explanation of the Site 839 trends, fully in accord with the previously discussed phenocryst assemblages, is that olivine is the major fractionating phase, with minor clinopyroxene, within the high MgO lavas of Site 839, resulting in increasing $Al_2O_3$ during fractionation. Interestingly, the basaltic andesites of this site seem to fall precisely at the high $Al_2O_3$ termination of this trend. Comparison of the CaO vs. $SiO_2$ plot with the $Al_2O_3$ plot shows that the olivine-rich Units 3 and 6 of Site 839 are low in CaO compared with the clinopyroxene–olivine-bearing Unit 4; this may indicate an increase and then a decrease of CaO with increasing $SiO_2$, related to the incoming of clinopyroxene after olivine. The remaining units at this site, as indeed in the other sites, exhibit a regular negative correlation of CaO and $SiO_2$, consistent with plagioclase and clinopyroxene (± olivine) controlled fractionation. Iron enrichment (expressed as $Fe_2O_3$ in Fig. 22) is characteristic of the lavas at most sites. This is consistent with the generally observed absence of Fe-Ti oxides

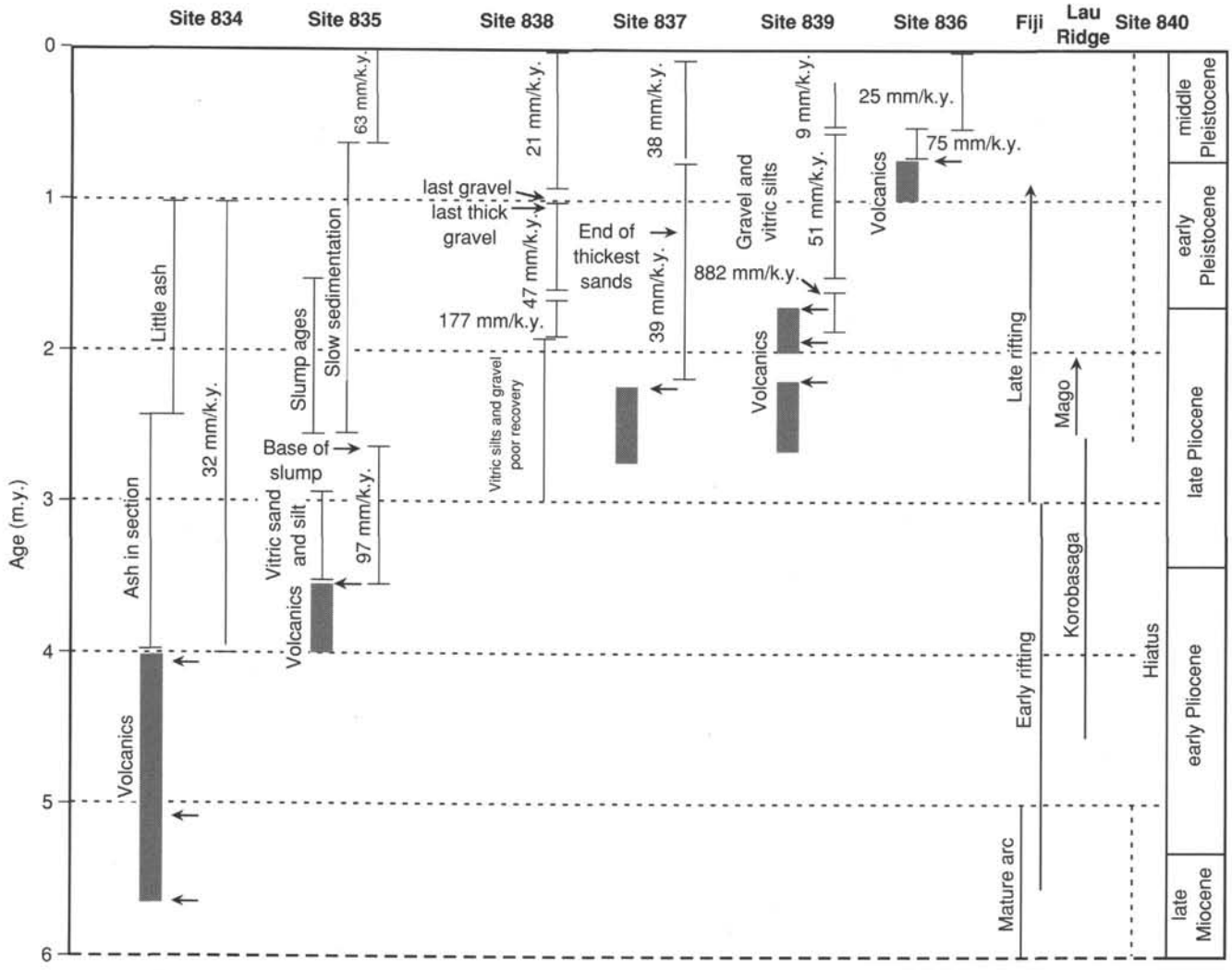


Figure 20. Timing of principal events in sites from the Lau Basin. Arrows along the volcanic intervals indicate where there are biostratigraphic age controls. Several of the volcanic units are separated by datable interbedded sediments. Sedimentation rates and sediment characteristics are taken from "Biostratigraphy" and "Lithostratigraphy" sections of the relevant chapters. Age ranges for volcanism on Fiji and the Lau Ridge are taken from Cole et al. (1985) and Whelan et al. (1985). The Korobasaga Group on the Lau Ridge is equivalent to the early rifting volcanics of Fiji; the Mago volcanics to the late rifting series. Dashed line indicates occurrence of volcanic debris in the recovered section at Site 840 on the Tonga platform; there is a long hiatus from 2.6 to 5 Ma in this hole.

in the phenocryst and microphenocryst assemblages. Units 3 and 4 of Site 836, which exhibit Fe depletion with increasing $SiO_2$, are exceptions.

The remaining elements ($Na_2O$, $P_2O_5$, $K_2O$, and $TiO_2$) show similar increases with $SiO_2$, illustrating their incompatible behavior. Of particular note are the relatively higher abundances of $Na_2O$, $P_2O_5$, and $TiO_2$ (for given $SiO_2$) of the Site 834 rocks, and their low concentrations in Site 839, indicative of important chemical differences in their respective sources. The basaltic and basaltic andesites are, as a group, relatively low $K_2O$, but positive correlations with $SiO_2$ are well defined, as are the intersite differences.

*Trace Element Geochemistry*

Trace element signatures of all Leg 135 samples show moderate to strong Rb, Ba, and K enrichments coupled with various degrees of depletion in Nb, Zr, Ti, and Y. In this respect, they more closely resemble island-arc magmas than typical mid-oceanic-ridge basalts (N-MORB). Figure 18 illustrates the average incompatible trace element concentrations normalized to N-MORB for each of the units defined at each site. Pattern shapes defined on these diagrams should not be affected by fractional crystallization and are likely to reflect variations in the mantle sources of these rocks. Detailed examination reveals subtle, yet significant, differences in incompatible element concentrations and ratios in the rocks of the various units. To facilitate comparisons, shaded regions for the range in modern Lau Basin basalts and Tonga-Kermadec arc compositions are included. Site 834 has the least enrichment in large-ion-lithophile elements (LILE: Rb, Ba, and K) and the least degree of depletion in high-field-strength elements (HFSE: Nb, Zr, Ti, and Y) and most closely resembles N-MORB (a horizontal line at 1 on these diagrams, Fig. 18). At the other extreme, rocks from Site 839 have lower HFSE contents and show pronounced enrichments in the LILE and most closely resemble rocks from the modern Tofua Arc. The composition of

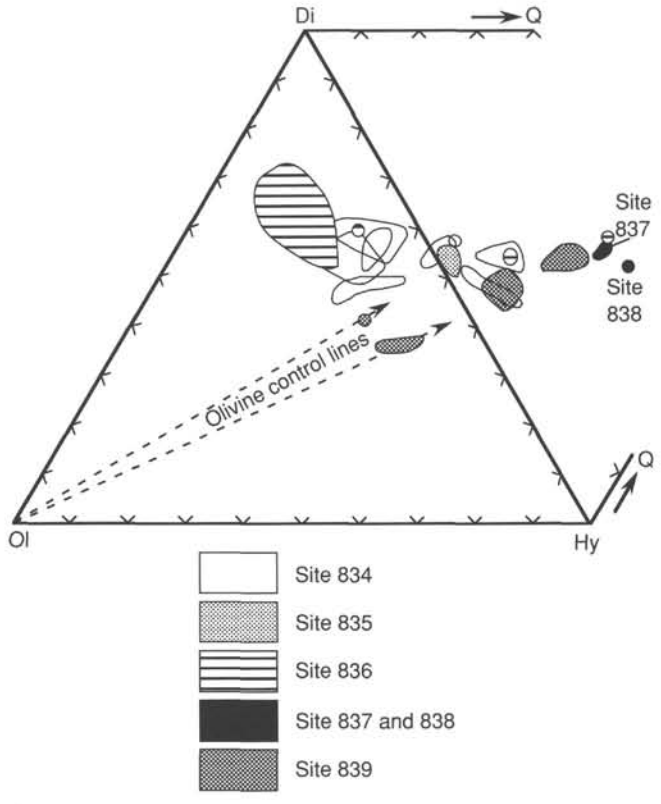


Figure 21. CIPW normative Ol-Di-Hy-Q for Leg 135 backarc sites. Calculated with $Fe_2O_3/FeO = 0.2$.

rocks from the remaining sites show signatures intermediate between the extremes defined by Sites 834 and 839.

Incompatible element signatures of these rocks are further illustrated in Figure 23, where the elements (or ratios) on the axes have been chosen to best discriminate island-arc signatures from those typical of N-MORB. In each of these plots, the Site 834 compositions plot within, or overlap, the fields defined by N-MORB, whereas those from Site 839 clearly overlap the Tonga-Kermadec field. The remaining sites tend to be in intermediate positions, as are volcanics from the modern Lau spreading centers. The plot of Zr/Nb vs. Zr/Y (Fig. 23) suggests that the Site 834 rocks have some trace element characteristics intermediate between island-arc magmas and N-MORB. Although they are somewhat displaced to MORB-like Zr/Y, the Site 834 rocks plot toward higher Zr/Nb values, more typical of the arc field. These ratios are also potentially useful in highlighting melting and source differences. Increasing Zr/Nb is an indication of higher degrees of melting and/or increased source depletions, whereas increased Zr/Y is correlated with lower degrees of melting and/or increasingly enriched mantle sources. Thus, the general decrease of Zr/Y ratios from Sites 834 to 839 may well reflect an increasingly depleted mantle source.

*Vesicularity*

All of the volcanic rocks recovered in the backarc basin drill sites are highly vesicular. This feature is shared by dredged rocks from the CLSC and ELSC as well as nearly all parts of the Lau Basin (e.g., Hawkins, 1976; Hawkins and Melchior, 1985). The reason for this is their high content of volatiles, that is, $H_2O$ and $CO_2$ with $H_2O$ being more abundant. The majority of the drill-site samples have 10%–30% vesicles (Fig. 24), with >40% vesicles in some rare samples. Only Unit 7 at Site 834 is nonvesicular. Glassy margins in all units tend to be either nonvesicular or poorly vesicular, indicating that most vesiculation occurred rapidly after eruption and during the lava flow.

Many larger vesicles (up to 10 mm), usually elongated and in some cases forming vesicle pipes and trails, are partially infilled by very dark gray, highly vesicular, aphyric, quench-textured basalt. These fillings also are characterized by the development of fairly large and usually irregular vesicles, and their degree of vesiculation is much higher than that of the host lavas, in many cases reaching >70 vol%. These dark infillings may be highly vesicular analogs to the segregation vesicles described by Smith (1968) that are common in deep-sea basalts (e.g., Sato, 1978). Similar vesicles have recently been described in lavas from the Troodos ophiolite (Bednarz et al., 1987). In this interpretation, late-stage interstitial melt (partially fractionated chemically) is squeezed into preexisting vesicles; presumably volatile enrichment in the late-stage melt results in the high degree of vesiculation in the segregations. Although partial infillings of low-temperature alteration products/zeolites are variously present in vesicles within many units, the segregation vesicles, where present, are usually remarkably free of secondary mineral deposition.

Recent measurements of volatile abundances in Lau and North Fiji Basin low-$K_2O$ backarc basaltic glasses (Aggrey et al., 1988; Newman, 1989) indicate $H_2O$ and $CO_2$ contents of 0.14%–1.4% and 0.07%–0.17%, respectively. Volatile contents are even higher in the more K-enriched and less MORB-like basalts. At the water depths in which the Leg 135 backarc sites were drilled (approaching 3000 m, or approximately 300 bars) volatile concentrations at the higher end of these ranges would be required to produce the observed levels of vesicularity (i.e., >1% total $H_2O$ and $CO_2$; MacPherson, 1984). Significantly, the almost complete absence of sulfides within vesicles seems to indicate that sulfur contents were below saturation levels in the volatile phase.

***Regional Comparisons***

It is useful to compare the compositions of the drilled rocks with the volcanics of the modern Lau Basin spreading centers. Although the data for the modern Lau Basin rocks show somewhat more scatter than is exhibited by the trace element compositions of individual drilled sites, the trace compositions from Sites 835–839, as well as the modern Lau Basin rocks, for the most part are distinct from N-MORB. Chemical data for representative modern Lau Basin (Hawkins and Melchior, 1985; Ernewein et al., in press), Tofua and Kermadec arcs (Ewart et al., 1977; Ewart and Hawkesworth, 1987), and the major units occurring in Sites 834–839 are summarized in Table 1. A comparison of the selected lava compositions among the sites reinforces the previous discussion of the main differences and gradations found between Sites 834 and 839. A particularly significant comparison is that between the basaltic andesites of Site 839 (Unit 9) and those of the Tofua-Kermadec arc. Their similar geochemical signatures are matched by the similarity of phenocryst assemblages (plagioclase-clinopyroxene-orthopyroxene) previously described. Further comparisons will need to await detailed analyses of trace elements and mineral phases, but it is already clear that not only do lavas with chemical and mineralogical arc affinities exist within the central Lau Basin, but that the Unit 9 lavas at Site 839 are almost indistinguishable from the Tonga-Kermadec arc lavas. This, coupled with the chemical signatures gradational between MORB-like and arc-like observed in the rocks from Sites 834–839, emphasizes that such geochemical characteristics are not confined to the active Tofua Arc as has been traditionally supposed. Moreover, the age range of the volcanic sequences at Sites 834 through 839 indicate that these geochemical features, interpreted as primary source characteristics, have evolved with the developing Lau Basin over the past 4–5 m.y. (minimum age of Site 834).

The Leg 135 data tend to exhibit a generalized, but not regular spatial (i.e., northwest to southeast), increase in the development of arc-like geochemistry. It is, therefore, important to note that the samples dredged from the neovolcanic zones associated with the spreading centers of the central Lau Basin (Ernewein et al., in press), as previously noted, exhibit increasing subduction-type chemistry both eastward toward the ELSC and southward along the ELSC to the Valu Fa Ridge (i.e., toward the Tofua Arc axis). In contrast, Hawkins and Melchior (1985) and Volpe et al. (1988) presented data supporting the inference that, except for Sr isotopes, the CLSC has a strong MORB-like signature. However, none of the lavas analyzed from the ELSC show the degree of resemblance to the Tofua basaltic andesites as do the Site 839 volcanic rocks (minimum age approximately 1.7 Ma). This can be clearly seen, for example, by comparing the average compositions of the Tofua basaltic andesites with similarly silica-enriched lavas from the ELSC (Sample CD33–D25; Table 1). Thus, it is possible that the current ELSC volcanism reflects a gradual reverse shift away from arc-like geochemical imprints toward N-MORB. Previous studies in the northern and central portions of the Lau Basin suggest that it is floored by MORB-type oceanic crust (e.g., Hawkins and Melchior, 1985; Volpe et al., 1988) with little, if any, contribution from the subducted slab. Comparison of the major element compositions (Table 1) of the T-type basalts from these areas, however, reveals some marked similarities with the Kermadec arc basaltic andesites (Ewart et al., 1977; Ewart and Hawkesworth, 1987; Cole, 1982), although trace element differences are clearly apparent.

The available data demonstrate the complexity and heterogeneity of the Lau Basin mantle sources, as previously suggested by Hawkins and Melchior (1985) and Volpe et al. (1988). The results from Leg 135 show even greater diversity than previously recognized. The tectonic implications of the recognition of arc-like, and "near-arc-like," lavas within the southern to central Lau Basin and the implication of a long, continuous dynamic interchange between the Lau Basin mantle and the subduction zone (the presumed source of the "arc-like" geochemical signatures) remains to be explored. One possibility, however, is an eastward migration of the Tofua Arc over the past 3 or more m.y., concurrent with the evolving Lau Basin.

A further aspect of petrological interest is the recovery of the high MgO–high $SiO_2$ tholeiites (Unit 3, Site 839), certainly candidates for possible parental "arc-like" magmas, as previously noted. These are quite distinct from the high-MgO lavas from the Intermediate Lau Spreading Center (ILSC), the short active spreading-ridge segment lying between the southern end of the CLSC and the northern end of the ELSC (Fig. 1 and Table 1; Sample CD33–D18; Ernewein et al., in press). Moreover, they possess the "arc-like" trace element imprints, which are not as well developed in the ILSC lavas. Compared with the calculated parental magma composition of the Mariana Trough and north-central Lau Basin (table 12 in Hawkins and Melchior, 1985), the Unit 3 lavas (Site 839) are lower in Ti, Al, Fe, and Na and higher in MgO, Cr, and Ni, although similar in $SiO_2$ to their more silica-rich compositions. Thus, the Unit 3 lavas may be considered even more "primitive" than the calculated model compositions and, in certain respects, may even be considered as becoming intermediate toward boninitic compositions.

It should be noted that silicic pyroclastic materials have been encountered at all sites and range from Pleistocene to late Miocene in age (see individual site reports, this volume). Pumice clasts from Sites 837 through 839 are low-$K_2O$ rhyolites with trace element abundance patterns showing the same "arc-like" or "near-arc-like" features as found in the basalt and basaltic andesite lavas from Sites 836 to 839 (based on three XRF analyses). The origin and sources of these rhyolitic rocks are unknown, but the pumices clearly document a hitherto unrecognized and continuous silicic volcanism throughout the evolution of the Lau Basin. The source of this volcanic material may well have been the Lau Ridge or the Tofua Arc; however, silicic rocks are known on Zephyr Shoal and on the Valu Fa Ridge, and arc-like andesites were drilled at Site 839. Therefore, an intrabasin source is also a possibility.

### *Alteration*

The secondary minerals determined at Sites 834 through 839 are listed in Table 2. The most prominent are clay minerals, smectite coated by iron-hydroxide (palagonitization of volcanic glass), iron-hydroxide stains and calcite in veins, and aragonite forming radiating crystals in cavities. Zeolites are less common, occurring as partial infillings of vesicles and miaroles. Celadonite(?), talc, quartz, opal(?), and analcime/chabazite(?) are of minor abundance and appear only occasionally in the sections.

Clay minerals (mainly of the smectite group, identified by X-ray diffraction analyses) appear throughout the rocks, either locally replacing the mesostasis or as a partial alteration product of olivine. In addition, vesicles are partially lined by green to bluish gray clays often extending to either side of an alteration front. To a lesser extent, clays also occur as vein fillings and fracture coatings.

Iron-hydroxide staining is most common on fractures and in vesicles. It is also produced during smectite formation from volcanic glass (palagonization). Smectite that is stained yellow to pale green forms vesicle linings and often shows a spherical texture with radiating extinction under crossed nicols.

Aragonite and calcite only occur in rocks from Sites 834, 836, 838, and 839, where interbedded sediment layers have been recovered or recorded during logging. Aragonite appears as acicular pseudohexagonal shapes, sometimes with radiating crystals up to 1 cm in length. These are elongated parallel to the c-axis and grow in large cavities, whereas veins are filled by calcite.

Although they are minor constituents, zeolites are widespread throughout the cores as vesicle fillings and miaroles. They exhibit acicular, globular, platy, and cubic shapes. Crystals differ in color from clear and transparent to white, yellow, and sometimes light red. Optical properties indicate that phillipsite is the major zeolite, but natrolite and other zeolites may also be present.

The formation of quartz on fractures and the probable presence of cryptocrystalline silica (opal?) as patches on the surface of rock samples from Site 838 can be related to an elevated $SiO_2$ content in the overlying sediment column. Here, dissolved $SiO_2$ is four times higher than measured in other holes (see "Inorganic Geochemistry" section, this chapter). The high dissolved silica may be a result of the high temperature gradient in the sedimentary sequence (8.7°C/100 m; see "Downhole Measurements" section, this chapter).

Traces of other minerals have been observed only locally in samples from Sites 834 (celadonite, stilpnomelane) and 839 (talc, analcime/chabazite). Dark green celadonite appears as a devitrification product in vesicles. White analcime/chabazite was observed partly filling vesicles and replacing the groundmass in a few samples of Unit 1 in Site 839. On a fracture of a single hand-specimen of the same unit, talc could be identified, exhibiting an unusual white, soft, globular form.

The least altered rocks occur in Units 2–9 of Site 839. Here, the localized breakdown of volcanic glass is the only observed alteration feature, accompanied by an early stage of yellow smectite and minor iron-hydroxide formation.

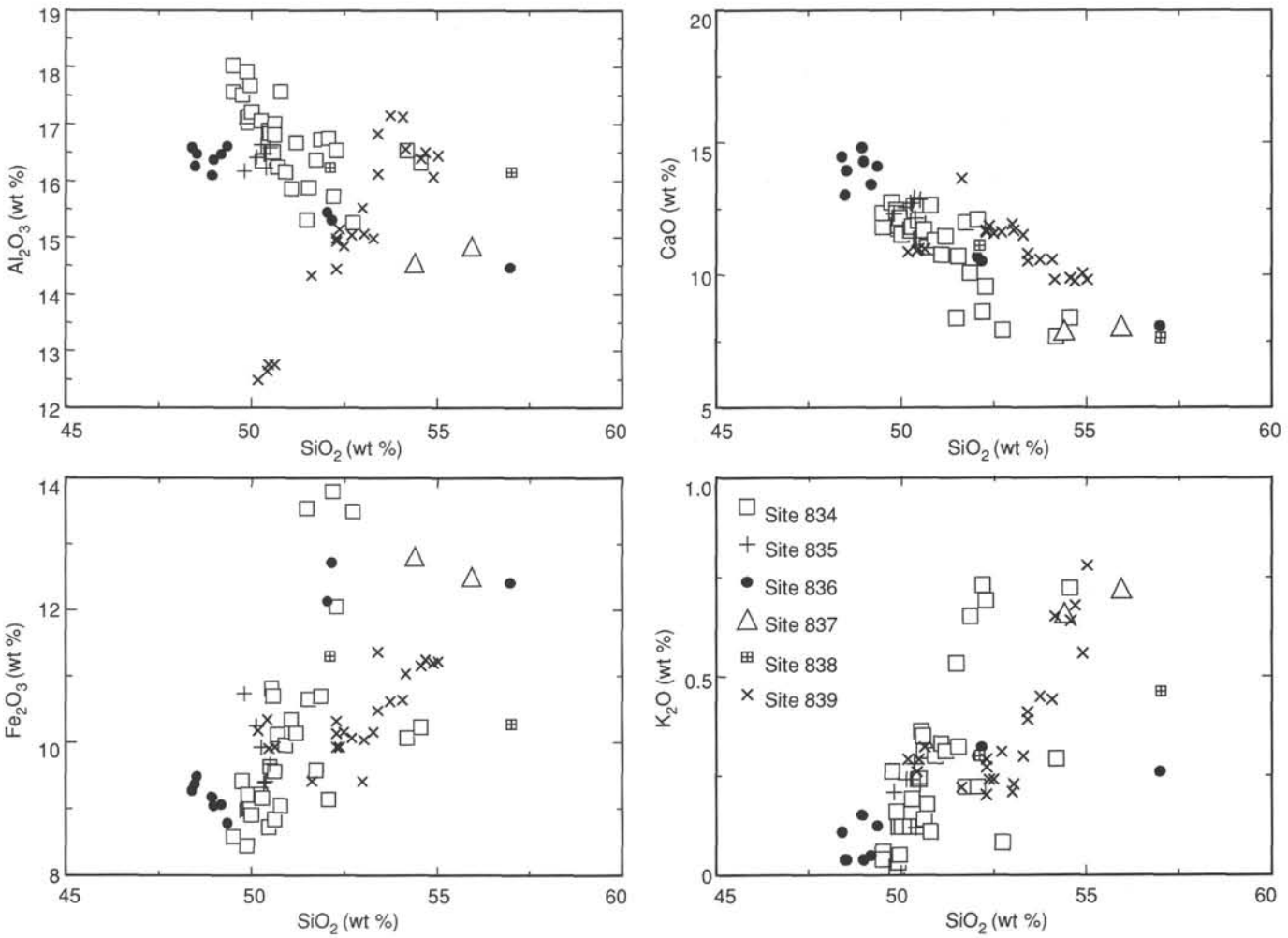


Figure 22. Harker diagrams for volcanic rocks from Leg 135 backarc sites. All oxides in weight percent.

### *Arc and Forearc Summary*

#### *Sites 840 and 841 Summary*

Site 840 is located on the Tonga Ridge between Tongatapu and Ata, and Site 841 is located near a trench-slope break approximately 30 km west of the axis of the Tonga Trench and 60 km east of the crest of the Tonga Ridge at a water depth of 4825 m. One of the principal objectives at both sites was to recover a sequence of volcaniclastic sediments spanning the Eocene to the Pleistocene volcanic history of the Tonga region. Volcaniclastic and lithic sediments of middle Pleistocene, upper Miocene, lower middle Miocene, lower Oligocene, and upper Eocene age were recovered. The initial sedimentologic and biostratigraphic data do not show any obvious, long hiatuses in arc volcanism in the region. The recovered materials include basaltic andesites to siliceous pumices. Shore-based investigations of their compositions should provide some detailed constraints on the chemical and petrologic evolution of the arc since the latest Eocene.

The second major objective of forearc Site 841 was to determine the age and composition of the forearc basement. In particular, determining the identity of the basement was critical for testing hypotheses for the origin of the forearc as a trapped fragment of old oceanic crust or as an Eocene arc volcanic complex equivalent to the basement on 'Eua.

Two major igneous sequences were recovered from Hole 841B. The first (Unit 1, 324.76–497.68 mbsf) is a sequence of nine basaltic andesite intervals within upper Miocene and lower middle Miocene volcanic siltstones and sandstones. The contacts between the basaltic andesites and sediments include chilled margins in the volcanics, hyaloclastite breccias, and indurated sedimentary material, all suggesting intrusion of the volcanics into the sedimentary pile. Chilled margins suggest intrusion as relatively steep dikes and flatter lying pillows or possibly sills. Their occurrence in upper Miocene sediments indicates that volcanism and heating is possible in forearc regions much later in the history of an arc than has generally been recognized. The basaltic andesites are extensively veined. Thaumasite, and a suite of sulfide minerals including mainly pyrite with lesser marcasite and chalcopyrite, fill the veins. The pyrite in the veins has abundant silicate inclusions and is rimmed by at least two generations of marcasite. Pyrite and chalcopyrite also occur as secondary sulfide minerals in the ground mass. Prehnite is a common secondary mineral in the sediments intruded by the basaltic andesites.

The second major igneous sequence recovered at Site 841 (Units 2 through 6, 605.05–815.1 mbsf) comprises a series of low-K rhyolites, rhyolitic tuffs, breccias, welded tuffs, and lapilli tuffs and appears to constitute volcanic basement in this part of the forearc. Evidence for welding in some of the rhyolitic clasts and tuffs and the complete absence of interbedded sediments and

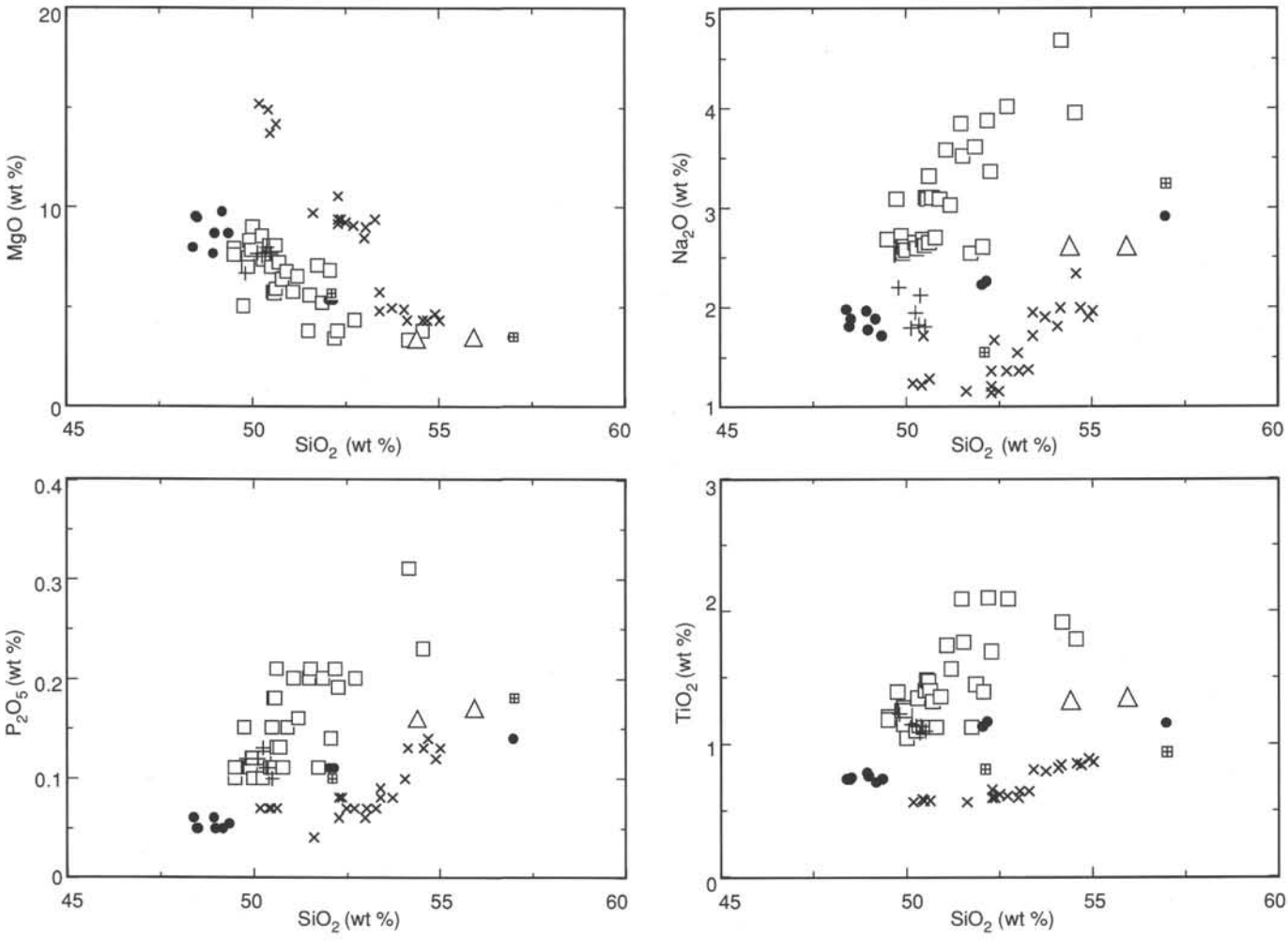


Figure 22 (continued).

fossil flora or fauna indicate subaerial emplacement. The silicic rocks are structurally overlain by upper Eocene shallow-water calcareous volcanic sandstones with reef fauna (approximately 38 Ma). The eruptives are predominantly low-$K_2O$ rhyolites; they generally have lower Ba contents than do similar high-$SiO_2$ pumices from the modern Tonga Arc (Hawkins, 1985) and pumices in Miocene to Pleistocene sediments recovered at Site 840. The rhyolitic breccias are locally kaolinitized and illitized, accompanied by extensive disseminated sulfide mineralization. Pyrite, occasionally with pyrrhotite inclusions, is the dominant ore mineral. In the lowermost part of the section, magnetite(?) was observed rimming pyrite and filling cracks.

The identification of these rhyolitic eruptives is important in several regards. First, their inferred subaerial origin indicates that this portion of the forearc was at or above sea level when erupted and has subsequently subsided over 5000 m. The age of eruption is not known, but the oldest sediments overlying the rhyolitic volcanics are of late Eocene age. These late Eocene calcareous volcanic sandstones are probably faulted against the volcanics but they contain abundant rhyolitic debris that must have been eroded from a nearby source. The absence of any older reworked fauna, the lack of any flora or fauna within the volcanic sequence, and the lack of any radiometric or biostratigraphic ages older than mid-Eocene from any part of the Tonga Ridge, forearc, or Trench all suggest that the upper Eocene is a reasonable minimum age for the rhyolitic volcanic complex.

This thick, high-$SiO_2$ eruptive complex is unusual in an intraoceanic island arc. High-silica rocks do occur in the Pacific (e.g., on Saipan and in the Mariana forearc; Meijer, 1982; Bloomer, 1983), but most are dacitic and few form true ignimbritic complexes. There are two hypotheses that we have considered for the origin of this low-K rhyolitic complex. The first is that they are part of a mid-Eocene volcanic complex that formed during the initial phases of subduction in the Tonga system. This arc platform then formed the foundation for the Tonga platform and Lau Ridge.

Although intraoceanic arcs may indeed produce high-$SiO_2$ eruptives, perhaps in part by remelting or older arc material, the position and composition of the forearc basement rocks raises the intriguing second hypothesis that the Site 841 silicic complex is related to similar rocks from rhyolitic complexes in northeastern Australia and the Lord Howe Rise in the Tasman Sea. In DSDP Hole 207 on the Lord Howe Rise (Burns and Andrews, 1973), 140 m of Late Cretaceous (93.7 ± 1.2 Ma) rhyolitic lavas was encountered. The rhyolites, tuffs, and fragmental rocks are interpreted as having formed subaerially or in shallow water (van der Lingen, 1973). The bottom of the rhyolitic series was not reached; they are overlain by Upper Cretaceous (Maestrichtian) silty claystone deposited in a shallow-marine environment (van der Lingen, 1973; Burns and Andrews, 1973). Cretaceous rhyolites are also recorded from New Caledonia (Paris and Lille, 1977). The Lord Howe Rise and New Caledonian sequences are both overlain by

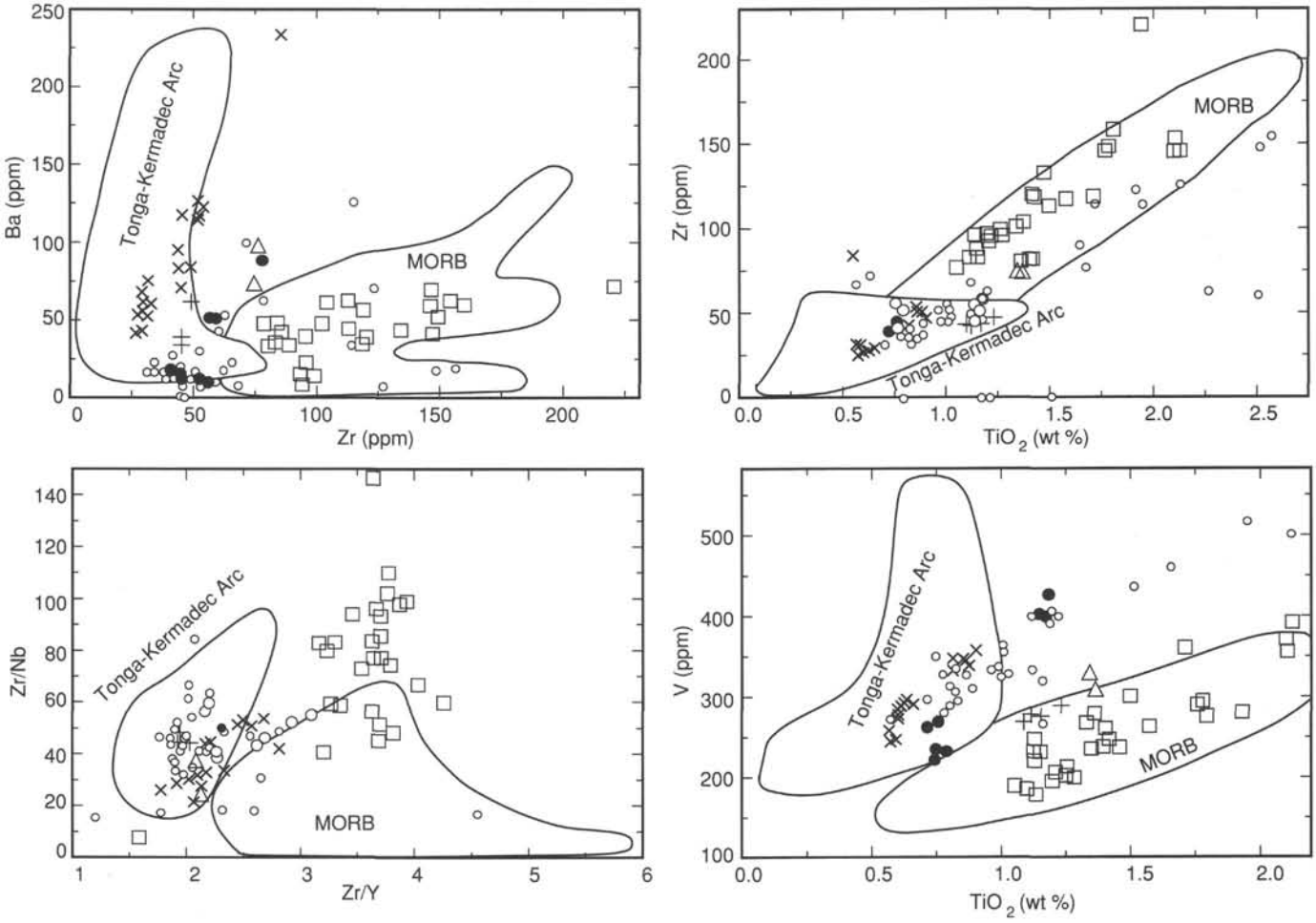


Figure 23. Incompatible element variation diagrams for volcanic rocks from Leg 135 backarc sites. Reference field for Tonga-Kermadec arcs is from Ewart and Hawkesworth (1987); MORB fields are based on reference sources in Sun and McDonough (1989). Small open circles are values for Lau Basin volcanics from Ernewein et al. (in press); other symbols as in Figure 22.

dolomite and shallow-water detrital sediments of Coniacian-Campanian age (89–72 Ma; Paris and Lille, 1977). Both of these occurrences are interpreted as associated with the formation of a small rift basin along the extension of the present eastern Australian coast, which preceded the break-up of eastern Australia and the opening of the Tasman Sea (Wilcox et al., 1980).

The occurrence of such a Cretaceous crustal fragment in the Tonga forearc would require a major reevaluation of tectonic models for the Southwest Pacific. Both the Australian and Tasman Sea occurrences are Cretaceous in age, however. As no fossiliferous horizons were encountered within the Site 841 rhyolitic units, their age is unknown, except as pre-upper Eocene. Moreover, no fauna or flora older than the upper Eocene have been identified anywhere in the Tonga region (e.g., Vallier et al., 1985; Cawood, 1985).

## Physical Properties

### *Index Properties and Compressional Wave Velocity*

Physical property gradients of sediments sampled in the Lau Basin, particularly at Sites 834 through 837, were negligible within the sediment column. Observed variations in physical properties were related to distinct changes in lithology. For example, the nannofossil ooze recovered in the backarc sites displayed a constant density of about 1.5 g/cm$^3$, water contents and porosity of about 120% and 80%, respectively, and compressional wave velocities of about 1500 m/s. Turbidite layers showed significantly greater values in both density and compressional wave velocity; vitric ash layers were marked by lower bulk density. Sites 838 and 839 showed considerably more variation in physical properties than the earlier backarc sites because the lithologies recovered were more varied. Nannofossil ooze was the dominant lithology recovered at all sites, but Sites 838 and 839 had a larger percentage of silt and sand interbeds within the nannofossil ooze than the backarc sites. Water content (and related properties) correlated positively with the carbonate content of the sediments. Nannofossil ooze, the dominant lithology, had a higher water content, porosity, and void ratio and a lower compressional wave velocity than did silts and sands, which resulted in oscillating values of index properties and compressional wave velocity.

The absence of physical property gradients within the sediment column and, in the case of Site 835, an increase in water content, porosity, and void ratio and a decrease in density values below 150 mbsf suggest that the fluid is carrying a significant portion of the overburden load, thus preventing normal consolidation of the sediment in the backarc sites. In addition, the high water content of the sediment below 150 mbsf and above the basalts in Site 835 suggest that fluid is migrating laterally between the sediment and basalt.

Changes in density and velocity of the basalts sampled in the Lau Basin are related to the degree of vesicularity and, therefore, the effective porosity of the basalts. Basalt velocities measured

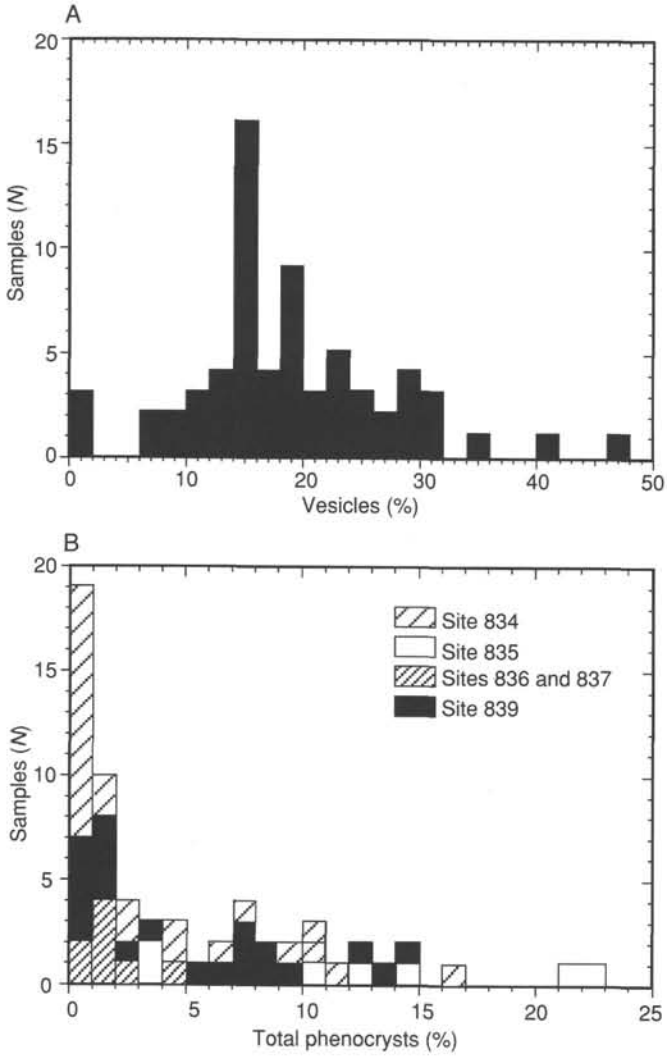


Figure 24. **A.** Vesicularity distribution in volcanic rocks from the Lau Basin based on point-counted modal data on 62 samples. **B.** Summary of phenocryst percentages in volcanic rocks from the Lau Basin based on point-counted modal data.

on discrete samples ranged from 3600 to 4500 m/s in vesicular basalts and from 4500 and 5400 m/s on very dense basalt samples. All of the basalts were isotropic with respect to velocity.

At Sites 840 and 841, the rapid lithologic changes in the turbidites lead to wide variations in index properties and compressional wave velocity. At Site 840, the turbidite signature was a gradual increase upward in velocity, density, and related properties in marked contrast to the usual decreasing upward values found in sand-shale turbidites. The increasing-upward values are a consequence of the large grain-size fraction predominantly composed of vitric and pumiceous volcanic grains with large pore spaces.

One of the primary goals of drilling Site 840 in the Tonga forearc was to penetrate a horizon identified on seismic reflection data as an unconformity. The horizon was mapped at about 0.4 to 0.45 s TWT at the drill site. This reflector, termed Horizon A, was presumed to mark a period of erosion or nondeposition within the sedimentary sequence and was interpreted by Scholl et al. (1985) to have formed during separation of the Lau Ridge from the Tonga forearc. No pronounced lithologic break or paleontologic break was found in the drilled section at a depth corresponding to the observed seismic reflection time for Horizon A. However, a significant velocity and density break at 383 mbsf falls at a two-way traveltime of 0.42 s, or almost exactly at the seismostratigraphic level of Horizon A. Furthermore, we note that the Horizon A seismic reflector corresponds to the zone of sediment alteration and an increased smectite content that extends from about 383 to about 420 mbsf.

Physical properties measured from Tonga forearc Site 841 samples reflect structural changes as well as lithologic changes within a sedimentary section. For example, a basalt dike at 390 to 395 mbsf prevents the sediment immediately beneath it from consolidating normally. This is reflected in the increased water content and associated index properties below the structure. Faults also have an effect on physical properties. In Hole 841B, the values for density, compressional wave velocity, and thermal conductivity decreased and the water content, porosity, and void ratio increased significantly at about 460 mbsf, an intersection with a major fault. A similar drop in measured values occurred below 610 mbsf, the depth of a second fault, although "normal" consolidation occurred below this fault.

### *Thermal Gradients and Calculated Heat Flow*

Considerable variability is evident in the temperature gradients and calculated heat flow values from the Lau Basin sites (Table 3 and Fig. 25). Thermal gradients range from a low of 0.7°C/100 m at Site 839 to a high of 8.7°C/100 m at Site 838. The heat flow values display a similar pattern. The heat flow measured in all the backarc sites is low when compared with the theoretical heat flow values of 175 to 200 MW/m$^2$ predicted for young crust (Anderson et al., 1977). This suggests that the sediments are not thick or diagenetically altered enough to function as a barrier to fluid-flow exchange between the sediments and seawater and that the fluid circulation in the backarc is sufficient to dissipate large amounts of heat.

In contrast, thermal gradients from the two forearc sites are similar to each other and to two earlier measurements from the Tonga forearc (Maung et al., 1981). The sediment cover is much thicker and undoubtedly impedes free fluid circulation, thus preventing heat dissipation.

## Downhole Measurements

### *Operations Summary*

During Leg 135, eight sites were drilled, and six of these sites were logged with either a partial or full set of logging tools. All logging tool strings were run at Holes 834B and 839B; the quad combination (or its component parts), the geochemical tool, and the FMS were run at Holes 838B and 840B; and only the quad tool and the FMS were run in Holes 835B and 841C. No logs were run at Sites 836 or 837.

### *Backarc: Sites 834, 835, 838, and 839*

Sites in the Lau Basin are similar in that they penetrate varying thicknesses of nannofossil-ooze-dominated sedimentary sequences and then core into the underlying basalt; the exception is Site 838, which bottoms in sediment. However, only a short section of basalt was drilled at Site 835, and the logging tools obtained measurements in only the uppermost part of that short section. Thus, results for basalt logging are mainly confined to Sites 834 and 839.

In the holes that were logged (834B, 835B, 838B, and 839B), the logs commonly showed variable values within ash, vitric sand, vitric gravel, and carbonate turbidite units, and showed only small variations within nannofossil ooze sections between turbidite

**Table 1. Average analyses of representative units from backarc sites drilled during Leg 135.**

| Site | 834 | 834 | 834 | 834 | 834 | 834 | 835 | 836 | 836 | 837 | 839 | 839 | 839 | 839 |
|---|---|---|---|---|---|---|---|---|---|---|---|---|---|---|
| Unit | 2 | 5 | 6 | 7 | 10 | 12 | 1 | 4 | 5 | 1 | 1 | 3 | 4 | 9 |
| Major elements (wt%): | | | | | | | | | | | | | | |
| $SiO_2$ | 50.70 | 50.27 | 51.28 | 49.79 | 53.68 | 52.15 | 50.25 | 48.74 | 52.11 | 55.17 | 52.64 | 50.42 | 51.64 | 53.98 |
| $TiO_2$ | 1.41 | 1.11 | 1.59 | 1.23 | 1.80 | 2.09 | 1.14 | 0.76 | 1.16 | 1.35 | 0.62 | 0.58 | 0.57 | 0.83 |
| $Al_2O_3$ | 16.34 | 16.99 | 16.36 | 17.56 | 16.46 | 15.43 | 16.42 | 16.39 | 15.38 | 14.71 | 15.00 | 12.63 | 14.33 | 16.69 |
| $Fe_2O_3$ | 10.39 | 8.98 | 10.32 | 8.76 | 10.77 | 13.61 | 9.90 | 9.24 | 12.44 | 12.66 | 10.02 | 10.16 | 9.42 | 10.93 |
| MnO | 0.15 | 0.14 | 0.17 | 0.13 | 0.16 | 0.18 | 0.16 | 0.14 | 0.20 | 0.21 | 0.17 | 0.17 | 0.17 | 0.18 |
| MgO | 6.33 | 8.39 | 5.59 | 7.67 | 3.62 | 3.83 | 7.53 | 8.85 | 5.35 | 3.41 | 9.28 | 14.74 | 9.72 | 4.84 |
| CaO | 11.28 | 11.74 | 10.73 | 12.15 | 8.52 | 8.29 | 12.59 | 14.01 | 10.62 | 8.00 | 11.68 | 10.93 | 13.64 | 10.35 |
| $Na_2O$ | 3.08 | 2.61 | 3.50 | 2.62 | 3.99 | 3.90 | 1.94 | 1.88 | 2.24 | 2.62 | 1.35 | 1.24 | 1.15 | 1.95 |
| $K_2O$ | 0.30 | 0.12 | 0.40 | 0.06 | 0.56 | 0.44 | 0.22 | 0.05 | 0.32 | 0.69 | 0.25 | 0.29 | 0.22 | 0.50 |
| $P_2O_5$ | 0.16 | 0.11 | 0.20 | 0.11 | 0.24 | 0.20 | 0.11 | 0.05 | 0.11 | 0.16 | 0.07 | 0.07 | 0.04 | 0.10 |
| Trace elements (ppm): | | | | | | | | | | | | | | |
| Nb | 2 | 1 | 2 | 1 | 2 | 2 | 1 | 1 | 1 | 2 | 1 | 1 | 1 | 1 |
| Zr | 108 | 86 | 137 | 96 | 166 | 149 | 46 | 47 | 58 | 76 | 30 | 33 | 27 | 48 |
| Y | 29 | 23 | 37 | 26 | 48 | 41 | 23 | 18 | 26 | 36 | 15 | 14 | 15 | 20 |
| Sr | 203 | 176 | 182 | 163 | 178 | 193 | 133 | 224 | 150 | 161 | 144 | 146 | 117 | 196 |
| Rb | 4 | 1 | 7 | 1 | 9 | 8 | 4 | 2 | 5 | 10 | 9 | 4 | 3 | 7 |
| Zn | 64 | 42 | 72 | 47 | 95 | 110 | 63 | 44 | 88 | 104 | 99 | 76 | 105 | 74 |
| Cu | 66 | 81 | 61 | 68 | 42 | 46 | 84 | 109 | 109 | 40 | 54 | 56 | 51 | 89 |
| Ni | 37 | 84 | 46 | 97 | 17 | 9 | 73 | 116 | 28 | 4 | 137 | 308 | 92 | 17 |
| Cr | 23 | 171 | 108 | 288 | 6 | 0 | 162 | 312 | 17 | 0 | 624 | 1456 | 445 | 14 |
| V | 285 | 200 | 266 | 200 | 305 | 373 | 275 | 241 | 415 | 322 | 287 | 243 | 256 | 344 |
| Ce | 14 | 8 | 14 | 10 | 18 | 13 | 7 | 7 | 13 | 12 | 7 | 10 | 6 | 11 |
| Ba | 55 | 47 | 45 | 17 | 63 | 64 | 42 | 16 | 53 | 86 | 62 | 57 | 44 | 102 |
| Ratios: | | | | | | | | | | | | | | |
| Ba/Zr | 0.51 | 0.55 | 0.33 | 0.18 | 0.38 | 0.43 | 0.91 | 0.34 | 0.91 | 1.13 | 2.07 | 1.72 | 1.6 | 2.13 |
| K/Ba | 45 | 21 | 74 | 29 | 74 | 57 | 43 | 26 | 50 | 67 | 33 | 42 | 42 | 41 |
| Zr/Y | 3.7 | 3.7 | 3.7 | 3.7 | 3.5 | 3.6 | 2.0 | 2.6 | 2.2 | 2.1 | 2.0 | 2.4 | 1.8 | 2.4 |
| Zr/Nb | 54 | 86 | 68 | 96 | 83 | 74 | 46 | 47 | 58 | 38 | 30 | 33 | 27 | 48 |

Notes: Oxide values are given in weight percent, trace elements in ppm. For comparative purposes, analyses include N-type (normal) and T-type (transitional) Lau Basin basalts from Hawkins and Melchior (1985); average Tonga and Kermadec Arc basaltic andesites from Ewart and Hawkesworth (1987); and analyses from the Intermediate Lau Spreading Center (ILSC) and Eastern Lau Spreading Center (ELSC) from Ernewein et al. (in press).

units. Within the turbidite units, velocity, density, and resistivity all tended to show increased values, responding to the higher grain size and density within the turbidites, whereas porosity decreased.

The most detailed variations were recorded on the FMS images, which showed light to dark banding in turbidite units, with low resistivities (and thus dark bands) characteristic of nannofossil oozes, and high resistivities (light bands) characteristic of ash or calcareous turbidite horizons. Regions of mottled images tended to be associated with thick, volcaniclastic gravels and are clearly differentiated from the uniform response of relatively featureless nannofossil oozes (e.g., at Site 838). Mottled textures may also correlate to disrupted bedding or conglomeratic beds (e.g., within and around slumped units at Site 835).

The FMS data were processed for dip information. Dips at Site 834 tended to be horizontal to dipping 1°–2°, and at Site 835, dips on both measured cores and FMS data tended to lie between 0° and 10°. At Site 838, the FMS data delineated a fracture zone with a maximum dip of 75° separating gently dipping beds above from bedded sediments with 15°–30° dips below.

All the logs showed large variations in the transition from sedimentary rocks to basalt, with large increases in velocity, density, resistivity, and geochemical values as well as gamma-ray intensities. The logs are even more valuable in delineating the depth and thickness of sedimentary rocks interbedded within the volcanics at Holes 834B and 839B. Some of these sedimentary interbeds were not sampled during coring and thus were not recognized until the logging data were available.

Logging data clearly correspond to changing petrological and physical characteristics within the basalts. In Hole 834B, for example, the transition from probable fractured and rubbly pillow lavas at flow margins to the more solid flow interior was accompanied by distinct changes in the velocity, density, and resistivity logs. The pillow lavas tended to correlate with widened areas in the hole recorded by the caliper logs, whereas the solid flow unit tended to maintain a narrow, straight hole. The characteristic signature thus formed is a wide, extremely rugose hole that narrows downward.

The FMS images in the basalts show numerous regions of fracturing, both horizontal and vertical. Although no positive pillows were identified, rounded forms are common within the images and may be the edges of pillows. The FMS images commonly suffer from hole size and rugosity in the basalt sequences, however, as the numerous washouts and rapid size changes resulted in large segments of poor quality images.

### *Tonga Ridge and Forearc: Sites 840 and 841*

Logs from Hole 840B all show significant variations that correlate with changes in the lithology of the drilled section. In particular, increases in velocity, density, and resistivity and a decrease in porosity at 383 mbsf correlate with the zone of sediment alteration where pore space is filled with clay cement. The gamma-ray and Fe geochemical log also display corresponding changes, reflecting the increased clay content of the section. The changes were recognized in the shipboard physical properties data, but they are more completely observed in the logging data. When velocity data are combined with depth to yield a time-to-depth conversion, the changes in the logging values from 383 mbsf are seen to occur at about 0.4–0.42 s on our single-channel

**Table 1 (continued).**

| Site | Lau Basin 123-74-1 | Lau Basin Ant 225-1 | Tonga basaltic | Kermadec basaltic | CD33–D18 | CD33–D25 |
|---|---|---|---|---|---|---|
| Unit | N-type | T-type | andesite | andesite | ILSC | ELSC |
| Major elements (wt%): | | | | | | |
| $SiO_2$ | 50.24 | 53.59 | 52.80 | 52.83 | 48.2 | 52.53 |
| $TiO_2$ | 0.76 | 1.05 | 0.51 | 0.90 | 1.14 | 1.94 |
| $Al_2O_3$ | 15.80 | 14.56 | 16.96 | 16.98 | 16.94 | 13.87 |
| $Fe_2O_3$ | 10.13 | 12.82 | 10.91 | 12.07 | 9.90 | 14.40 |
| MnO | 0.21 | 0.21 | 0.18 | 0.20 | 0.16 | 0.22 |
| MgO | 7.39 | 5.27 | 5.33 | 4.68 | 10.12 | 4.09 |
| CaO | 13.37 | 10.22 | 11.36 | 9.78 | 11.68 | 8.25 |
| $Na_2O$ | 2.10 | 2.34 | 1.56 | 2.19 | 2.43 | 3.05 |
| $K_2O$ | 0.11 | 0.17 | 0.34 | 0.30 | 0.04 | 0.29 |
| $P_2O_5$ | 0.09 | 0.11 | 0.07 | 0.06 | 0.04 | 0.17 |
| Trace elements (ppm): | | | | | | |
| Nb | 3 | 7 | 0.56 | 0.76 | 0.75 | 2.1 |
| Zr | 40 | 45 | 18 | 39 | 50 | 115 |
| Y | 21 | 26 | 12 | 21 | 24.5 | 44.8 |
| Sr | 166 | 98 | 196 | 174 | 103 | 98 |
| Rb | 2 | 0.5 | 4.4 | 4.9 | <2 | 4 |
| Zn | 40 | | 84 | 92 | 70 | 126 |
| Cu | 89 | 107 | 133 | | 111 | 39 |
| Ni | 94 | 33 | 23 | 16 | 209 | 9 |
| Cr | 300 | 50 | 54 | 27 | 423 | 7 |
| V | | | 305 | 346 | 258 | 518 |
| Ce | 5.1 | | 3.7 | 6.2 | 5.4 | 12.91 |
| Ba | 10.8 | 32.5 | 88 | 111 | 16 | 34.5 |
| Ratios: | | | | | | |
| Ba/Zr | 0.27 | 0.72 | 4.89 | 2.85 | 0.32 | 0.30 |
| K/Ba | 85 | 43 | 32 | 22 | 21 | 70 |
| Zr/Y | 1.9 | 1.7 | 1.5 | 1.9 | 2.0 | 2.6 |
| Zr/Nb | 13 | 6 | 32 | 51 | 67 | 55 |

**Table 2. Secondary minerals observed in Holes 834–839.**

| Hole 834 (106–435 mbsf) (8.8°–25.3°C) | Hole 835 (155–183 mbsf) (5.9°–6.3°C) | Hole 838 (150–259 mbsf) (16.6°–26.0°C) | Hole 837 (80–100 mbsf) (5.2°–5.6°C) | Hole 839 (218–517 mbsf) (5.0°–7.2°C) | Hole 836 (17–58 mbsf) (no data) |
|---|---|---|---|---|---|
| Clay minerals | Clay minerals | Quartz, opal? | Clay minerals | Clay minerals | Clay minerals |
| Palagonite→ smectite | Palagonite→ smectite ± zeolite-rim | Zeolites | Palagonite→ smectite | Palagonite→ smectite | Palagonite→ smectite |
| Cubic zeolites | Dark green | Calcite | Fe-hydroxide | Iddingsite | Fe-hydroxide |
| Calcite veins | Vein infilling (sepiolite?) | | | Zeolites | Aragonite in cavities |
| Iddingsite | | | | Analcime/chabazite? | Zeolites |
| Fe-hydroxide | | | | Aragonite in cavities | |
| Celadonite? | | | | | |
| Chrysotile? | | | Remarks: | Remarks: | Remarks: |
| Stilpnomelane? | | | No interbedded sediments | Interbedded sediments; talc on fractures | Interbedded sediments |
| Remarks: Interbedded sediments | Remarks: No interbedded sediments | Remarks: Poor recovery; 600 µM Si in pore water; highest temperature gradient (8.7°C/100 m) | | | |

Note: Minerals have been listed from the westernmost to the easternmost location and include depths and estimated borehole temperatures.

seismic reflection profiles. The seismic unconformity at that traveltime was interpreted as being related to the time of break-up of the Tonga Ridge and the initial opening of the Lau Basin; this was the primary target of drilling at Site 840. Previous interpretations (by Scholl et al., 1985) that relate this horizon to the earliest rifting and formation of the Lau Basin require modification.

All of the logs from Hole 840B contain a high degree of variability about average values that may be caused by the large lithologic changes within the turbidite units comprising the drilled section. Velocity, density, and resistivity lows and porosity highs coincide with the coarse, volcaniclastic-rich lower part of the turbidite units and reflect the large amount of pore space within these vitric sediments. The typical downlog profile of the turbidites is a sawtooth with gradually increasing velocity, density, and resistivity, followed by a sharp break to lower values. This is the opposite to what is normally observed in nonvitric, sand-domi-

**Table 3. Calculated heat flow for Leg 135 forearc and backarc sites.**

| Site | Temperature gradient (°C/100 m) | Calculated heat flow ($mW/m^2$) |
|---|---|---|
| Backarc: | | |
| 834 | 5.0 | 50.0 |
| 835 | 1.5 | 14.5 |
| 837 | 2.1 | 24.4 |
| 838 | 8.7 | 50.6 |
| 839 | 0.7 | 9.3 |
| Forearc: | | |
| 840 | 2.9 | 27.5 |
| 841 | 2.8 | 29.5 |

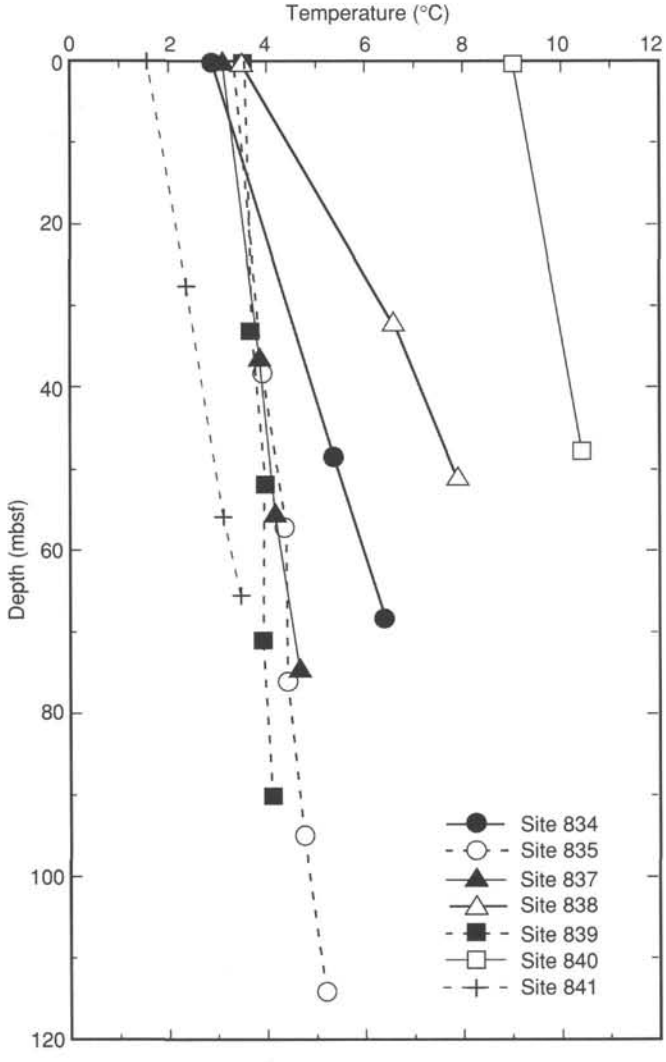


Figure 25. Thermal gradients observed at Leg 135 sites.

nated turbidites, in which the sand component causes high velocity, density, and resistivity values at the base of the section, gradually decreasing upward.

High-quality FMS images were obtained between 250 and 516 mbsf that show spectacular banding within the turbidite section. Images from the upper part of the hole between 87 and 250 mbsf were degraded by the large hole size and rugosity. In the sequence imaged below 250 mbsf, high-resistivity light bands correlate with the fine-grained turbidite chalk tops, and dark low-resistivity bands correspond to the vitric- and volcanic-rich turbidite bases. Banding within the FMS images may eventually permit correlation of individual turbidite units sampled in the cores with the units seen on the images, thus allowing us to make better estimates of unit thickness and depth. This, in turn, will permit detailed studies of sedimentation rates and lithologic changes within turbidite units or groups of units.

High-quality dipmeter data was also obtained from the FMS data. From 250 to 516 mbsf, the dip is extremely consistent and averages about 2° from 250 to 350 mbsf, then gradually increases to about 4.5° by 500 mbsf. The range of values is up to 10°, but most of the values are within 2° of the average. The dip azimuth averages 0° from 250 to 400 mbsf, with a range of about 30° west and east. The azimuth gradually changes to a slightly western direction beginning at about 350 mbsf and averages about 345° at the base of the hole.

Hole 841B was logged with the quad and FMS tools. The geophysical logs show changes that delineate the location of the mafic igneous intrusions identified as dikes or sills within the sedimentary section. These logs also show changes associated with the fault at about 455 mbsf. The FMS data also image this fault, and dip information from the FMS data indicate the presence of an unconformity at around 555 mbsf.

## REFERENCES


Adams, C. G., 1970. A reconsideration of the East Indian Letter Classification. *Bull. Br. Mus. Nat. Hist. Geol.*, 19:87–137.

Aggarwal, Y. P., Barazangi, M., and Isacks, B., 1972. P and S travel times in the Tonga-Fiji region: a zone of low velocity in the uppermost mantle behind the Tonga Island arc. *J. Geophys. Res.*, 77:6427–6434.

Aggery, K. E., Muenow, D. W., and Sinton, J. M., 1988. Volatile abundances in submarine glasses from the North Fiji and Lau back-arc basins. *Geochim. Cosmochim. Acta*, 52:2501–2506.

Anderson, R. N., Langseth, M. G., and Sclater, J. G., 1977. The mechanisms of heat transfer through the floor of the Indian Ocean. *J. Geophys. Res.*, 82:3391–3409.

Austin, J., Taylor, F. W., and Cagle, C. D., 1989. Seismic stratigraphy of the Central Tonga Ridge. *Mar. Pet. Geol.*, 6:71–92.

Ballance, P. F., Vallier, T. L., Nelson, C. S., and Frisch, R. S., in press. Petrology and sedimentology of mixed volcaniclastic and pelagic sedimentary rocks from the southern Tonga platform, trench slope and trench, and the Lau Ridge. *In* Ballance, P. F., Herzer, R. H., and Vallier, T. L. (Eds.), *Geology of the Tonga Ridge, Lau Basin and Lau Ridge Region, Southwest Pacific*. Circum-Pac. Counc. Energy Miner. Resour., Earth Sci. Ser.

Barazangi, M., and Isacks, B., 1971. Lateral variations of seismic wave attenuation in the upper mantle behind the Tonga Island arc. *J. Geophys. Res.*, 76:8493–816.

Bednarz, U., Sunkel, G., and Schmincke, H. U., 1987. The basaltic andesite-andesite and the andesite-dacite series from the ICRDG Drill Holes CY-2 and CY-2a. I. Lithology, petrology, and geochemistry. *In* Robinson, P. T., Gibson, I. L., and Panayiotou, A. (Eds.), *Cyprus Crustal Study Project: Initial Report, Holes CY-2 and CY-2a*. Pap.—Geol. Surv. Can., 85-29:183–204.

Bentz, F. P., 1974. Marine geology of the southern Lord Howe Rise, southwest Pacific. *In* Burk, C. A., and Drake, C. L. (Eds.), *The Geology of Continental Margins:* New York (Springer-Verlag), 537–547.

Berger, A. L., 1978. Long-term variations of caloric solar insolation resulting from earth's orbital variations. *Quat. Res.*, 9:139–167.

Berggren, W. A., Kent, D. V., Flynn, J. J., and Van Couvering, J. A., 1985. Cenozoic geochronology. *Geol. Soc. Am. Bull.*, 96:1407–1418.

Billington, S., 1980. The morphology and tectonics of the subducted lithosphere in the Tonga-Kermadec-Fiji region from seismicity and focal mechanism solutions [Ph.D. dissert.]. Cornell Univ., Ithaca, NY.

Bloemendal, J., and deMenocal, P., 1989. Evidence for a change in the periodicity of tropical climate cycles at 2.4 Myr from whole-core magnetic susceptibility measurements. *Nature*, 342:897–899.

Bloomer, S. H., 1983. The distribution and origin of igneous rocks from the landward slopes of the Mariana Trench. *J. Geophys. Res.*, 88:7411–7428.

Bloomer, S. H., and Fisher, R. L., 1985. Petrology and geochemistry of igneous rocks from the Tonga Trench—a non-accreting plate boundary. *J. Geol.*, 95:469–495.

Blow, W. H., 1969. Late middle Eocene to Recent planktonic foraminiferal biostratigraphy. *In* Brönniman, P., and Renz, H. H. (Eds.), *Proc. First Int. Conf. Planktonic Microfossils*, Geneva, 1967. Leiden (E. J. Brill), 1:199–422.

Bolli, H. M., and Premoli-Silva, I., 1973. Oligocene to Recent planktonic foraminifera and stratigraphy of the Leg 15 Sites in the Caribbean Sea. *In* Edgar, N. T., Saunders, J. B., et al., *Init. Repts. DSDP*, 15: Washington (U.S. Govt. Printing Office), 475–497.

Buchbinder, B., and Halley, R. B., 1985. Source rock evaluation of outcrop and borehole samples from Tongatapu and 'Eua Islands, Tonga, and from Viti Levu and Vanua Levu Islands, Fiji. *In* Scholl, D. W., and Vallier, T. L. (Eds.), *Geology and Offshore Resources of Pacific Island Arcs—Tonga Region.* Circum-Pac. Counc. Energy Miner. Resour., Earth Sci. Ser., 2:335–349.

Bukry, D., 1973. Low-latitude coccolith biostratigraphic zonation. *In* Edgar, N. T., Saunders, J. B., et al., *Init. Repts. DSDP*, 15: Washington (U.S. Govt. Printing Office), 685–703.

_____, 1975. Coccolith and silicoflagellate stratigraphy, northwestern Pacific Ocean, Deep Sea Drilling Project Leg 32. *In* Larson, R. L., Moberly, R., et al., *Init. Repts. DSDP*, 32: Washington (U.S. Govt. Printing Office), 677–701.

Burns, R., and Andrews, J., 1973. Regional aspects of drilling in the southwest Pacific. *In* Burns, R. E., Andrews, J. E., et al., *Init. Repts. DSDP*, 21: Washington (U.S. Govt. Printing Office), 897–906.

Cawood, P., 1985. Petrography, phase chemistry and provenance of volcanogenic debris from the southern Tonga Ridge: implications for arc history and magmatism. *In* Scholl, D. W., and Vallier, T. L. (Eds.), *Geology and Offshore Resources of Pacific Island Arcs—Tonga Region.* Circum-Pac. Counc. Energy Miner. Resour., Earth Sci. Ser., 149–170.

Chaproniere, G.C.H., in press. Pleistocene to Holocene planktic foraminiferal biostratigraphy of the Coral Sea, offshore Queensland, Australia. *BMR J. Aust. Geol. Geophys.*

Chase, C. G., 1971. Tectonic history of the Fiji plateau. *Geol. Soc. Am. Bull.*, 82:3087–3110.

Clement, B. M., and Robinson, F., 1987. The magnetostratigraphy of Leg 94 sediments. *In* Ruddiman, W. F., Kidd, R. B., et al., *Init. Repts. DSDP*, 94, Pt. 2: Washington (U.S. Govt. Printing Office), 635–650.

Cole, J. W., 1982. Regional distribution and character of active andesite volcanism, Tonga-Kermadec-New Zealand. *In* Thorpe, R. S. (Ed.), *Andesites and Related Rocks:* New York (Wiley), 25–95.

Cole, J. W., Gill, J. B., and Woodhall, D., 1985. Petrologic history of the Lau Ridge, Fiji. *In* Scholl, D. W., and Vallier, T. L. (Eds.), *Geology and Offshore Resources of Pacific Island Arcs—Tonga Region.* Circum-Pac. Counc. Energy Miner. Resour., Earth Sci. Ser., 379–414.

Cole, W. S., 1960. Upper Eocene and Oligocene larger foraminifera from Viti Levu, Fiji. *Geol. Surv. Prof. Pap. U.S.*, No. 374-A.

Colley, H., Hindle, W. H., and Hathaway, B., 1986. Early arc and basinal activity on Viti Levu, Fiji. Internat. Volcanol. Congr., New Zealand, 140. (Abstract)

Cunningham, J. K., and Anscombe, K. J., 1985. Geology of 'Eua and other islands, Kingdom of Tonga. *In* Scholl, D. W., and Vallier, T. L. (Eds.), *Geology and Offshore Resources of Pacific Island Arcs—Tonga Region.* Circum-Pac. Counc. Energy Miner. Resour., Earth Sci. Ser., 221–258.

Davey, F. J., 1982. The structure of the South Fiji Basin. *Tectonophysics*, 87:185–241.

Delaney, J. R., Muenow, D. W., and Graham, D. G., 1978. Abundance and distribution of water, carbon, and sulfur in the glassy rims of submarine pillow basalts. *Geochim. Cosmochim. Acta*, 42:581–594.

Duncan, R. A., Vallier, T., and Falvey, D. A., 1985. Volcanic episodes at 'Eua Tonga. *In* Scholl, D. W., and Vallier, T. L. (Eds.), *Geology and Offshore Resources of Pacific Island Arcs—Tonga Region.* Circum-Pac. Counc. Energy Miner. Resour., 281–290.

Eguchi, T., 1984. Seismotectonics of the Fiji Plateau and Lau Basin. *Tectonophysics*, 102:17–32.

Ernewein, M., Pearce, J. A., Bloomer, S. H., Parson, L. M., Murton, B. J., Johnson, L. E., in press. Geochemistry of Lau Basin volcanic rocks: influence of ridge segmentation and arc proximity. *Contrib. Mineral. Petrol.*

Ewart, A., Brothers, R. N., and Mateen, A., 1977. An outline of the geology and geochemistry, and the possible petrogenetic evolution of the volcanic rocks of the Tonga-Kermadec-New Zealand island arc. *J. Volcanol. Geotherm. Res.*, 2:205–250.

Ewart, A., and Bryan, W., 1972. Petrography and geochemistry of the igneous rocks from 'Eua, Tonga Islands. *Geol. Soc. Am. Bull.*, 83:3281–3298.

Ewart, A., and Hawkesworth, C. J., 1987. The Pleistocene-Recent Tonga-Kermadec arc lavas: interpretation of new isotope and rare earth data in terms of a depleted mantle source model. *J. Petrol.*, 28:495–530.

Exon, N. F., Herzer, R. H., and Cole, J., 1985. Mixed volcaniclastic and sedimentary rocks from the Cenozoic southern Tonga platform and their petroleum potential. *In* Scholl, D. W., and Vallier, T. L. (Eds.), *Geology and Offshore Resources of Pacific Island Arcs—Tonga Region.* Circum-Pac. Counc. Energy Miner. Resour., Earth Sci. Ser., 75–108.

Fisher, R. L., and Engel, C. G., 1969. Ultramafic and basaltic rocks dredged from the nearshore flank of the Tonga Trench. *Geol. Soc. Am. Bull.*, 80:1373–1378.

Fryer, P., Sinton, J., and Philpotts, J., 1981. Basaltic glasses from the Mariana Trough. *In* Hussong, D. M., and Uyeda, S., et al., *Init. Repts. DSDP*, 60: Washington (U.S. Govt. Printing Office), 601–610.

Garcia, M. O., Liu, N.W.K., and Muenow, D. W., 1979. Volatiles in submarine volcanic rocks from the Mariana island arc and trough. *Geochim. Cosmochim. Acta*, 43:305–312.

Giardini, D., and Woodhouse, J., 1984. Deep seismicity and modes of deformation in Tonga subduction zone. *Nature*, 307:505–509.

Gill, J. B., 1976. Composition and age of Lau basin and ridge volcanic rocks: implications for evolution of an interarc basin and remnant arc. *Geol. Soc. Am. Bull.*, 87:1384–1395.

Hamburger, M. W., and Isacks, B. L., 1988. Diffuse backarc deformation in the southwestern Pacific. *Nature*, 332:599–604.

Harland, W. B., Cox, A. V., Llewellyn, P. G., Pickton, C.A.G., Smith, D. G., and Walters, R., 1982. *A Geologic Time Scale:* Cambridge (Cambridge Univ. Press).

Hart, S. R., Glassley, W., and Karig, D. E., 1972. Basalts and seafloor spreading behind the Mariana Island arc. *Earth Planet. Sci. Lett.*, 15:12–18.

Hawkins, J. W., 1974. Geology of the Lau Basin, a marginal sea behind the Tonga Arc. *In* Burk, C., and Drake, C. (Eds.), *The Geology of Continental Margins:* Berlin (Springer-Verlag), 505–520.

_____, 1976. Petrology and geochemistry of basaltic rocks of the Lau Basin. *Earth Planet. Sci. Lett.*, 28:283–297.

_____, 1977. Petrologic and geochemical characteristics of marginal basin basalts. *In* Talwani, M., and Pitman, W. (Eds.), *Island Arcs, Deep Sea Trenches and Back-Arc Basins*, Am. Geophys. Union, Maurice Ewing Ser., 1:355–365.

_____, 1985. Low-K rhyolitic pumice from the Tonga ridge. *In* Scholl, D. W., and Vallier, T. L. (Eds.), *Geology and Offshore Resources of Pacific Island Arcs—Tonga Region.* Circum-Pac. Counc. Energy and Miner. Resour., Earth Sci. Ser., 2:171–178.

_____, 1988. Cruise Report—PAPATUA Expedition, Leg 04, R/V *Thomas Washington.* SIO Ref. Ser., No. 88-14.

_____, 1989. Cruise Report—ROUNDABOUT Expedition, Legs 14, 15, R/V *Thomas Washington.* SIO Ref. Ser., No. 89-13.

Hawkins, J. W., and Batiza, R., 1975. Tholeiitic basalt from an active spreading center on the North Fiji Plateau near 15°30'S, 173°30'E. *Eos*, 56:1078.

Hawkins, J. W., Bloomer, S. H., Evans, C., and Melchior, J., 1984. Evolution of intra-oceanic arc-trench systems. *Tectonophysics*, 102:174–205.

Hawkins, J. W., and Falvey, D. A., 1985. Petrology of andesitic dikes and flows from 'Eua, Tonga. *In* Scholl, D. W., and Vallier, T. L. (Eds.), *Geology and Offshore Resources of Pacific Island Arcs—Tonga Region.* Circum-Pac. Counc. Energy Miner. Resour., 269–280.

Hawkins, J. W., Lonsdale, P. F., Macdougall, J. D., and Volpe, A. M., 1990. Petrology of the axial ridge of the Mariana Trough back arc spreading center. *Earth Planet. Sci. Lett.*, 100:226–256.

Hawkins, J. W., and Melchior, J. T., 1985. Petrology of Mariana Trough and Lau Basin basalts. *J. Geophys. Res.*, 90:11431–11468.

Hawkins, J. W., Melchior, J., Florendo, F., and Nilsson, K., 1989. Evolution of backarc basin magmas and their mantle sources—examples from the Lau Basin and Mariana Trough. *Eos*, 70:1389.

Herzer, R. H., and Exon, N., 1985. Structure and basin analysis of the southern Tonga forearc. *In* Scholl, D. W., and Vallier, T. L. (Eds.), *Geology and Offshore Resources of Pacific Island Arcs—Tonga Region*. Circum-Pac. Counc. Energy Miner. Resour., Earth Sci. Ser., 2:55–74.

Hey, R. N., Naar, D. F., Kleinrock, M. C., Phipps Morgan, W. J., Morales, E., and Schilling, J., 1985. Microplate tectonics along a superfast seafloor spreading system near Easter Island. *Nature*, 317:320–325.

Hoffmeister, J. E., 1932. Geology of 'Eua, Tonga. *Bull. B.P. Bishop Museum*, No. 96.

Hunt, J. M., 1979. *Petroleum Geochemistry and Geology:* San Francisco (W. H. Freeman).

Hussong, D. M., and Fryer, P., 1985. Fore-arc tectonics in the northern Mariana Arc. *In* Nasu, N., Kobayashi, K., Uyeda, S., et al. (Eds.), *Formation of Active Ocean Margins:* Tokyo (Terra Scientific Publishing), 273–290.

Isacks, B. L., and Barazangi, M., 1977. Geometry of Benioff zones: lateral segmentation and downwards bending of the subducted lithosphere. *In* Talwani, M., and Pitman, W. (Eds.), *Island Arcs, Deep Sea Trenches and Back-Arc Basins*, Am. Geophys. Union, Maurice Ewing Ser., 1:99–114.

Karig, D. E., 1970. Ridges and basins of the Tonga-Kermadec island arc system. *J. Geophys. Res.*, 75:239–254.

_____, 1971. Structural history of the Mariana Island arc system. *Geol. Soc. Am. Bull.*, 82:323–344.

Katz, H. R., 1986. Hydrocarbon potential in the SW Pacific. *In* Cronan, D. (Ed.), *Sedimentation and Mineral Deposits in the Southwestern Pacific Ocean:* London (Academic Press).

Kennett, J. P., and Srinivasan, M. S., 1983. *Neogene Planktonic Foraminifera:* New York (Van Nostrand Reinhold).

Kroenke, L., 1984. *Cenozoic Development of the Southwest Pacific.* CCOP/SOPAC, Tech. Bull., No. 6. U. N. Econ. Soc. Comm. Asia Pac., Suva.

Lancelot, Y., Larson, R., et al., 1990. *Proc. ODP, Init. Repts.*, 129: College Station, TX (Ocean Drilling Program).

Lawver, L. A., Hawkins, J. W., and Sclater, J. G., 1976. Magnetic anomalies and crustal dilation in the Lau basin. *Earth Planet. Sci. Lett.*, 33:27–35.

Lonsdale, P., 1986. A multibeam reconnaissance of the Tonga Trench axis and its intersection with Louisville Guyot Chain. *Mar. Geophys. Res.*, 8:295–327.

Louat, R., and Dupont, B., 1982. Seismicité de l'arc des Tonga-Kermadec. *Trav. Doc. ORSTOM*, 147:299–317.

MacPherson, G. J., 1984. A model for predicting the volumes of vesicles in submarine basalts. *J. Geol.*, 92:73–82.

Malahoff, A., Feden, R. H., and Fleming, H. S., 1982. Magnetic anomalies and tectonic fabric of marginal basins north of New Zealand. *J. Geophys. Res.*, 87:4109–4125.

Malahoff, A., Kroenke, L. W., Cherkis, N., and Brozena, J., in press. Magnetic and tectonic fabric of the North Fiji Basin and Lau Basin. *In* Kroenke, L., and Eade, J. V. (Eds.), *Basin Formation, Ridge Crest Processes, and Metallogenesis in the North Fiji Basin.* Circum-Pac. Counc. Energy and Miner. Resour., Earth Sci. Ser.

Mankinen, E. A., Donnelly, J. M., and Grommé, C. S., 1978. Geomagnetic polarity event recorded at 1.1. m.y. B.P. on Cobb mountain, Clear Lake volcanic field, California. *Geology*, 6:653–656.

Martini, E., 1971. Standard Tertiary and Quaternary calcareous nannoplankton zonation. *In* Farinacci, A. (Ed.), *Proc. 2nd Planktonic Conf. Roma:* Rome (Ed. Technosci.), 2:739–785.

Mattey, D. P., Marsh, N. G., and Tarney, J., 1980. The geochemistry, mineralogy, and petrology of basalts from the West Philippine and Parece Vela basins and from the Palau-Kyushu and West Mariana ridges, Deep Sea Drilling Project Leg 59. *In* Kroenke, L., and Scott, R., et al., *Init. Repts. DSDP*, 59: Washington (U.S. Govt. Printing Office), 753–796.

Maung, T. U., Anscombe, K. J., and Tongilava, S. L., 1981. Assessment of petroleum potential of the southern and northern parts of the Tonga platform. *Tech. Rep.—U. N. Econ. Soc. Comm. Asia Pac., CCOP/SOPAC*, No. 18.

Meijer, A., 1983. The origin of low-K rhyolites from the Mariana frontal arc. *Contrib. Mineral. Petrol.*, 83:45–51.

Melson, W. G., Jarosewich, E., and Lundquist, C. A., 1970. Volcanic eruption at Metis Shoal, Tonga, 1967–1968. Description and petrology. *Smithson. Contrib. Earth Sci.*, No. 4.

Moberly, R., 1972. Origin of lithosphere behind island arcs with reference to the western Pacific. *Mem.—Geol. Soc. Am.*, 132:35–55.

Newman, S., 1989. Water and carbon dioxide in the basaltic glasses from the Mariana Trough. *Eos*, 70:1387.

Nilsson, K., Florendo, F. F., and Hawkins, J. W., et al., 1989. Petrology of a nascent triple junction, northeastern Lau Basin. *Eos*, 70:1389.

Okada, H., and Bukry, D., 1980. Supplementary modification and introduction of code numbers to the low-latitude coccolith biostratigraphic zonation (Bukry, 1973; 1975). *Mar. Micropaleontol.*, 5:321–325.

Packham, G. H., 1985. Vertical tectonics on the Tonga Ridge from the Tongatapu oil exploration wells. *In* Scholl, D. W., and Vallier, T. L. (Eds.), *Geology and Offshore Resources of Pacific Island Arcs—Tonga Region*. Circum-Pac. Counc. Energy Miner. Resour., Earth Sci. Ser., 301–316.

Packham, G. H., and Falvey, D. A., 1971. An hypothesis for the formation of marginal seas in the western Pacific. *Tectonophysics*, 11:79–109.

Parris, J. P., and Lille, R., 1977. New Caledonia: evolution from Permian to Miocene: mapping data and hypothesis about geotectonics. *Int. Symp. Geodynamics of the Southwest Pacific New Caledonia*, August–September 1976. Paris (Edition Technip.), 195–208.

Parson, L. M., et al., 1989. RRS *Charles Darwin* Cruise 33/8, 5 May–1 June 1988. Geophysical and geological investigations of the Lau back-arc basin, SW Pacific. Institute of Oceanographic Studies, Deacon Laboratory, Cruise Rep., No. 206.

Parson, L. M., Pearce, J. A., Murton, B. A., Hodkinson, R. A., Bloomer, S., Ernewein, M., Huggett, Q. J., Miller, S., Johnson, L., Rodda, P., and Helu, S., 1990. Role of ridge jumps and ridge propagation in the tectonic evolution of the Lau backarc basin, southwest Pacific. *Geology*, 18:470–473.

Pelletier, B., and Louat, R., 1989. Seismotectonics and present day relative plate motions in the Tonga-Lau and Kermadec-Havre region. *Tectonophysics*, 165:237–250.

Raitt, R. W., Fisher. R. L., and Mason, R. G., 1955. Tonga Trench. *In* Poldervaart, A. (Ed.), *Crust of the Earth*. Spec. Pap.—Geol. Soc. Am., 62:237–254.

Ruddiman, W. F., and McIntyre, A., 1981. Oceanic mechanisms for amplification of the 23,000 year ice volume cycle. *Science*, 212:617–627.

Ruddiman, W. F., and Sandstrom, M. W., 1985. Organic geochemistry of dredge samples and oil seeps from the southern Tonga Platform. *In* Scholl, D. W., and Vallier, T. L. (Eds.), *Geology and Offshore Resources of Pacific Island Arcs—Tonga Region*. Circum-Pac. Counc. Energy Miner. Resour., Earth Sci. Ser., 2:121–129.

Sager, W. W., and Hall, S. A., 1990. Magnetic properties of black mud turbidites from ODP Leg 116, Distal Bengal Fan, Indian Ocean. *In* Cochran, J. R., Stow, D.A.V., et al., *Proc. ODP, Sci. Results*, 116: College Station, TX (Ocean Drilling Program), 317–336.

Sandstrom, M. W., 1985. Organic chemistry of dredge samples and oil seeps from the southern Tonga platform. *In* Scholl, D. W., and Vallier, T. L. (Eds.), *Geology and Offshore Resources of Pacific Island Arcs—Tonga Region*. Circum-Pac. Counc. Energy and Miner. Resour., Earth Sci. Ser., 2:121–129.

Sato, H., 1979. Segregation vesicles and immiscible liquid droplets in ocean-floor basalt of Hole 396B, DSDP Leg 46. *In* Dmitriev, L., Heirtzler, J., et al., *Init. Repts. DSDP*, 46: Washington (U.S. Govt. Printing Office), 283–291.

Scholl, D. W., and Vallier, T. L. (Eds.), 1985. *Geology and Offshore Resources of Pacific Island Arcs—Tonga Region*. Circum-Pac. Counc. Energy Miner. Resour., Earth Sci. Ser., No. 2.

Scholl, D. W., Vallier, T. L., and Packham, G. H., 1985. Framework geology and resource potential of the southern Tonga platform and adjacent terranes—a synthesis. *In* Scholl, D. W., and Vallier, T. L. (Eds.), *Geology and Offshore Resources of Pacific Island Arcs—Tonga Region*. Circum-Pac. Counc. Energy Miner. Resour., Earth Sci. Ser., 2:457—488.

Sclater, J. G., 1972. Heat flow and elevation of the marginal basins of the Western Pacific. *J. Geophys. Res.*, 77:5685–5696.

Sclater, J. G., Anderson, R. N., and Bell, M. L., 1971. Elevation of ridges and evolution of the central Eastern Pacific, *J. Geophys. Res.*, 76:7888–7915.

Sclater, J. G., Hawkins, J. W., Mammerickx, J., and Chase, C. G., 1972. Crustal extension between the Tonga and Lau Ridges: Petrologic and geophysical evidence. *Geol. Soc. Am. Bull.*, 83:505–518.

Shor, G. G., Jr., Kirk, H. K., and Menard, H. W., 1971. Crustal structure of the Melanesian area. *J. Geophys. Res.*, 76:2562–2586.

Smith, R. E., 1968. Segregation vesicles in basaltic lava. *Am. J. Sci.*, 265:696–713.

Sun, S.-S., and McDonough, W. F., 1989. Chemical and isotopic systematics of oceanic basalts: implications for mantle composition and processes. *In* Saunders, A. D., and Norry, M. J. (Eds.), *Magmatism in the Ocean Basins*. Geol. Soc. Spec. Publ. London, 42:313–345.

Tappin, D. R., and Ballance, P. F., in press. Contributions to the sedimentary geology of 'Eua Island—Kingdom of Tonga: reworking in an oceanic forearc. *In* Stevenson, A., and Ballance, P. (Eds.), *Tonga Arc:* Berlin (Springer-Verlag).

Tappin, D. R., Herzer, R. H., and Stevenson, A. J., in press. Structure and history of an oceanic forearc—the Tonga Ridge 22 to 26 South. *In* Stevenson, A., and Ballance, P. (Eds.), *Tonga Arc:* Berlin (Springer-Verlag).

Tatsumi, Y., Hamilton, D. L., and Nesbitt, R. W., 1986. Chemical characteristics of fluid phase released from a subducted lithosphere and origin of arc magmas: evidence from high pressure experiments and natural rocks. *J. Volcanol. Geotherm. Res.*, 29:293–309.

Taylor, B., Fujioka, K., et al., 1990. *Proc. ODP, Init. Repts.*, 126: College Station, TX (Ocean Drilling Program).

Tissot, B. P., and Welte, D. H., 1984. *Petroleum Formation and Occurrence* (2nd ed.): Heidelberg (Springer-Verlag).

Vallier, T. L., O'Connor, R. M., Scholl, D. W., Stevenson, A. J., and Quinterno, P. J., 1985. Petrology of rocks dredged from the landward slope of the Tonga Trench: implications for middle Miocene volcanism and subsidence of the Tonga Ridge. *In* Scholl, D. W., and Vallier, T. L. (Eds.), *Geology and Offshore Resources of Pacific Island Arcs—Tonga Region*. Circum-Pac. Counc. Energy Miner. Resour., 2:109–120.

Vallier, T. L., Stevenson, A. J., and Scholl, D. W., 1985. Petrology of igneous rocks from Ata Island, Kingdom of Tonga. *In* Scholl, D. W., and Vallier, T. L. (Eds.), *Geology and Offshore Resources of Pacific Island Arcs—Tonga Region*. Circum.-Pac. Counc. Energy Miner. Resour., Earth Sci. Ser., 2:301–316.

van der Lingen, G., 1973. The Lord Howe rhyolites. *In* Burns, R. E., Andrews, J. E., et al., *Init. Repts. DSDP*, 21: Washington (U.S. Govt. Printing Office), 523–540.

Volpe, A. M., Macdougall, J. D., and Hawkins, J. W., 1987. Mariana Trough basalts (MTB): trace element and Sr-Nd isotopic evidence for mixing between MORB-like and Arc-like melts. *Earth Planet. Sci. Lett.*, 82:241–254.

_____, 1988. Lau Basin basalts (LBB): trace element and Sr-Nd isotopic evidence for heterogeneity in back arc basin mantle. *Earth Planet. Sci. Lett.*, 90:174–186.

von Stackelberg, U., 1990. R. V. Sonne cruise S048: summary of results testing a model of mineralization. *Mar. Min.*, 9:135–144.

von Stackelberg, U., and von Rad, U., 1990. Geological evolution and hydrothermal activity in the northern Lau and North Fiji Basins (Sonne Cruise SO-35—a synthesis. *Jahrb., Reihe D, Mineral., Petrog., Geoch., Lagerstatt.*, 92:629–660.

Walker, R. G., 1978. Deep water sandstone facies and ancient submarine fans: models for exploration of stratigraphic traps. *AAPG Bull.*, 62:932–966.

Wegener, A., 1929. *The Origin of Continents and Oceans:* New York (Dover Publ.). Transl. J. Biram, 1966.

Weissel, J. K., 1977. Evolution of the Lau Basin by the growth of small plates. *In* Talwani, M., and Pitman, W. C. (Eds.), *Island Arcs, Deep Sea Trenches and Back Arc Basins*. Am. Geophys. Union, Maurice Ewing Ser., 1:429–436.

Whelan, P. M., Gill, J. B., Kollman, E., Duncan, R., and Drake, R. E., 1985. Radiometric dating of magmatic stages in Fiji. *In* Scholl, D. W., and Vallier, T. L. (Eds.), *Geology and Offshore Resources of Pacific Island Arcs—Tonga Region*. Circum-Pac. Counc. Energy Miner. Resour., Earth Sci. Ser., 2:415–440.

Wilcox, J. B., Symonds, P. A., Hinz, K., Bennet, D., 1980. Lord Howe Rise, Tasman Sea—preliminary geophysical results and petroleum prospects. *BMR J. Aust. Geol. Geophys.*, 5:225–236.

Woodhall, D., 1985. Geology of the Lau Ridge. *In* Scholl, D. W., and Vallier, T. L. (Eds.), *Geology and Offshore Resources of Pacific Island Arc—Tonga Region*. Circum-Pac. Counc. Energy Miner. Resour., Earth Sci. Ser., 2:351–378.

**Ms 135A-101**